Universidad de Oviedo

Programa de Doctorado en Materiales

Mejora del comportamiento en servicio y optimización microestructural de la capa de trabajo de cilindros de laminación fabricada en fundición Ni-Hard con grafito, aleada con Mo, Nb y Mg.

TESIS DOCTORAL

Alberto Cofiño Villar

Diciembre 2021

Universidad de Oviedo

Programa de Doctorado en Materiales

Mejora del comportamiento en servicio y optimización microestructural de la capa de trabajo de cilindros de laminación fabricada en fundición Ni-Hard con grafito, aleada con Mo, Nb y Mg.

TESIS DOCTORAL

Director de tesis

Dr. D. José Florentino Alvarez Antolín

Universidad de Oviedo
Universidá d'Uviéu
University of Oviedo

RESUMEN DEL CONTENIDO DE TESIS DOCTORAL

1.- Título de la Tesis	
Español: Mejora del comportamiento en servicio y optimización microestructural de la capa de trabajo de cilindros de laminación fabricada en fundición Ni-Hard con grafito, aleada con Mo, Nb y Mg.	Inglés: Enhancement of service bahviour and microstructural optimization in the working layer of rolling cylinders manufactured in Ni-Hard Cast Iron alloyed with Mo, Nb and Mg.

2.- Autor	
Nombre: Alberto Cofiño Villar	DNI: ´
Programa de Doctorado: Materiales	
Órgano responsable: Comisión Académica Programa de Doctorado en Materiales	

RESUMEN (en español)

Los cilindros de laminación dúplex fabricados mediante temple indefinido y doble colada son muy utilizados en cajas acabadoras de tren de bandas en caliente. Estos cilindros están compuestos por una capa externa de trabajo de fundición Ni-Hard atruchada y un núcleo de fundición gris nodular. Los principales motivos de fallo en servicio que se pueden dar son el desgaste, agrietamiento y desconchamiento de la capa de trabajo, o la rotura de la unión entre la capa de trabajo y el núcleo por una mala formación de la zona intermedia que se crea entre ellas. El primer fallo se ve influenciado en gran medida por la presencia de carburos y la continuidad de la red. El segundo se deriva del proceso de colada en el que se debe conseguir la fusión completa de la zona de la intercara, pero evitando una mezcla excesiva entre las dos capas y la formación de estructuras duras y frágiles.

Para realizar este estudio se utilizó el método de Diseño de Experimentos tomando como variables 6 parámetros metalúrgicos específicos de la fabricación de los cilindros, a saber, la temperatura líquidus, el porcentaje de silicio final presente en la aleación, el porcentaje final de Mg en la aleación, y la inoculación con diferentes cantidades de FeB, SiCaMn y FeSi-La. Para medir la mejoría o empeoramiento de la idoneidad de la aleación se tomaron respuestas sobre las propiedades del material, de los diferentes experimentos realizados, como la dureza o la resistencia al impacto y a la flexión, así como parámetros microestructurales como la fracción en volumen de precipitados o la morfología del grafito. Se obtuvieron aquellos factores que generaban un efecto sobre los valores de las respuestas y se analizó las modificaciones que producían, explicando la relación entre la mejora de las propiedades y el comportamiento en servicio de los cilindros.

RESUMEN (en Inglés)

Duplex rolling mill rolls are manufactured through indefinite chilling and double pouring are commonly used in the finishing stands of hot rolling mills. These rolls are made of an external working zone manufactured in Ni-hard white cast iron, and a core manufactured in Nodular cast iron. The main causes of service failure are wear, cracking and spalling of the working layer, or the break of the bond between the working layer and the core due to poor formation of the intermediate zone created between them. The first failure is largely influenced by the presence of carbides and the continuity of the carbide network. The second one derives from

the casting process, in which complete melting of the interlayer area must be achieved, but excessive mixing between the two layers and formation of hard and brittle structures must be avoided.

To carry out this study, the Design of Experiments method was used, taking as variables 6 metallurgical parameters specific to the manufacture of the cylinders, namely the liquidus temperature, the final percentage of Silicon present in the alloy, and the inoculation with different amounts of FeB, SiCaMn and FeSi-La. To measure the improvement or worsening of the alloy's suitability, responses on material properties, such as hardness, impact and flexural strength, as well as microstructural parameters such as precipitate volume fraction or graphite morphology, were taken from the different experiments carried out. Those factors that generated an effect on the response values were obtained and the modifications they produced were analysed, explaining the relationships between the improvement of the properties and the behaviour of the cylinders in service.

SR. PRESIDENTE DE LA COMISIÓN ACADÉMICA DEL PROGRAMA DE DOCTORADO EN MATERIALES

Agradecimientos

A José Florentino Álvarez Antolín, por toda la ayuda que me prestó durante la realización de esta tesis y la eterna paciencia que tuvo conmigo, al enseñarme todo lo necesario para poder llevar a cabo el trabajo de forma satisfactoria. A mi familia por estar siempre conmigo durante los mejores y los peores momentos a los que me tuve que enfrentar a lo largo de los años dedicados a este viaje.

A todos los que en algún momento participaron y ayudaron con la investigación.

Gracias

Índice

Resumen

Los cilindros de laminación dúplex fabricados mediante temple indefinido y doble colada son muy utilizados en cajas acabadoras de tren de bandas en caliente. Estos cilindros están compuestos por una capa externa de trabajo de fundición Ni-Hard atruchada y un núcleo de fundición gris nodular. Los principales motivos de fallo en servicio que se pueden dar son el agrietamiento y desconchamiento de la capa de trabajo, o la rotura de la unión entre la capa de trabajo y el núcleo por una mala formación de la zona intermedia que se crea entre ellas. El primer fallo se ve influenciado en gran medida por la presencia de carburos y la continuidad de la red. El segundo se deriva del proceso de colada en el que se debe conseguir la fusión completa de la zona de la intercara, pero evitando una mezcla excesiva entre las dos capas y la formación de estructuras duras y frágiles.

Para realizar este estudio se utilizó el método de Diseño de Experimentos tomando como variables 6 parámetros metalúrgicos específicos de la fabricación de los cilindros, a saber, la temperatura líquidus, el porcentaje de silicio final presente en la aleación, el porcentaje final de Mg en la aleación, y la inoculación con diferentes cantidades de FeB, SiCaMn y FeSi-La. Para medir la mejoría o empeoramiento de la idoneidad de la aleación se tomaron respuestas sobre las propiedades del material, de los diferentes experimentos realizados, como la dureza o la resistencia al impacto y a la flexión, así como parámetros microestructurales como la fracción en volumen de precipitados o la morfología del grafito. Se obtuvieron aquellos factores que generaban un efecto sobre los valores de las respuestas y se analizó las modificaciones que producían, explicando la relación entre la mejora de las propiedades y el comportamiento en servicio de los cilindros.

1. INTRODUCCIÓN

1.1. Conceptos generales de la laminación

El proceso de laminación, aun siendo desarrollado por primera vez en el siglo XVI, no fue predominante en la fabricación de piezas metálicas hasta la industrialización ocurrida durante el siglo XIX, comenzándose a laminar en primer lugar perfiles (railes, vigas, etc.) y, a partir de la década de los 30 productos planos.

La laminación es el proceso de conformado por deformación consistente en la reducción del espesor de una pieza aplicando fuerzas de compresión mediante cilindros. Este proceso es uno de los más importantes dentro del sector metalmecánico, estimándose que el 90% de la producción de piezas metálicas han sido sometidas, en algún momento del proceso productivo, a etapas de laminación.

En términos generales se pueden hacer diferentes distinciones a la hora de categorizar el proceso. Si tenemos en cuenta la temperatura a la que se realizan las pasadas de laminación tenemos laminación en caliente y laminación en frío; teniendo en cuenta al formato final de la pieza final se distinguen laminación plana y laminación de forma. [1]

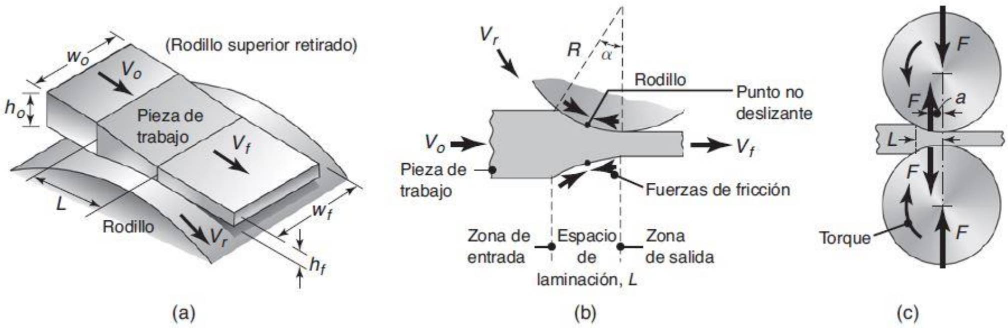

Figura 1.1 Esquema de laminación plana

Los avances principales que ocurrieron fueron sobre la disposición de los cilindros en los trenes de laminación y la fabricación de los cilindros (método y materiales usados).

En los cilindros de laminación se pueden distinguir tres zonas:

1. Zona de trabajo o tabla: Ocupa la mayor parte del cilindro de laminación, es la parte del cilindro en contacto con la pieza trabajada. Dependiendo del tipo de pieza a deformar la tabla puede ser lisa (productos planos) o tener mecanizada sobre ella unas estrías (productos largos y perfiles).

2. Cuello: parte intermedia de los cilindros que se encuentran alojadas en los cojinetes de la caja.

3. Trébedes: Extremos de los cilindros que se encuentran acoplados a la transmisión del motor que acciona el giro de los cilindros.

En cuanto a la disposición de los cilindros nos podemos encontrar, entre otras disposiciones, con cajas dúo, trio, cuatro, quinto, sexto, Sendzimir y cajas de laminación para productos largos.

Las cajas dúo están construidas por dos cilindros de trabajo, las cajas trío están formadas por tres cilindros de trabajo en las que se pueden realizar dos pasadas de laminación al mismo tiempo. Las cajas cuatro poseen dos cilindros de trabajo y dos cilindros de apoyo. Las cajas quinto son cajas trio a las que se les han añadido dos cilindros de apoyo. Las cajas sexto pueden ser cajas dúo con dos cilindros de apoyo o cajas cuatro con un cilindro intermedio que pasaría a ser el cilindro motor. Cajas con múltiples cilindro de apoyo y cilindros intermedios como la caja tipo Sendzimir. Y, por último, cajas universales que además de los cilindros de trabajo horizontales poseen cilindros canteadores verticales.

De entre todas estas configuraciones, las cajas dúo y cuatro son capaces de trabajar en régimen tanto de un solo sentido de avance como en régimen reversible.

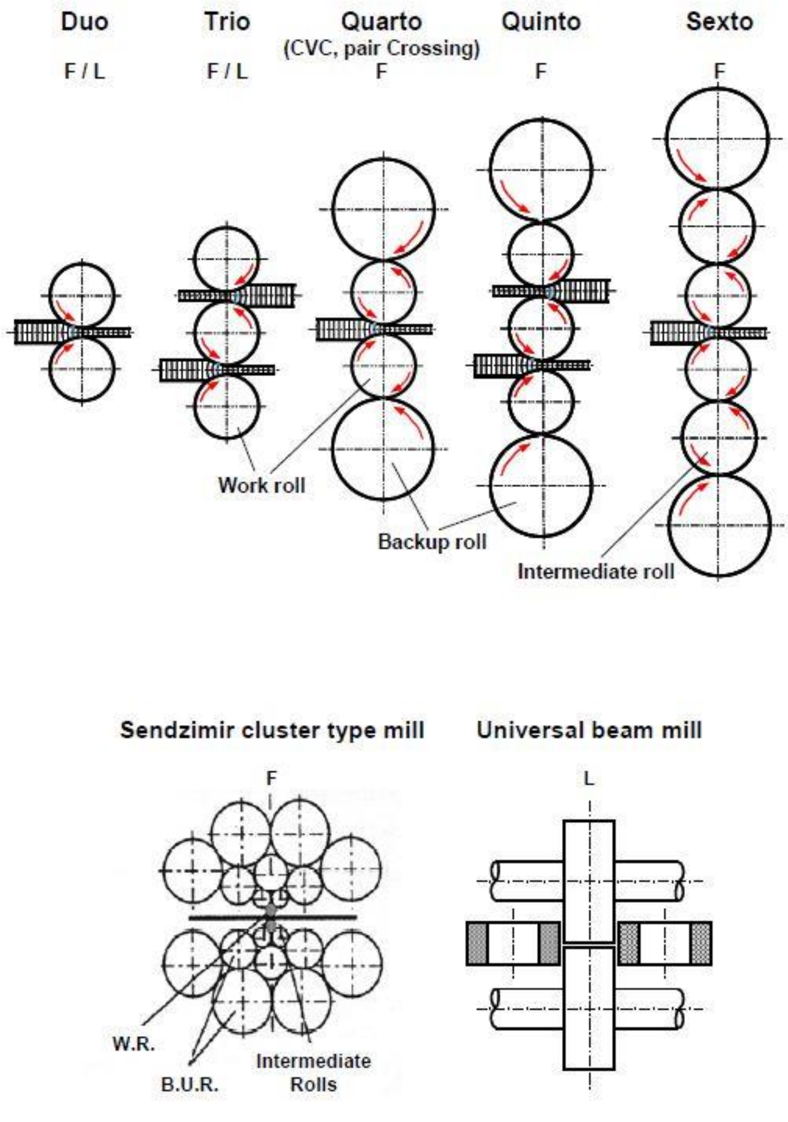

Figura 1.2 Disposiciones posibles de cajas de laminación

Los trenes de laminación son el conjunto de cajas de laminación que realizan el proceso de laminación completo. Las cajas están dispuestas en serie, de tal forma que la pieza laminada está siendo trabajada por al menos dos de las cajas.

Se pueden clasificar los trenes de laminación por el producto laminado:

1. Trenes desbastadores: Se laminan los productos obtenidos por colada continua o colada en lingotera. Se obtienen grandes reducciones de espesor para obtener productos conocidos como desbastes. Si el producto inicial es cuadrado se tienen trenes de “blooming” en los que los tochos se transforman en palanquilla. Si el producto inicial es plano se tienen trenes de “slabbing” obteniéndose un producto plano conocido como “slab”.

2. Trenes de planos: Utilizan el producto obtenido de los trenes de “slabbing” para obtener planchón o bobinas de chapa más fina. Se pueden tener tres tipos de trenes planos, trenes de planchas, trenes continuos para chapa fina y trenes semicontinuos, también para la obtención de chapa fina.

3. Trenes de largos: En estos trenes se utiliza la palanquilla para obtener perfiles, barras, carril u otros productos largos. Se utilizan cilindros acanalados con la forma pertinente para el producto a obtener.

4. Trenes especiales: Se utilizan para la laminación de productos concretos como tubos, laminación de llantas de vehículos, anillos, etc. Dentro de esta categoría se encontrarían los trenes universales, que se utilizan para la laminación de perfiles estructurales, como por ejemplo vigas. [2]

En cuanto a los materiales utilizados nos encontramos con cilindros fabricados en fundición gris y acero forjado a finales del siglo XIX y principios del siglo XX. A partir de los años 30 del siglo XX se comienza a utilizar cilindros fabricados mediante ICDP (Indefinite Chill Double Poured) en los trenes de laminación en caliente, siendo posteriormente modificados con carburos en los años 90 del siglo XX. En la década de los 50 se desarrolla la fundición nodular y se introdujo como tecnología para la fabricación de cilindros de laminación. Posteriormente, a mediados de los años 80, se introdujeron las calidades de acero rápido (HSS) y semi-rápido a la fabricación de cilindros, llevando asociado una modificación sustancial de las condiciones de laminación con ellos. Estas calidades de material son utilizadas para laminación de forma general, sin embargo, para aplicaciones más específicas se utilizan calidades especiales como por ejemplo cilindros de carburos sinterizados o cilindros de material cerámico.

La tecnología que rodea el proceso de laminación ha evolucionado rápidamente en el pasado reciente, manteniéndose los rodillos como la parte crítica del proceso.[3]

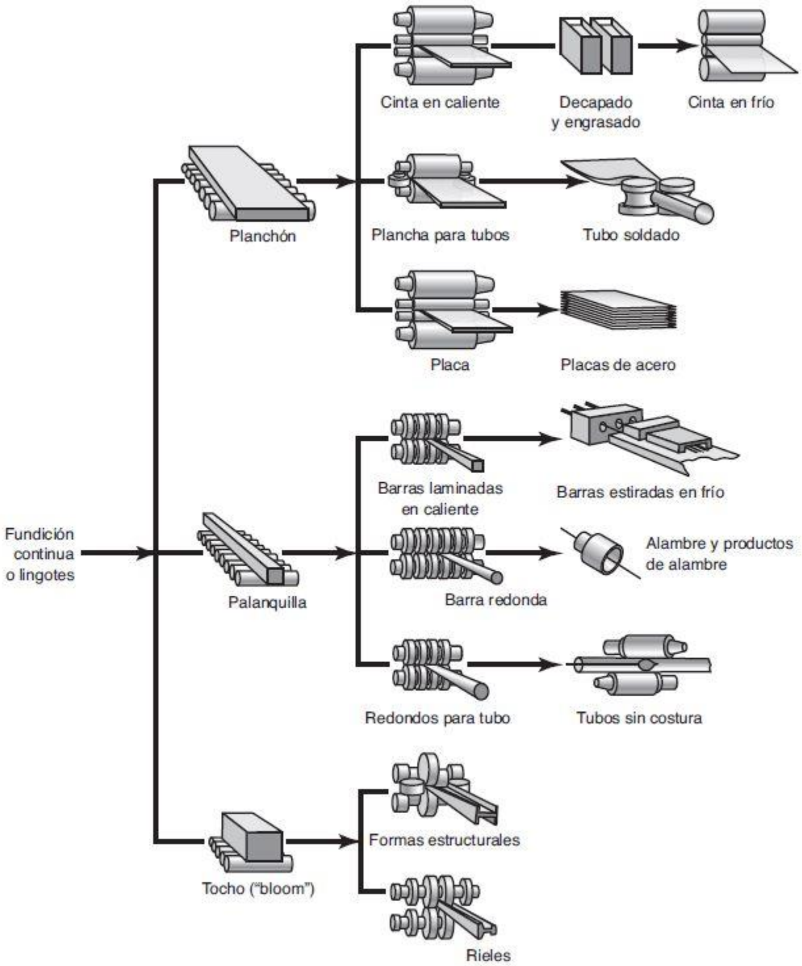

Figura 1.3 Formatos de productos laminados [1]

1.2. Conceptos generales de la deformación en caliente

Las deformaciones en caliente se realizan a temperaturas lo suficientemente altas (Temperatura de trabajo > 0.75 Temperatura de fusión) como para que, al mismo tiempo, coexistan fenómenos de endurecimiento por deformación y ablandamiento del material deformado. Ocurren simultáneamente la conferencia de acritud al material y la restauración o recristalización a la temperatura de deformación dependiendo de la energía de los defectos de apilamiento de la aleación deformada. Los metales con alta energía de defectos de apilamiento como los aluminios sufren un proceso de restauración dinámica seguido de otro proceso de restauración estática después de haber sufrido la reducción de espesor. Por el contrario, los metales de baja energía de defectos de apilamiento, como por ejemplo los aceros al carbono austenizados, sufren un proceso de restauración dinámica durante el deformado y un proceso de recristalización estática después de haber sufrido la reducción de espesor.

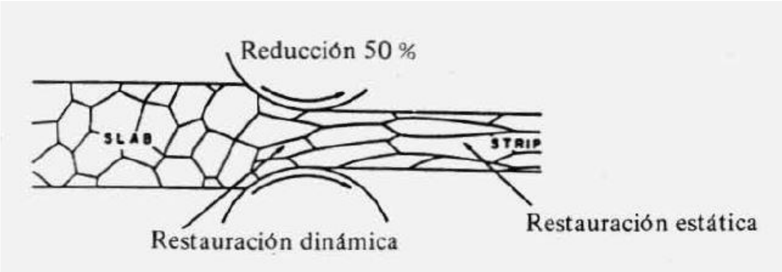

Figura 1.4 Esquema de laminación de aleaciones de alta energía de defectos de apilamiento

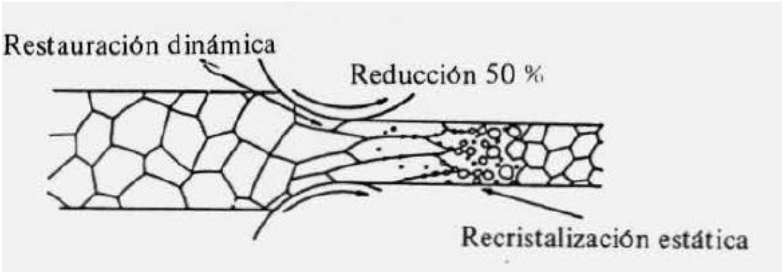

Figura 1.5 Esquema de laminación de aleaciones de baja energía de defectos de apilamiento

De forma general se alcanza un equilibrio entre el endurecimiento por deformación y los mecanismos de ablandamiento señalados anteriormente lo que conlleva la posibilidad de obtener materiales que son deformados sin la introducción de acritud, incluso pudiéndose reducir la tensión necesaria si se produce el fenómeno de la recristalización dinámica.

Las piezas en estado de bruto de moldeo poseen heterogeneidades físicas, estructuras no homogéneas, posibles defectos como sopladuras o rechupes, así como heterogeneidades químicas. La deformación en caliente en general y, más en concreto, en el caso de productos largos o planos, el proceso de laminación permite eliminar en gran medida estas heterogeneidades y defectos. El aplastamiento de granos dendríticos permite la homogeneización de la estructura. Además, el proceso de recristalización de la estructura, si los defectos internos tienen las superficies libres y limpias son capaces de desaparecer, obteniéndose una pieza libre de defectos. [4]

Esto se puede comprobar con ensayos de compresión uniaxial en caliente, obteniéndose a partir de estos las curvas de fluencia de los materiales ensayados. En estas curvas se pueden distinguir tres fases del proceso, una primera fase de endurecimiento en la que la restauración/recristalización no ha comenzado a actuar, la segunda fase o fase de transición en la que comienza a surtir efecto los fenómenos de ablandamiento y la tercera fase o fase de estabilidad en la que la tensión verdadera permanece constante. Se pueden distinguir tres tipos de comportamientos en función del material ensayado y de la velocidad de deformación aplicada [5]:

1. Los materiales en los que solo tiene efecto la restauración dinámica
2. Los materiales en los que la caída de la tensión en la fase de transición verdadera debida a la recristalización dinámica se produce de forma continua.
3. Los materiales en los que la caída de la tensión verdadera en la fase de transición se produce de forma oscilatoria.

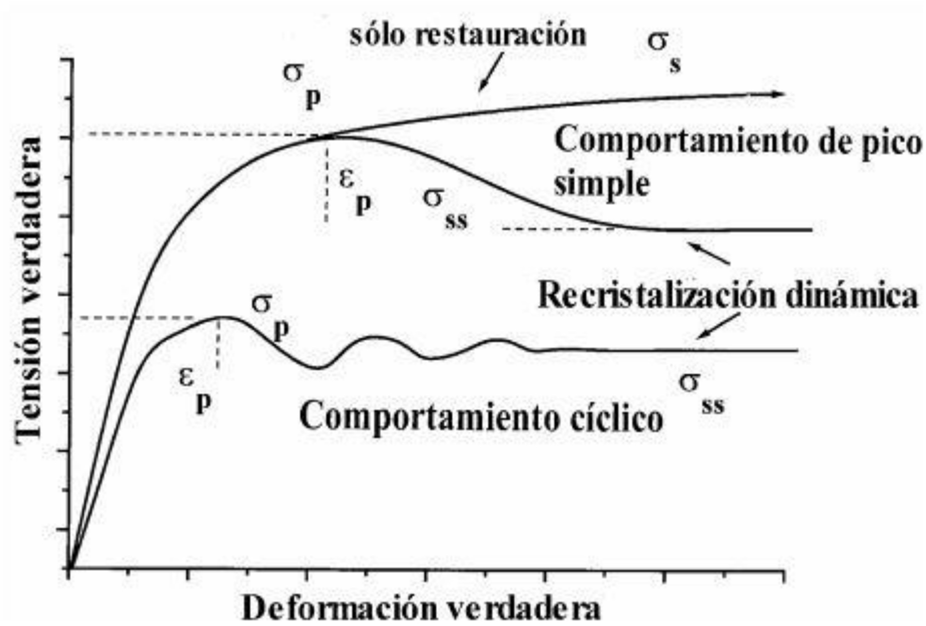

Figura 1.6 Comportamiento de diferentes materiales frente a deformaciones en caliente

En el caso de la laminación en caliente primero se debe aumentar la temperatura de la pieza a trabajar hasta; tomando como ejemplo la laminación de acero, los 1250ºC, realizándose las pasadas de laminación requeridas inmediatamente después de alcanzar dicha temperatura. Los cilindros de laminación alcanzarán una temperatura de en torno a los 500ºC y serán enfriados mediante duchas de agua fría alcanzando los 80ºC tras la salida del material laminado de la caja de laminación. Este gradiente térmico generado en el cilindro provoca que tenga que soportar ciclos de fatiga térmica. [6]

Este ciclo térmico genera en el cilindro una expansión térmica opuesta a las fuerzas de laminación, generándose en el cilindro ciclos de esfuerzos mecánicos y térmicos complementarios que suponen que la vida útil de los cilindros se vea influenciada por el desgaste, y por el comportamiento de los cilindros frente a fatiga producida por los ciclos de tensiones debidas a la temperatura y las tensiones mecánicas. [7-9]

1.3. Tren de bandas en caliente

El tren de bandas en caliente es la instalación que transforma los “slabs” o planchón en bobinas de unas dimensiones determinadas. Generalmente existen dos disposiciones, trenes semicontinuos o trenes continuos. El primero está formado por una caja cuatro reversible que realiza las pasadas de desbaste y un conjunto de cajas acabadoras en serie. El segundo está formado por varias cajas en serie que realizan tanto las funciones de desbaste, las primeras cajas del conjunto, y las funciones de acabado, el segundo conjunto de cajas. En los trenes en continuo el material está siendo trabajado por varias cajas a la vez.

Así una configuración típica de un tren de bandas en caliente estaría formada por:

1. Zona de hornos de recalentamiento
2. Zona de desbastes
3. Zona de acabado

4. Zona de enfriamiento
5. Zona de bobinado

1.3.1. Zona de hornos de recalentamiento

Para realizar laminación en caliente se requiere que las piezas se encuentren a una temperatura mayor a la de recristalización del material. Para ello se ha de calentar el material antes de realizar el proceso de laminación. Con este fin, antes de la entrada al tren de desbaste se hace pasar el producto de partida por hornos que los calientan hasta la temperatura de trabajo. El horno más utilizado es el denominado horno de vigas galopantes, aunque también se pueden utilizar hornos de fosa, hornos de inducción, etc.

Para el tren de bandas en caliente, es recomendable que los hornos utilizados sean continuos con el objetivo de la realización del proceso de laminación sin interrupción. Es por esto que el horno de vigas galopantes sea el elegido actualmente.

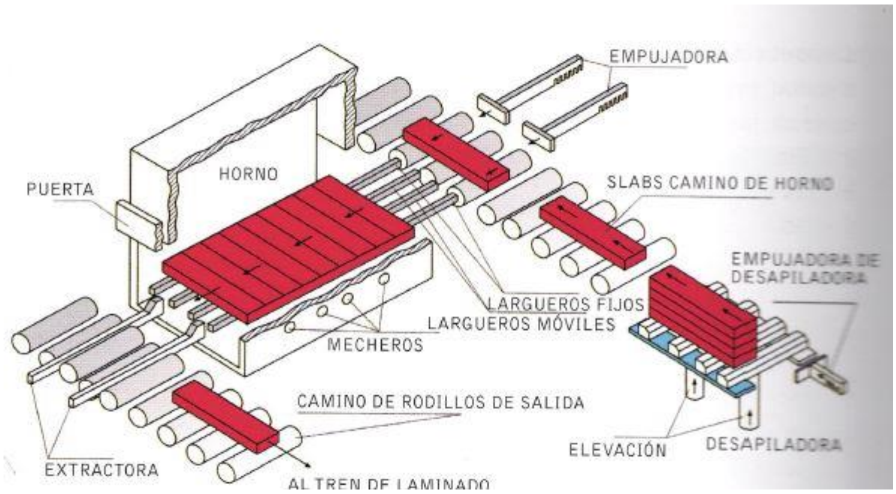

Figura 1.7 Esquema horno de vías galopantes

1.3.2. Zona de desbastes

Esta zona se encuentra entre la zona de hornos y la zona de acabado. En esta zona se persiguen dos objetivos, el descascarillado de las piezas salidas del horno y la reducción del espesor de la pieza.

El descascarillado se realiza mediante la rotura de las capas de cascarilla utilizando rompedores verticales, cilindros canteadores verticales, que además le dan a la pieza el ancho óptimo para la entrada al tren desbastador. Una vez se haya roto la cascarilla se ha de desprender utilizando, de forma general, chorros de agua a presión.

Una vez descascarillado se hace pasar por una caja cuatro reversible, con cilindros canteadores a la entrada y a la salida, transformando los planchones en piezas para ser laminados en las cajas acabadoras.

1.3.3. Zona de acabado

Se encuentra después de las cajas de desbaste y comprende hasta las mesas de enfriamiento.

Primero se realiza el despuntado, es decir, se cortan los extremos del planchón ya desbastado. Esto puede realizarse de forma manual, automática u optimizada.

1. Manual: Se elige la distancia a cortar en función del planchón.
2. Automática: El corte se realiza con unas distancias predeterminadas.
3. Optimizada: La cantidad cortada se escoge atendiendo a cálculos

Los trenes acabadores están formados por cajas cuatro, reduciéndose el espesor de la chapa hasta espesores entre 20 mm y 1.5 mm. Esto implica que la velocidad de la chapa a lo largo del tren va aumentando conforme se va reduciendo el espesor.

Las partes del tren acabador, en la dirección del avance de la plancha es:

1. Sistema de descascarillado
2. Guías laterales, que mantienen centradas las planchas a la entrada de la caja.
3. Sistema de refrigeración de los cilindros
4. Reguladores de lazo: Cilindros basculantes que mantienen la tensión de la chapa entre cajas de laminación.
5. Sistemas de refrigeración de la chapa. Refrigerando con cortinas de agua se consigue evitar la formación de cascarilla que puede generar daños en los cilindros de trabajo.
6. Sistemas de medición de la chapa a la salida de la última caja.
7. Sistemas de inspección de calidad.

1.3.4. Zona de enfriamiento

Están situadas a la salida de la última caja del tren de acabado. Es esta zona se reduce la temperatura de la chapa ya laminada hasta la temperatura de bobinado. El sistema de refrigeración empleado es el mojado de la piezas con cortinas de agua. El enfriamiento se controla mediante la regulación del caudal de agua.

1.3.5. Zona de bobinado

Una vez se tiene la chapa enfriada se debe de embobinar, de tal forma que no se generen defectos en la chapa. Para ello se debe regular al velocidad de enhebrado y los elementos de la bobinadora deben configurarse de forma correcta.

La bobinadora consta de los siguiente elementos:

1. Guías de entrada para posicionar la chapa
2. Rodillo pisón: mantiene la tensión de la chapa constante.

3. Rodillos arrastradores: le dan el avance de la chapa hacia el mandril de la bobinadora.
4. Mandril: Sirve tanto de eje de la bobina a la vez que realiza el bobinado de la chapa. Permite sujetar la chapa expandiéndose para realizar el bobinado y, para extraer la bobina, se contrae. La velocidad de giro depende de la velocidad de salida del tren acabador.
5. Rodillos de bloqueo: Sujetan las primeras espiras de la bobina al mandril y las últimas espiras al terminar el bobinado.
6. Carro extractor: Recoge las bobinas terminadas y las deposita en la cinta transportadora que llevará las bobinas a almacenaje.
7. Flejadoras: Realizan un flejado circunferencial para evitar el desbobinado de la chapa durante el transporte.
8. Salida de la zona de bobinado: Se voltean las bobinas de tal forma que el eje quede vertical y se depositan sobre una transportador. En el recorrido de la cinta transportadora se controla el peso de la bobina, se realiza el marcado, se prensa la bobina y se realiza un proceso de detección de telescopidad (comprobar que la bobina no se deshaga por la parte del centro). [10]

1.4. Daños producidos sobre los cilindros

Durante el proceso de laminación, entendido como el ciclo completo de pasada de laminación y enfriamiento del cilindro, se pueden generar sobre el cilindro daños que requieran de parada de producción para la sustitución de la pieza dañada o su reparación. Se puede hacer una distinción entre dos tipos de daños, fallos catastróficos y daño superficial.

Entre los fallos catastróficos nos podemos encontrar, por ejemplo, la rotura de los cuellos del cilindro, agrietamientos del cilindro o desconchamientos. Estos fallos catastróficos pueden ser generados por choque térmico, sobrecarga de los cuellos del cilindro, o sobrecargas puntuales en la tabla del cilindro.

El daño superficial se produce por diferentes factores como, por ejemplo, fenómenos de desgaste o fenómenos de fatiga. Esto se debe, entre otros factores, a la oxidación de la superficie de esta por la conjunción de las altas temperaturas a las que se realiza la laminación y la presencia de aire, generándose óxidos de hierro en la laminación de aceros. Estos óxidos son muy fácilmente desprendibles y extremadamente duros produciendo fenómenos de abrasión en 3 cuerpos dañando la superficie de la tabla.

Otro de los problemas a los que pueden estar sometidos los cilindros de laminación en caliente es la oxidación de la capa de trabajo. Debido a la utilización de agua como medio de enfriamiento de los cilindros después de cada pasada se genera una atmósfera de vapor de agua que es capaz de generar capas de oxido en la superficie del cilindro, produciendo daños en la superficie de la pieza laminada, siendo los óxidos más comunes la hematita y la magnetita. [11]

Por otro lado, la tabla del cilindro puede estar sometida a procesos de corrosión durante el proceso de enfriado con agua, generándose picaduras que deterioran significativamente la superficie de trabajo del cilindro.[12]

Dentro de los daños producidos por el choque térmico se tiene la generación de grietas en la superficie del cilindro. Estas grietas pueden llegar a ser peligrosas si se propagan los suficiente pudiendo llegar a generar roturas del cilindro y desconchamientos. Estas grietas se generan principalmente en los carburos precipitados y tienen a crecer siguiendo la red de carburos y el grafito, siendo más acentuado este crecimiento cuando el grafito tiene morfología laminar. Así mismo, mayores gradientes de temperatura generan mayores densidades de grietas. Esto se puede solucionar mediante el refinamiento de los carburos, la rotura de la red de carburos, incrementando la nodularidad del grafito y utilizando tratamientos térmicos adecuados. [13]

Unido a las grietas generadas por choque térmico, en ocasiones la presión sufrida por los cilindros, que depende de factores geométricos del proceso de laminación, puede ser lo suficientemente grande como para producir el aplastamiento de algún carburo, generando grietas y pudiendo ser propagadas a través de la red de carburos [14], Esto se ve fuertemente influenciado por las características microestructurales de la capa de trabajo, especialmente por la presencia de carburos en ella. [15,8]

Los daños por fatiga, si no se tiene un control estricto del estado del cilindro, pueden generar fallos catastróficos importantes. Lo que en un principio son pequeñas grietas formadas por diferentes motivos, como, por ejemplo, sobrecargas localizadas en la tabla del cilindro, son capaces de propagarse con las pasadas de laminación hasta generar desconchamientos grandes. Uno de los modos en los que se puede dar la rotura del cilindro es la denominada “ribbon fatigue spalling” en el que las grietas se propagan circunferencialmente alrededor de la tabla del cilindro produciendo al final desprendimientos grandes de material. [16]

Es, el fenómeno de desgaste, uno de los daños más importantes que pueden sufrir piezas en contacto con otras piezas, por lo que ha sido estudiado de forma exhaustiva, con el fin de minimizar los paros en la producción.

Sin embargo, este fenómeno es extremadamente complejo debido a la gran multitud de variables que gobiernan el comportamiento de un material dado. Entre otras están:

- El material y sus propiedades intrínsecas
- El material con el que se encuentra en contacto
- Las condiciones del contacto entre los cuerpos
- La posible existencia de agentes externos a los cuerpos en contacto.

De entre estos factores el más sencillo de estudiar es el primero, el material utilizado y sus propiedades, y más concretamente como afecta la composición de un material frente al comportamiento al desgaste de este.

En términos generales se tiene que un mayor contenido de aleantes produce un material más resistente ante fenómenos de desgaste y más concretamente se tiene que para un mismo material de partida se tiene:

- Para un mismo valor de dureza la presencia de elementos de aleación mejora el comportamiento frente al desgaste.
- Altos tenores de carbono y aleantes producen un aumento de la resistencia al desgaste a menores durezas que aleaciones con bajos tenores de aleantes.

- El potencial de una determinada aleación a tener una buena resistencia al desgates aumenta con los tenores de aleantes.

Todo ello se resume en el denominado diagrama de Khruschov en el que se representa la resistencia relativa al desgaste frente a la dureza del material para aleaciones de base hierro con diferentes aleantes y cantidades de carbono. [17, 18]

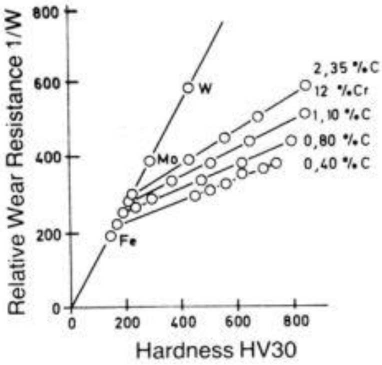

Figura 1.8 Diagrama de Khruschov

Es importante señalar que en sí misma la dureza no es un parámetro que determine la resistencia al desgaste de una determinada aleación. El contenido de elementos carburígenos precipitados en forma de carburos y la microestructura del material son extremadamente importantes a la hora de mejorar la resistencia al desgaste del material de tal forma que para una misma macrodureza, la resistencia al desgaste aumenta con el contenido en carburos del material. Del mismo modo se puede estimar la resistencia al desgaste con el parámetro "alloy equivalent" de tal forma que cuanto mayor sea este mayor será la resistencia al desgaste. [19, 20]

Además de factores microestructurales y composicionales de la capa de trabajo, el desgaste de un cilindro de laminación se ve influenciado principalmente por la temperatura de trabajo, la velocidad de deslizamiento y de la carga aplicada. [21]

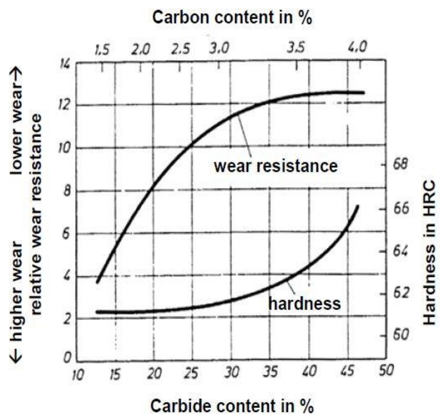

Figura 1.9 Relación entre contenido en carbono y carburos y la resistencia al desgaste relativa

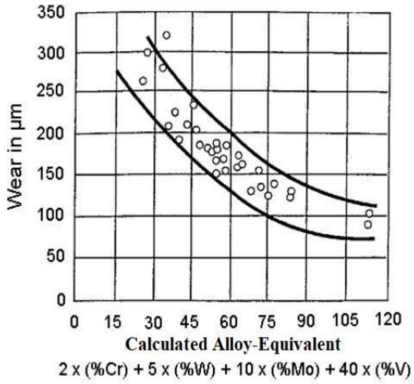

Figura 1.10 Relación entre el desgaste absoluto y el "alloy equivalent"

1.5. Cilindros de laminación ICDP

En cilindros dúplex fabricados mediante la técnica ICDP (Indefinite Chill Double Poured) se ha evolucionado en el material de la capa de trabajo.

Están fabricados en dos capas diferenciadas, una capa exterior que debe soportar los esfuerzos y el desgaste durante las pasadas de laminación, generalmente se utilizan calidades de material duro (Aceros de herramientas, fundiciones blancas aleadas) y un núcleo que debe absorber y soportar los esfuerzos que le transmite la capa de trabajo, fabricada en materiales tenaces (fundiciones grises de matriz perlítica).

La calificación de “Indefinite” hace referencia al “atruchamiento” de la fundición blanca, es decir, la presencia de carbono tanto en forma de grafito, así como la formando parte de carburos metálicos.[22] Dicho grafito cumple una doble función durante el uso de los cilindros, como lubricante seco, desprendiéndose por el funcionamiento normal del proceso, reduciendo el coeficiente de fricción entre cilindro y pieza laminada; así como mejorando la conductividad térmica del cilindro, siendo capaz de evacuar más calor.[23-25]

Se tiene dos grandes grupos de cilindros ICDP los cilindros convencionales y los cilindros denominados “carbide enhanced”.

Los cilindros convencionales poseen una microestructura formada por grafito libre, con alta tendencia del grafito hacia morfologías laminares, una red carburos duros pero muy frágiles y una matriz de austenita transformada parcialmente en bainita o martensita. Al mismo tiempo se observa una alta caída de la dureza cuanto más cerca de la transición entre capa más externa y núcleo, esto es debido a una baja penetración del temple.

Estas calidades de cilindros fueron mejoradas en los años 90 con el desarrollo de los cilindros CE ICDP o “carbide enhanced Indefinite Chill Double Poured”. Este tipo de cilindros utiliza como material base de la capa de trabajo los mismos materiales base que los convencionales, sin embargo, se alean con elementos que afinan la microestructura tanto en la precipitación de carburos más duros que los cementíticos y distribuidos de forma homogénea por todo el volumen del cilindro, como en el afino de la precipitación del grafito, obteniéndose partículas más compactas. Además, la introducción de esos elementos de aleación permite la penetración del temple en mayor medida, no observándose esa reducción de la dureza con el espesor del cilindro. [26]

Para fabricar estos cilindros se realiza mediante colada centrífuga vertical constando la operación de tres etapas bien diferenciadas. En la primera etapa se hace la colada de la capa de trabajo. Una vez solidificada esta capa se cuela una parte del material del núcleo (también colada centrífuga) de tal forma que se consiga una buena interfase entre capa de trabajo y núcleo. Para conseguirlo la zona más interna de la capa de trabajo se vuelve a fundir y se mezcla con esa primera colada del núcleo. Una vez se ha solidificado esa capa intermedia se cuela, por gravedad y en estático, el resto del núcleo. El desmoldeo se produce 5 días después de la solidificación, se realiza una austenización y temple al aire para posteriormente realizar un doble revenido, obteniéndose así el producto finalizado. Estos cilindros dúplex han de ser fabricados con sumo cuidado para conseguir una unión entre capa de trabajo y núcleo satisfactoria. Durante el proceso de fabricación de los cilindros ocurrirá, inevitablemente, una mezcla entre los materiales de la capa de trabajo y el núcleo, contaminándose la unión con elementos de aleación de la capa de trabajo como el Cr, formándose un material cuya microestructura está compuesta de una fundición gris con grafito esferoidal, junto con presencia de ledeburita. Así mismo durante el enfriamiento lento de los cilindros se pueden producir fenómenos de difusión entre núcleo y capa de trabajo, lo que puede llevar a la formación de microestructuras frágiles. Así mismo la presencia de inclusiones y microcavidades afectan de forma negativa a la calidad de la unión, pudiendo llegar a producir desconchamientos en el cilindro. [27-35]

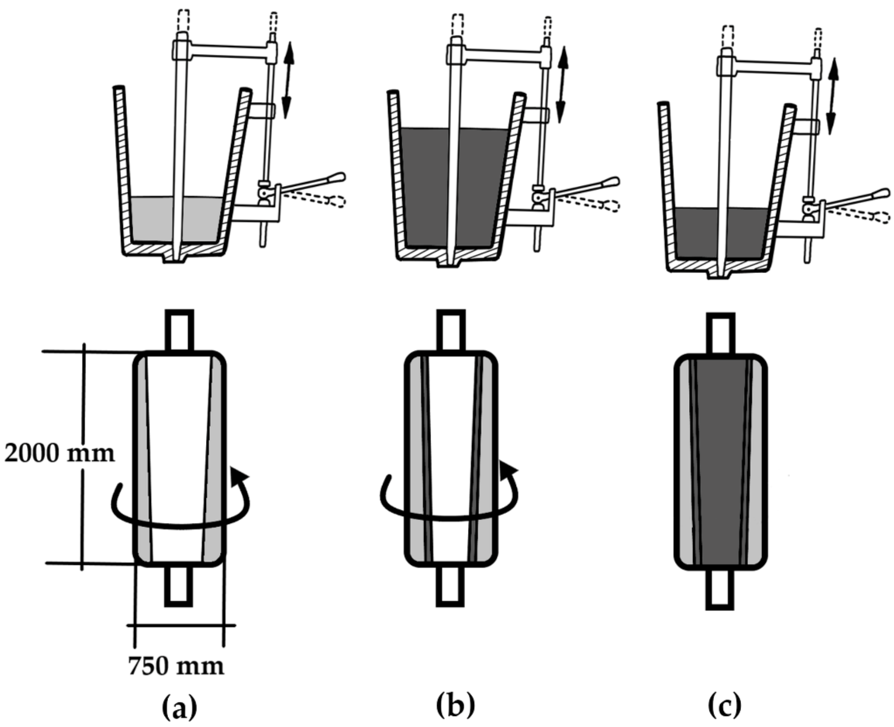

Figura 1.11 Esquema de colada de los cilindros ICDP a) colada de la capa de trabajo, b) colada de la interfase entre capa de trabajo y núcleo y c) colada del núcleo

1.6. Procesos de fabricación de cilindros de laminación

El desarrollo de procesos de fabricación de los cilindros ha sido una constante comenzó a finales de los años 80, al mismo tiempo que nuevos métodos de fabricación se comenzaron a utilizar VSC, HIP, ESR, CPC. [36]

El método VSC consiste en la colada centrífuga vertical de los cilindros. Es el mismo método señalado en el apartado anterior. Este método es uno de los más utilizados en la fabricación de cilindros HSS y ICDP.

El método CPC consisten en la deposición del material sobre el núcleo, previamente recubierto con fundentes, calentado por inducción y realizándose la colada del material de la capa de trabajo dentro de un molde de cobre. Una pequeña capa del material del núcleo debe de ser refundida para poder obtener una unión entre capa de trabajo y núcleo sana.

El método ESR es extremadamente similar al CPC con la diferencia de que el calentamiento se produce mediante electroescoria y el núcleo no necesita ser recubierto. El núcleo se introduce de forma que se induce un giro y se funde una capa fina del núcleo para asegurar la unión entre capas.

El método HIP se utiliza para la sinterización de cilindros fabricados mediante pulvimetalurgia. Aunque se utilice ya para cilindros de tamaño pequeño, el escalado de instalaciones para la fabricación de cilindros de tamaño estándar so es viable económicamente. El producto obtenido mediante pulvimetalurgia posee excelentes propiedades, una unión entre capas sana y una microestructura de grano extremadamente fino.

Es con el método CPC como se fabrican estos cilindros obteniéndose una capa de trabajo de acero altamente aleada, con una microestructura de grano fino por la rápida solidificación de este proceso, además de obtenerse núcleos de los cilindros altamente resistentes. Estos cilindros poseen carburos muy duros, finos y dispersos, junto con una matriz que posee una alta dureza trabajando a altas temperaturas. [37]

1.6.1. Métodos de fabricación avanzados

Además de los métodos anteriormente señalados se pueden encontrar procesos de fabricación de cilindros más avanzados: el método Osprey y el método CCR.

El método Osprey, desarrollado en los años 70, consiste en la deposición del material de la capa de trabajo mediante atomización del metal fundido por la aplicación de un gas inerte comprimido. Este gas junto con el metal líquido atomizado produce una niebla del metal líquido que se deposita sobre el sustrato que será el núcleo del cilindro. La solidificación del metal ocurre en dos fases, la primera por convección durante el tiempo de vuelo y la segunda por conducción en el momento del impacto.

Es necesario controlar de forma precisa la superficie de adherencia del sustrato, además del tamaño y el enfriamiento de las partículas metálicas. Para conseguir esto se tienen que controlar entre otros parámetros: La temperatura de fusión, el flujo de metal líquido a través del atomizador o la presión del gas.

La deposición puede realizarse de dos formas, en estado particulado o no particulado. En el primer caso la deposición se realiza con las partículas en estado sólido y se genera una capa heterogénea, siendo este caso no deseable. El caso más deseable ocurre cuando las gotas están parcialmente solidificadas generándose una capa densa, libre de segregación y de grano extremadamente fino.

Este proceso de fabricación ha encontrado su nicho de mercado en las fabricaciones de aleaciones in situ, la fabricación de piezas en materiales reforzados y la fabricación de materiales compuestos. [38]

El método CCR llamado así por sus siglas en inglés "Complex Carbide Reinforcement". Este método consiste en la adición de partículas de carburos sólidos al caldo de colada. Estas partículas se han recubierto de un metal de tal forma que pueden ser mojadas por el metal fundido que va a ser colado. De esta forma se pueden conseguir distribuciones uniformes de las partículas, evitando fenómenos de segregación.

Esta tecnología puede ser aplicada a métodos tradicionales de colada, resultando muy rentable económicamente por la posibilidad de usar instalaciones ya existentes para la fabricación de cilindros de laminación, así como las altas velocidades de producción que se pueden alcanzar en comparación con métodos como el Osprey. [39]

1.7. Fundición Ni-Hard atruchada

La elección de un material que sea capaz de resistir al desgaste por abrasión, en muchas ocasiones responde a motivaciones económicas que técnicas, siempre y cuando solo se requiera resistencia al desgaste. Toda pieza sometida a procesos de desgaste requiere de una sustitución periódica. Para esa sustitución podría, por ejemplo, utilizarse un material como una fundición blanca no aleada en cambio de una función altamente aleada, aunque sea necesario cambiarla más a menudo.

Una posibilidad para solucionar el problema de la frecuencia de la sustitución de las piezas es la utilización de materiales en los que la austenita haya sido transformada en martensita. El uso de fundiciones hipoeutécticas cuyo constituyente disperso sea martensita aumenta de forma considerable el comportamiento frente al desgaste. Sin embargo, es la transformación la que genera problemas debido a la imposibilidad de obtener esa microestructura sin que se produzcan agrietamiento o rotura de la pieza realizándose un temple en agua. Para evitar ese problema, se puede conseguir la transformación con un simple temple al aire utilizando aleaciones en las que la austenita esté enriquecida con elementos de aleación, como las fundiciones denominadas Ni-Hard.

La aleación utilizada para la capa de trabajo, como ya se ha dicho, es una fundición blanca hipoeutéctica Ni-Hard atruchada, aleada con molibdeno, cromo, niobio y magnesio.

La presencia del Cr, Ni y Mo le confiere una alta templabilidad permitiendo la transformación parcial de la austenita en martensita, tanto eutéctica como pro-eutéctica, durante la solidificación. Esa martensita será el constituyente disperso mientras que la matriz será ladeburítica, formada por la austenita eutéctica y carburos mixtos del tipo M3C. Además, se tendrá disperso grafito esferoidal que se forma por la presencia de líquido de composición eutéctica residual durante el proceso de solidificación.

Aun teniendo una alta templabilidad, la baja severidad del medio de temple y el efecto estabilizador de la austenita de los elementos de aleación presentes en este tipo de aleaciones favorecen la presencia de austenita retenida a temperatura ambiente. Esto es desfavorable para la resistencia de la pieza final a la abrasión y al desgaste, siendo uno de los principales usos de esta aleación la fabricación de piezas que trabajan en ambientes de alto desgaste. Por ello se han desarrollado dos estrategias para evitar la presencia de dicha austenita retenida. La primera de ellas es la realización de temples bajo cero, con temperaturas entre los -50ºC y -80ºC. Esta estrategia es solamente viable si las condiciones económicas son propicias para ello

El segundo método, y el utilizado para la fabricación de las piezas usadas en esta tesis, es la realización de revenidos después del temple. Los revenidos desestabilizan la austenita retenida durante el calentamiento, produciendo la precipitación de carburos, reduciéndose la cantidad de carbono disuelto en la austenita. Esa austenita empobrecida se trasformará finalmente en martensita durante el enfriamiento, obteniéndose un material más duradero frente a procesos de desgaste.

Los principales aleantes de las aleaciones Ni-Hard son el cromo, el níquel y el molibdeno.

El cromo minimiza la formación de grafito, ya que es un elemento carburígeno, formando carburos del tipo Kc. Es precisamente esa capacidad para precipitar en forma de carburos lo que reduce la mejora en la templabilidad, al encontrarse precipitado en vez de en solución sólida, en comparación con otros elementos de aleación como el níquel. Con porcentajes de cromo menores al 15% los carburos formados son del tipo M3C con una dureza del 1200HV.

El níquel, al contrario que el cromo, es un elemento grafitizante, sin embargo, los tenores de níquel que estas aleaciones tienen comúnmente son menores al 5% viéndose este efecto minimizado hasta no ser relevante. Por el contrario, sí que aumenta la templabilidad de la aleación.

Por último, el molibdeno tiene una funcionalidad similar a la del cromo. Se trata de un elemento altamente carburígeno pero que en los tenores que este tipo de aleaciones poseen éste se mantiene en solución sólida mejorando la templabilidad, sin modificar sensiblemente la temperatura de fin de transformación martensítica Ms. [40]

Adicionalmente el Molibdeno en porcentajes cercanos al 1% hace la función de afinador de los carburos y mejora la resistencia al desgaste de la aleación. [41]

Esta aleación, utilizada para la fabricación de cilindros de laminación dúplex requiere de una alta resistencia al desgaste, para ello se puede inocular con Niobio, un elemento altamente carburígeno, produce la precipitación de carburos de estequiometría MC extremadamente duros, en torno a los 2400 HV. Estos carburos aumentan de forma notable la resistencia al impacto y al desgaste de la capa de trabajo, al mismo tiempo que pueden favorecer la nucleación de las partículas de grafito. [42-46]

Para mejorar la resistencia al desgaste se pueden utilizar aleaciones con B como aleantes. Este elemento tiene el efecto de incrementar el porcentaje de carburos precipitados con el inconveniente de afectar negativamente a la resistencia a la flexión de la aleación final [46]. Para contrarrestar ese efecto de reducción de la resistencia mecánica del material se puede inocular con SiCa, reduciéndose el tamaño de grano de la austenita primaria, así como promoviendo la discontinuidad de la red de carburos. [47]

Por tanto, la microestructura de la capa de trabajo estará constituida por austenita primaria, transformada parcialmente en martensita durante la solidificación, y como resultado de varias reacciones eutécticas como austenita + carburos MC, austenita + grafito, o austenita + carburos M3C. [48]

La morfología del grafito es altamente importante tanto en lo referido a la transmisión de calor como a la resistencia mecánica de la aleación. Morfologías laminares de grafito favorecen la propagación de grietas generadas en los carburos, pero la transmisión de calor se ve favorecida por ellos. Por el contrario, morfologías esferoidales no transfieren el calor de manera tan eficiente, pero funcionan como barreras ante la propagación de grietas [50-53]. Esto hace que la presencia de grafito laminar sea más eficiente a la hora de evacuar calor, pero que la presencia de grafito esferoidal genere un material con mayor resistencia mecánica. [54-57]

El porcentaje óptimo de grafito, medido en fracción en volumen, se encuentra en el rango de entre 2 y 5% siendo recomendable a la hora de fabricar los cilindros controlar tanto la cantidad de grafito presente como su morfología. La cantidad de grafito se puede controlar con el carbono equivalente de la aleación, obteniéndose más carbono en forma de grafito cuanto mayor sea el carbono equivalente, mientras que la morfología del grafito se puede controlar con la adición de aleantes que promuevan la esferoidización del grafito como el Mg, actuando también como agente nucleante de grafito, el Ca o el La. Así mismo la adición de elementos de aleación que precipiten en forma de carburos pueden funcionar como agentes de nucleación heterogénea para las partículas de grafito. [58-63].

1.8. Motivación de la tesis

En esta tesis doctoral se busca obtener, mediante la aplicación de un diseño de experimentos, un material de la capa de trabajo y la zona de unión entre capa de trabajo y núcleo, de cilindros de laminación dúplex fabricados en fundición Ni-Hard atruchada (en la capa de trabajo) y fundición nodular (en el núcleo), cuyos valores de resistencia mecánica y resistencia al desgaste sean lo más altos posibles.

Para ello se variaron de forma controlada parámetros metalúrgicos relacionados con la inoculación con diferentes aleaciones, así como los tenores de elementos de aleación en la composición final de la capa de trabajo y la temperatura líquidus de la aleación final. El diseño de experimentos fraccionado aplicado a esta tesis constó de 8 experimentos. Los resultados de esta tesis servirán para que los fabricantes de cilindros de laminación puedan realizar el proceso de fabricación de los cilindros obteniendo unas piezas finales de mayor calidad, ofreciendo un material que resista tanto a problemas de desconchamiento como de desgaste del cilindro durante su vida en servicio.

1.9. Artículos publicados derivados de la investigación incluidos en esta tesis

1. ***Cofiño-Villar, A.; Alvarez-Antolin, J.F.; Asensio-Lozano, J. Enhanced Fracture Strength in the Working Layer of Rolls Manufactured in Ni-Hard Cast Iron Alloyed with Mo, Nb and Mg. Metals 2018, 8, 725. https://doi.org/10.3390/met8090725***

El objetivo principal de este trabajo fue analizar el efecto que tienen los parámetros seleccionados sobre la resistencia a la flexión y al impacto, así como la relación de estas con la rede de carburos precipitados.

2. ***Cofiño-Villar, A.; Alvarez-Antolin, F.; Asensio-Lozano, J.; Garcia-Garcia, M. Control over the Percentage, Shape and Size of the Graphite Particles in Martensitic White Castings Alloyed with Cr, Nb and Mg. Materials 2019, 12, 185. https://doi.org/10.3390/ma12010185***

El objetivo principal de este trabajo fue analizar el efecto de los parámetros seleccionados sobre la forma, tamaño y cantidad de grafito precipitado en la capa de trabajo, debido a la alta importancia de estas partículas de grafito en la vida útil del cilindro en servicio.

3. ***Cofiño-Villar, A.; Alvarez-Antolin, F.; Asensio-Lozano, J. Enhancement of the Quality of the Shell-Core Bond Interface in Duplex Work Rolls***

Manufactured by Centrifugal Casting Used in Hot Strip Mills. Materials 2019, 12, 1304. https://doi.org/10.3390/ma12081304

En este trabajo se tuvo como objetivo estudiar la resistencia mecánica de la unión entre la capa de trabajo y el núcleo del cilindro, atendiendo a los efectos generados por la variación de los parámetros metalúrgicos seleccionados para el diseño de experimentos realizado.

4. ***Cofiño-Villar, A.; Alvarez-Antolin, F.; Alvarez-Perez, C.H. Improvement in the Resistance to Wear of Work-Rolls Used in Finishing Stands of the Hot Strip Mills. Metals 2021, 11, 1873. https://doi.org/10.3390/met11111873***

Por último, se realizó un estudio sobre el desgaste que sufría esta aleación mediante ensayos Pin on Disc, los resultado de los ensayos se analizaron y se identificaron los parámetros metalúrgicos que afectaban a la resistencia al desgaste.

2. MÉTODO EXPERIMENTAL

2.1. Estrategia experimental

La experimentación trata de forzar de forma artificial circunstancias de tal forma que se puedan extraer conclusiones de la reacción que se derive de estas circunstancias. Este espíritu, llevado al mundo industrial se puede aplicar a dos grandes áreas, la mejora del producto y la mejora del proceso.

Siendo esto así damos ya con el primer problema, que es decidir que variables se han de modificar de tal forma que la respuesta obtenida sea lo más clara posible. A su vez decidir como variar éstas no es baladí y requiere de ciertas suposiciones sobre el comportamiento de la respuesta. La suposición principal es que la respuesta sigue el comportamiento de una función continua y con variaciones suaves o que, si existen discontinuidades, éstas sean conocidas.

Es aquí donde, para un determinado presupuesto, se pueden distinguir tres estrategias fundamentales de experimentación:

1. Experimentar sin planificar:

Guiado por la intuición para la realización de pruebas y ensayos en momentos en los que el funcionamiento normal de la producción se vea interrumpido. No se puede considerar como una estrategia viable para la realización de experimentación.

2. Decisión de la inversión total a priori:

Teniendo en cuenta el presupuesto disponible para la investigación se decide, después de estudiar de forma exhaustiva los objetivos y los aspectos que se conocen de la problemática estudiada, todos y cada uno de los experimentos a realizar.

3. Estrategia secuencial:

Al contrario que en la estrategia anterior, si se sigue una estrategia secuencial primero se decide en qué condiciones se van a realizar un número reducido de experimentos, gastando en torno al 40% del presupuesto en este primer paso. Teniendo en cuenta los resultados del primer paso, se deciden de manera secuencial los siguientes experimentos.

Este último método de decisión es el más recomendable, tanto en el ámbito económico (se reserva parte del presupuesto en cada paso), como en el ámbito de la obtención de resultados óptimos (se va aproximando a la zona en la que los experimentos producen mejores resultados).

Una vez se tiene fijada la estrategia experimental hay que decidir la planificación de los experimentos. En un estudio que comprenda un número determinado de variables se puede seguir esta secuencia de experimentación:

1. Se toma una de las variables y se prueban diferentes niveles hasta encontrar el que genera el mejor resultado.
2. Se fija esa variable y se pasa a la siguiente repitiéndose el proceso anterior.
3. Se repite este procedimiento hasta fijar cada variable en el valor que genera la máxima respuesta.

Este sistema parece correcto a la hora de obtener un máximo (en el caso de estar buscando una mejora en la cantidad de producción, por ejemplo), sin embargo, el valor que se obtiene puede no ser el valor más alto al que se puede llegar.

Contrariamente a lo que intuitivamente pueda parecer correcto, lo adecuado a la hora de obtener los mejores resultados es variar todos los factores estudiados en sus valores, de forma que, aunque se llegue a un máximo local, se pueda llegar al máximo absoluto. Los diseños de experimentos que permite realizar estas variaciones se denomina Diseños Factoriales.

Estos diseños se pueden usar de forma secuencial, permiten obtener el óptimo absoluto, son capaces de estimar las interacciones entre variables, proporcionan estimaciones de los efectos de las variables y son fáciles de construir y de analizar.

Sin embargo, para realizar un diseño factorial completo se requiere de un gran número de experimentos, por suerte existen métodos para reducirlo, siendo los más comunes fijar los niveles de las variables en 2 y utilizar los denominados diseños factoriales fraccionales.

La notación a la hora de nombrar los diseños de experimentos con 2 niveles es 2k donde k es el número de factores a estudiar. Esto se modifica cuando el diseño es fraccional donde la notación se modifica a 2k-pN donde k es el número de factores, p es el grado de fraccionamiento y N es la resolución del diseño.

El grado de fraccionamiento indica la proporción de experimentos que se han dejado de realizar en un diseño fraccionado en comparación con el mismo diseño si se hubiera realizado completo, por ejemplo, en un diseño con 6 factores se tendría que es completo si se realizan 26 experimentos (se harían 64 experimentos) frente a un diseño fraccionado de por ejemplo p=3 donde se realizarían 26-3 experimentos (se harían 8 experimentos), dando lugar a un diseño de la octava fracción.

La resolución indica el grado de confusión que se presentan en la estimación de los efectos. En general, un diseño de resolución N es aquel en el que ningún efecto de k factores se vea confundido con otro que tenga menos de N-k. Por ejemplo, un diseño con resolución III es aquel en el que los efectos principales se ven confundidos con las interacciones de 2 factores, si es IV las interacciones de 2 factores se confunden entre sí y los efectos principales se ven confundidos con las interacciones de tres factores.

Las interacciones son el resultado que se obtiene cuando dos o más factores, de los que se conoce perfectamente la respuesta, se aplican al mismo tiempo, generando una respuesta diferente a la que generan por separado. Un claro ejemplo de esto es lo que ocurre cuando se mezclan medicamentos (por ejemplo, ibuprofeno) con alcohol. Los medicamentos generan una sensación de bienestar (desaparición de dolor de cabeza), mientras que una cantidad reducida de alcohol suele generar euforia y desinhibición, pero en el momento en el que los introduces al mismo tiempo en el cuerpo el resultado final es de mareo y somnolencia.

En un mundo ideal se tendría que una misma acción realizada de la misma forma generaría exactamente el mismo resultado, sin embargo, la realidad nos ha mostrado que esto no ocurre, es decir, en la práctica ningún sistema estudiado es perfectamente determinista.

En el mundo industrial los sistemas son extremadamente complejos y esa complejidad afecta al análisis y diseño de experimentos. Suponiendo que una respuesta depende de dos variables de la producción (x1, x2), la respuesta sería función de esas variables f(x1, x2), sin embargo, el resultado final estará influenciado en menor medida por otras variables que no se explicarían en el diseño inicial. Esta parte aleatoria se designa con la letra ε y se ha de introducir en el modelo como un generador de ruido, quedando la función respuesta como:

$$Y = f(x_1, x_2) + \varepsilon(z_1, z_1, \dots, z_n) \qquad (2.1)$$

ε es función de todas aquellas variables no tenidas en cuenta por lo que para reducir el ruido aleatorio generado se tendrían que introducir variables contenidas en ε dentro de la función f que controla en mayor medida la respuesta.

Se ha hablado de efectos y factores, pero ¿cuál es la relación que hay entre ellos?

Se define efecto de un factor como la variación que tiene la función respuesta cuando se realiza una variación del factor en cuestión. Se distinguen los efectos principales de los efectos de las interacciones de segundo orden, tercer orden, etc.

Los efectos principales son aquellos que se derivan de variar los factores por separado, es decir, el efecto principal de un factor indica como cambia la respuesta en promedio al pasar éste de su valor -1 a su valor +1. Este efecto se calcula como el promedio de los valores de la respuesta cuando el factor está en +1 menos el promedio de los valores de la respuesta cuando el factor esté en su valor -1.

En el caso de las interacciones de 2 factores, su efecto se define como la variación que ocurre cuando manteniendo uno de los factores fijo se varía entre el valor -1 y +1 del factor con el que está interactuando.

Hay que tener en cuenta que en la mayoría de los casos las interacciones de 3 o más factores suelen tener poca relevancia y para la mayor parte de la investigación industrial es suficiente con analizar las interacciones de 2 factores.

Que un efecto tenga una estimación diferente de 0 no implica que realmente afecte a la respuesta de forma significativa, esto hace que una vez calculados los efectos sea necesario determinar mediante la técnica estadística adecuada aquellos efectos que sean significativamente diferente de 0 o, más corto, aquellos efectos que sean significativos.

Para calcular los efectos se puede utilizar el algoritmo de Yates. Los experimentos están sometidos a error, y éste suele seguir una ley normal con media cero y desviación típica, o en algún caso raro, son combinaciones lineales de la respuesta, lo que hace que aplicando el teorema del límite central se aproximan a una ley normal.

Si se representan los valores de los efectos en papel probabilístico normal estos estarán alineados, salvo en el caso de que alguno de los efectos sea significativo, en cuyo caso estará alejado de la normal. Esto es porque los efectos no significativos siguen la ley del tipo N(0,σ) mientras que si el efecto es significativo, la media no será 0 sino μ por lo que la ley que siguen es del tipo N(μ,σ), desplazando el punto en la representación gráfica sobre papel probabilístico normal.

Para realizar la representación se sigue la siguiente secuencia:

1. Ordenar los valores de los efectos de mayor a menor
2. Calcular la proporción de efectos menores que el que se está considerando mediante la siguiente ecuación:

$$P = 100 \times \frac{i - 0.5}{n} \qquad (2.2)$$

Donde i es el orden de cada efecto y n es el número total de efectos

1. Graduar el eje no probabilístico del papel
2. Representar las parejas (efecto, P)

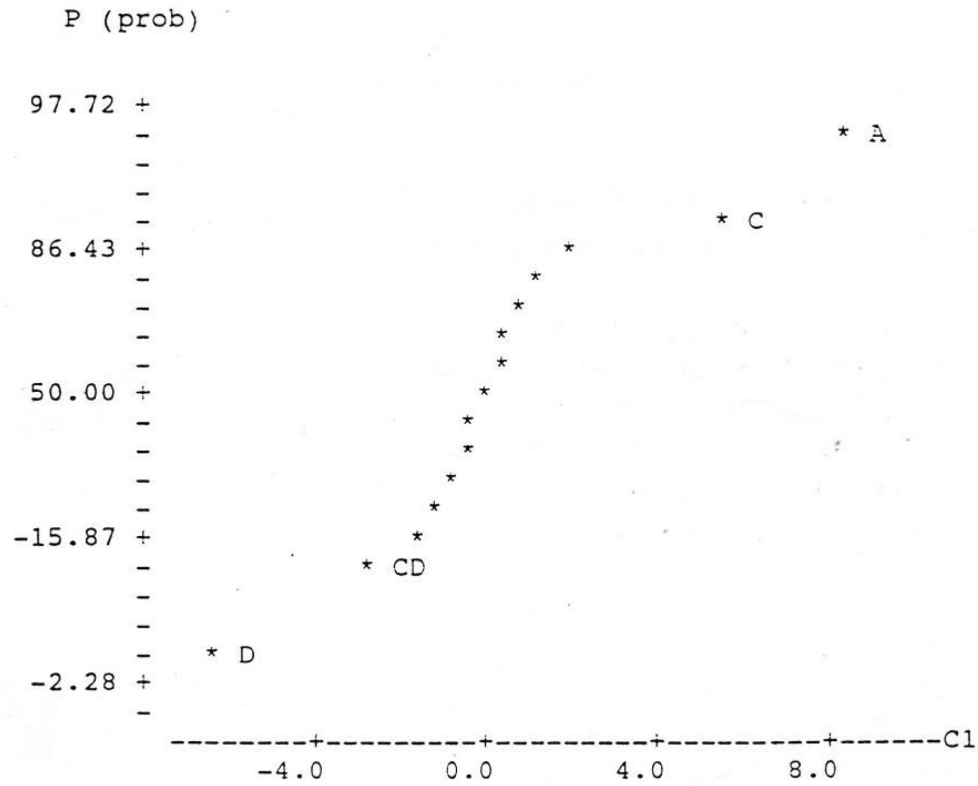

Figura 2.1 Ejemplo de diseño sobre papel probabilístico normal

Una vez se ha hecho la representación de los puntos se debe realizar la interpretación de los resultados.

Como los valores que generan un efecto real, no confundido por el error, aparecen desplazados de la recta que pasa por el punto (0, 50), en el ejemplo anterior se puede asegurar que para el diseño realizado los factores principales A, C y D, y la interacción entre los valores C y D son significativos. Para que así sea los valores que se encuentran en el extremo inferior de la recta deben estar desplazados hacia la izquierda y los que estén en el extremo superior deben estar desplazados hacia la derecha. El significado de estos desplazamientos, en términos del valor que toman los factores, es que, para una cierta respuesta, por ejemplo, la dureza de una aleación, cuando los valores de C y A se encuentran en si nivel +1 generan un aumento en la dureza del material, mientras que el factor D genera un aumento en la dureza cuando se encuentra en su nivel -1. En el caso de la interacción se debe calcular el efecto que tiene por separado.

El diseño de experimentos más simple de todos es aquel en el que se estudia la variación de las respuestas cuando se tienen dos factores de dos niveles, sin embargo, este tipo de DoE no son muy útiles a la hora de realizar estudios industriales. Los diseños más comunes son en los que se estudia la variación de 6, 7, 8 o incluso más factores.

Es por esto qué, si se realizase un diseño factorial completo con ese número tan elevado de factores exige la realización de un número desorbitado de experimentos. Tomando como ejemplo un diseño de 7 factores se tendrían que realizar 27 experimentos, con efectos obtenidos de los efectos principales (7), las interacciones de 2 factores (21), interacciones de 3 factores (35), interacciones de 4 factores (35), interacciones de 5 factores (21), interacciones de 6 factores (7), interacción de 7 factores (1) y la media.

En la práctica es muy difícil encontrar interacciones significativas de tres o más factores, o lo que es lo mismo, suele ser suficiente con estudiar las interacciones de dos factores, a parte de los efectos principales, para dar una explicación suficientemente precisa del comportamiento del sistema en estudio.

He aquí donde entran en juego los diseños factoriales fraccionados, en los que se pierde parte de la información (de las interacciones de orden superior) pero el número de experimentos a realizar es considerablemente menor.

Para estudiar los efectos requeridos es suficiente con realizar una parte o fracción de los experimentos del diseño completo. Estos diseños se denominan diseños factoriales fraccionales, o simplemente, diseños fraccionales. Estos diseños utilizan la notación 2k-p donde k es el número de factores y p es el grado de fraccionamiento. Para el ejemplo de 7 factores se puede tener:

- El fraccionamiento es de p=1 donde se realizarían 64 experimentos, se presupone que las interacciones de cuarto orden o superior son 0, y se pueden calcular los efectos principales y las interacciones de segundo y tercer orden
- El fraccionamiento es de p=3 donde se realizarían 16 experimentos, se presupone que las interacciones de orden superior a tres y parte de las de segundo orden son 0, estimándose los efectos principales y el resto de las interacciones de orden 2.
- El fraccionamiento es de p=4 donde se realizarían 8 experimentos, se presupone que todas las interacciones son 0 y se podrían estimar los efectos principales.

Para la construcción de la matriz de los diseños fraccionales se comienza escribiendo la matriz del diseño completo para el número de experimentos a realizar, en el caso de 27-1 se escribiría la matriz para un diseño de 26 con los factores A, B, C, D, E y F. Posteriormente se escribió la columna del factor G y se confundió deliberadamente con la interacción de sexto orden. Esta confusión deliberada se denomina generador, siendo el generador para este diseño:

$$G = A \times B \times C \times D \times E \times F \qquad (2.3)$$

Para calcular las confusiones no deliberadas introducidas se tienen que realizar operaciones entre las columnas, en particular se debe obtener el producto de los signos de las filas de las columnas en cuestión.

La media se corresponde con una columna en la que todos los signos son +, se designa por la letra I y tiene las siguientes propiedades:

- Cualquier columna multiplicada por si misma es la columna I.
- Cualquier columna multiplicada por la I es la columna original.

- Se cumple la propiedad asociativa.
- Se cumple la propiedad conmutativa.

Si utilizando estas propiedades se multiplican ambos miembros de la ecuación de generación por G se obtiene la relación de definición:

$$G \times G = G \times A \times B \times C \times D \times E \times F \qquad (2.4)$$

$$I = G \times A \times B \times C \times D \times E \times F = A \times B \times C \times D \times E \times F \times G \qquad (2.5)$$

La relación de definición está formada por todas aquellas interacciones que generan una columna I, es decir, que su efecto se vea confundido con la media.

A partir del grado de fraccionamiento introducido en un diseño de experimentos se pueden distinguir 3 familias de diseños fraccionales:

- Medias fracciones
- Diseños saturados
- Diseños intermedios

Medias fracciones

Son aquellos diseños en los que se divide el número de experimentos necesarios por la mitad. Se denotan de forma general por 2^{k-1} lo que implica que se diferencian del diseño completo por 1 factor. Para escribir la matriz de experimentos se toma el diseño completo para un factor menos y se asigna el factor restante a la interacción de mayor orden.

Por ejemplo, un diseño de 2^{3-1}_{III} se tendría:

- Diseño completo para 2^2
    - El generador sería C=AB
    - La relación de diseño es I=ABC
- La resolución es III
- El patrón de confusión es:
    - A+BC
    - B+AC
    - C+AB
    - Media + ABC
- La matriz de experimentos sería:

Tabla 2.1 Ejemplo de matriz de experimentos 2^{3-1}_{III}

Experimento	A	B	C=AB
1	-	-	+
2	+	-	-
3	-	+	-
4	+	+	+

Para diseños de más factores el método de fabricación de la matriz es similar, sólo sería necesario añadir más columnas en función del número de factores y filas en función del número de experimentos asociados a el número de factores.

Diseños saturados

Los diseños saturados son aquellos en los que se tiene el máximo fraccionamiento posible. Se obtienen a base de saturar un completo 2^k asignando a cada interacción una variable nueva, pudiéndose estudiar k factores en k+1 experimentos. Este tipo de diseños son siempre de resolución III.

También se los denomina diseños de efectos principales y su principal utilidad radica en la identificación de los factores activos, de tal forma que, en fases posteriores de la investigación y usando la estrategia secuencial, se estudie la posible interacción que hay entre ellos.

Sería un ejemplo de diseño saturado el anterior o por ejemplo el 2^{7-4}:

- Diseño completo para 2^3
- Se tienen 4 generadores:
  - D=AB
  - E=AC
  - F=BC
  - G=ABC
- La relación de diseño es I = ABD = ACE = BCF = ABCG = BCDE = ACDF = CDG = ABEF = BEG = AFG = DEF = ADEG = BDFG = CEFG = ABCDEFG
- La resolución es III
- El patrón de confusión es:
  - A+BC
  - B+AC
  - C+AB
  - Media + ABC

La matriz de experimentos sería:

Tabla 2.2 Ejemplo de matriz de experimentos 2^{7-4}

Experimento	A	B	C	D=AB	E=AC	F=BC	G=ABC
1	-	-	-	+	+	+	-
2	+	-	-	-	-	+	+
3	-	+	-	-	+	-	+
4	+	+	-	+	-	-	-
5	-	-	+	+	-	-	+
6	+	-	+	-	+	-	-
7	-	+	+	-	-	+	-
8	+	+	+	+	+	+	+

Diseños intermedios

Son aquellos diseños fraccionados que no se corresponden ni con una media fracción ni con un diseño saturado. Permiten realizar diseños con menos experimentos que las medias fracciones, pero con confusiones más favorables que los diseños saturados. La construcción de las matrices es análoga, se selecciona el número de experimentos a realizar y se asignan los factores restantes a interacciones. Sin embargo, este tipo de diseños tienen el problema de no poder discernir siempre con claridad que interacciones hay que asignar a que factores, siendo la regla del diseño la asignación de las interacciones que generen un diseño de máxima resolución. [64-66]

2.2. Fabricación de los cilindros

El proceso de fabricación de los cilindros usados en esta tesis fue el siguiente:

1. Fusión del material de la capa de trabajo a 1400ºC.
2. Sangrado del horno a 1380ºC y adición de los inoculantes en el fondo de la cuchara.
3. Colada sobre el molde centrífugo a 1320C con una velocidad de rotación de 600 rpm.
4. Fusión del material del núcleo a 1500ºC.
5. Sangrado del horno a 1480ºC.
6. Tratamiento de esferoidización.
7. Colada de la capa intermedia que generará la interfase entre la capa de trabajo y el núcleo del cilindro.
8. Colada final del núcleo.
9. Desmoldeo tras 4-5 días de la colada.
10. Austenización del cilindro a 1000ºC y temple al aire.
11. Doble revenido a 400ºC con permanencias en horno de 20h.
12. Mecanizado para obtener el producto finalizado.

Los rangos composicionales del material base de las capas de trabajo y núcleo se encuentran en la **Tabla 2.3**.

Tabla 2.3 Rangos composicionales de la capa de trabajo y núcleo (% peso)

Capa	C	Si	Mn	Ni	Cr	Nb	Mo	Mg
Trabajo	3.2-3.4	0.9-1.0	0.8-1.0	4.4-4.6	1.7-1.8	0.65-0.75	0.25	-
Núcleo	3-3.02	2.2-2.3	0.2-0.4	0.1-0.2	≤0.1	-	≤0.02	0.06-0.08

Los inoculantes utilizados, así como sus composiciones se encuentran en la Tabla 2.4.

Tabla 2.4 Composición química de los inoculantes utilizados (% peso) Resto Fe.

Inoculantes	Composición Química												
	Si	Ca	Al	Mn	Ti	Ba	C	Bi	S	P	B	La	Mg
FeSi-La	66.0	2.5	0.8	---	---	0.3	---	0.3	---	---	---	0.8	
FeSiMg	28.7												15
FeMn	2.0	---	---	69.4	---		5.8		0.014	0.130	---		
SiCa	58.3	16.4	1.1	14.8	0.030		0.6		0.030	0.030	---		
FeB	0.4	---	---	---	---		0.3		---	---	17.9		

2.3. Obtención de las probetas

El análisis de la capa de trabajo se realizó comenzando por la división de esta en dos partes según la profundidad a la que se obtenían las probetas. Las primeras probetas se extrajeron de la zona más externa que abarcaba desde la periferia del cilindro hasta una profundidad de 15 mm, siendo denominada esta zona “Zona I”. Las segundas probetas se extrajeron de una zona que abarcaba desde los 25 mm de profundidad hasta los 40 mm de profundidad, siendo denominada “Zona II”. Por último, se extrajeron probetas de la zona de unión entre la capa de trabajo y el núcleo del cilindro siendo denominada esta zona “Zona U”.

Se mecanizaron 3 probetas Charpy sin entalla para cada zona de dimensiones 10mm x 10mm x 50mm y 3 probetas de flexión de sección rectangular de dimensiones 10mm x 3mm x 60mm.

Se mecanizaron pines de 1 mm de diámetro obtenidos de los restos de las probetas Charpy después de ser ensayadas.

2.4. Preparación metalográfica

Para la preparación metalográfica se aprovecharon las probetas charpy después de la realización de los ensayos.

El proceso de preparación consistió en una primera etapa de desbaste, seguido de una etapa de pulido y se finalizó con un ataque químico.

La etapa de desbaste consistió en el lijado de la superficie con papel abrasivo de SiC de grit creciente desde grit 60 hasta grit 600.

El pulido se realizó en dos etapas consecutivas utilizando como abrasivo pasta de diamante de 6µm y 1µm.

Los ataques químicos utilizados para revelar la microestructura del material fue Nital 4 y Nital 5.

Se obtuvieron micrografías de las tres zonas (para cada experimento) tanto en estado pulido para el análisis de las partículas de grafito, como en estado atacado para el análisis de los carburos precipitados y la obtención de micrografías representativas de la estructura del material.

Dichas micrografías fueron realizadas tanto en microscopio óptico (estado pulido y estado atacado), como en microscopio electrónico de barrido (SEM por sus siglas en inglés) (estado atacado).

El microscopio óptico utilizado fue el modelo NIKON Epiphot 200 utilizando el software Omninet Enterprise para la toma de fotos.

El SEM utilizado fue el modelo JEOL JSM-5600, equipado con el módulo de microanálisis por dispersión de rayos X característicos (EDX).

2.5. Metalografía cuantitativa

Las respuestas fueron obtenidas mediante el software Image ProPlus en su versión 4.5.0.29 en conjunción con el módulo de análisis Materials-Pro.

Para el análisis de la fracción en volumen de carburos se obtuvieron 5 micrografías para cada experimento a 10X.

Para el análisis de las partículas de grafito se utilizaron 5 micrografías para cada experimento a 10X.

2.6. Microanálisis

Se realizaron análisis químicos semicuantitativos por dispersión de rayos X característicos sobre los carburos, obteniéndose el espectro composicional de los precipitados analizados en las Zonas I y II.

2.7. Ensayos de dureza

Se realizaron ensayos de dureza Vickers con una carga de 150kp, obteniéndose el resultado como la media de 10 indentaciones.

Para obtener el perfil de dureza de la Zona U, con el fin de describir la transición entre capa de trabajo y núcleo, se realizaron microdurezas Vickers con una carga de 0.5kp. Se realizaron 23 indentaciones separadas entre sí por 400 µm a largo de una distancia de 8.8 mm. El perfil de durezas final se calculó como la media de 3 perfiles.

2.8. Ensayos de resiliencia

Se realizaron 3 ensayos charpy para cada zona (I, II y U) sobre probetas sin entalla.

2.9. Ensayos de flexión en tres puntos

Se realizaron 3 ensayos de flexión en tres puntos, por Zona y experimento, en una máquina de ensayos universal de la marca Instrom modelo 5582, con una célula de carga de 100 kN, distancia entre apoyos de 50 mm.

2.10. Ensayos de desgaste

Se realizaron 3 ensayos de desgate Pin on Disc, utilizando los pines de las zonas I y II, y como contra probetas (disc) discos de acero F125-2 en estado de temple en aceite sin revenir.

Los ensayos se realizaron a alta temperatura (250ºC y 350ºC) con un radio de ensayo de 25 mm y una velocidad angular de 140 Rpm, la distancia de ensayo fue de 8 km y la velocidad lineal fue de 0.36 m/s. Se utilizo una carga de 20N.

La máquina de ensayos utilizada fue el modelo MT/30/SCM/T de la empresa MicroTest, número de serie V1041.

2.11. Análisis de los resultados

Para el análisis de los resultados se utilizó el programa informático Statgraphics Plus en su versión 5.1.

3. RESULTADOS

A continuación, se presentan los cuatro artículos que forman el conjunto de resultados de la tesis, en el siguiente orden:

1. Enhanced Fracture Strength in the Working Layer of Rolls Manufactured in Ni-Hard Cast Iron Alloyed with Mo, Nb and Mg.

   Publicado en la revista Metals el 15 de septiembre de 2018, Autores: Alberto Cofiño Villar, José Florentino Álvarez Antolín y Juan Asensio Lozano, DOI: 10.3390/met8090725

2. Control over the Percentage, Shape and Size of the Graphite Particles in Martensitic White Castings Alloyed with Cr, Nb and Mg

   Publicado en la revista Materials el 8 de enero de 2019, Autores: Alberto Cofiño Villar, José Florentino Álvarez Antolín, Juan Asensio Lozano y María Ángeles García García, DOI: doi:10.3390/ma12010185

3. Enhancement of the Quality of the Shell-Core Bond Interface in Duplex Work Rolls Manufactured by Centrifugal Casting Used in Hot Strip Mills.

   Publicado en la revista Materials el 20 de abril de 2019, Autores: Alberto Cofiño Villar, José Florentino Álvarez Antolín, y Juan Asensio Lozano. DOI: 10.3390/ma12081304

4. Improvement in the Resistance to Wear of Work-Rolls Used in Finishing Stands of the Hot Strip Mills

   Publicado en la revista Metals el 21 de noviembre de 2021, Autores: Alberto Cofiño Villar, José Florentino Álvarez Antolín y Carlos Hugo Álvarez Pérez DOI: 10.3390/met11111873

metals

Article

Enhanced Fracture Strength in the Working Layer of Rolls Manufactured in Ni-Hard Cast Iron Alloyed with Mo, Nb and Mg

Alberto Cofiño-Villar [1], Jose Florentino Alvarez-Antolin [1,*] and Juan Asensio-Lozano [2]

[1] Departamento de Ciencia de los Materiales e Ingeniería Metalúrgica, Edificio departamental Este, Universidad de Oviedo C/ Wifredo Ricart s/n-, 33204 Gijón (Asturias), Spain; uo229780@uniovi.es

[2] Departamento de Ciencia de los Materiales e Ingeniería Metalúrgica, Escuela de Ingeniería de Minas,

Energía y Materiales, Universidad de Oviedo, C/ Independencia 13, 33004 Oviedo (Asturias), Spain; jasensio@uniovi.es

* Correspondence: alvarezflorentino@uniovi.es; Tel.: +34-985-181-949

Received: 28 August 2018; Accepted: 13 September 2018; Published: 15 September 2018

Abstract: One of the main in-service failure mechanisms of the work-rolls used in hot strip mill finishing stands is surface spalling. The indefinite chill double-poured rolls usually comprise of a peripheral working layer made of crushed Ni-hard cast iron and a grey cast iron core, mostly pearlitic matrix with spheroidal graphite. To enhance its wear resistance, the working layer can be alloyed with Mo and Nb. The possible cracking and spalling of the surfaces of these work-rolls is strongly influenced by the presence of carbides and the continuity of their network. The flexural and impact toughness tests are reliable testing methods to assess these properties. The aim of this paper is to identify those manufacturing factors that have a significant effect on the flexural strength and toughness of this material, correlating the results with the volume fraction of precipitated carbides. It is worth highlighting, among the analysed factors are the liquidus temperature, the %Si, the use of an inoculant with traces of Lanthanum, and inoculation with different amounts of FeB, SiCa and Mg. Inoculation with SiCa is found to have a positive effect on the toughness of the material, breaking up the continuity of the carbide network, while FeB is found to act as a heterogeneous nucleant for NbC precipitation. However, high FeB contents reduce flexural strength and do not have a significant effect on the hardness of the material. To enhance the fracture toughness of the working layer, a liquidus temperature in the 1270–1275 ◦C range is recommended, as well as inoculating the ladle with Mg, 3 kg/T FeB and 0.6 kg/T SiCa.

Keywords: flexural strength; hot strip mills; hardness; white cast iron; toughness

1. Introduction

Indefinite chill double-poured (ICDP) work-rolls are usually used in the finishing stands of hot strip mills (HSMs). These rolls usually comprise a peripheral working layer made of crushed Ni-hard cast iron and a grey cast iron core with spheroidal graphite in a mostly pearlitic matrix. Table 1 shows the most usual chemical composition range for the working layer.

Table 1. Chemical composition range of the working layer, expressed in weight percent (wt.%).

C	Mn	Si	S	P	Cr	Ni	Mo	Nb
3.2–3.4	0.8–1.0	0.9–1.0	<0.015	<0.035	1.7–1.8	4.4–4.6	0.25	0.65–0.75

These rolls are manufactured by means of vertical centrifugal casting. The working layer is cast first and the core is subsequently cast in two stages. In the first, an intermediate layer is cast which ensures optimum binding with the outer layer. The remainder of the core is then cast in a second stage. The microstructure of the working layer is formed by primary austenite, which is partially transformed into martensite during solidification, and by the result of several eutectic reactions, such as austenite + MC carbides, austenite + graphite, and austenite + M3C carbides [1]. The presence of graphite is intended to increase the thermal conductivity and the resistance to thermal shock of the working layer. In turn, the graphite performs dry lubrication functions [2,3], reducing the coefficient of friction between the work-roll and the steel strip to be rolled [4]. These rolls should also have a high resistance to wear. To enhance this property, they can be alloyed with Mo and Nb. The addition of Nb favours the formation of hard MC carbides, whose hardness is around 2400 HV [5,6], which promotes enhanced wear resistance and increases the material's impact toughness [7,8]. Mo improves austenite hardenability, and with increasing percentages up to 1%, refines carbides and improves wear resistance [9].

During the rolling pass, the roll undergoes compression forces that oppose thermal expansion. The service life of these rolls depends on their wear resistance, as well as on their fatigue behaviour versus cyclic loadings of thermal stresses and cyclic mechanical strain [10]. The rolling process commences with the slab at 1250 ◦C, the work-roll reaches up to 500–600 ◦C in a single second when entering into contact with the slab, subsequently being water-cooled to the 80 ◦C in 4 s as the slab exits the rolls. These thermal variations generate severe thermal fatigue cycles [11]. The thermal stresses are proportional to the thermal gradient, which reaches a maximum during the cooling at the exit of the rolling pass. After a few cycles, thermally induced cracks may begin to appear and may advance inwards into the roll. In this case, the ledeburite microstructure plays an important role in the formation of these cracks and their development [12]. Furthermore, in addition to the yield stress of the material, the amount of pressure the roll must support will depend on geometric factors such as the roll radius, the reduction in thickness, and the final thickness of the slab between passes. The pressures exerted during rolling can lead to the crushing of some carbides and the subsequent transmission of the cracks generated through the network of these carbides [13]. Aside from the rolling process, the possible cracking and spalling of the surfaces of these rolls is strongly influenced by the microstructural characteristics of the working layer [14], especially by the presence of carbides [15].

For the above reasons, it follows that in addition to wear resistance in the working layer of these rolls, they must also present a high mechanical strength and a high fracture strength. The flexural test [16] and the impact toughness test [17] are reliable methods to assess these properties in this type of alloy, where the presence of a continuous carbide network is crucial. Via the application of a Design of Experiments (DoE), the aim of this paper is to identify those manufacturing factors that have a significant effect on the flexural strength and toughness of this material, correlating the results with the volume fraction of precipitated carbides and the material's hardness. For this purpose, manufacturing factors such as the liquidus temperature, the %Si, the use of an inoculant with traces of Lanthanum, and inoculation with different amounts of FeB, SiCa and Mg were analysed. Previous research concludes that additions of B promote an increase in the percentage of carbides and an increase in wear resistance. However, their addition could affect the flexural strength of the material [18]. Moreover, the addition of Mg and other elements such as Ca and La promote the precipitation of graphite with a nodular morphology [19]. Mg acts as a nucleator of graphite [20]. Inoculation with SiCa promotes a decrease in the grain size of the primary austenite and discontinuity of the carbide network [21], which could increase the toughness of the material. The presence of Lanthanum improves the mechanical properties of white cast irons [22]. The research was conducted at an industrial scale, for which purpose eight rolls with a diameter between 680 and 700 mm, a length between 1800 and 2000 mm, and a thickness of the working layer between 50 and 55 mm, were cast.

2. Materials and Methods

The experimental method applied was a fractional factorial Design of Experiments (DoE) with six factors, two levels for each factor, and eight experiments in all. The resolution of this Design of Experiments was III [23].

The working layer was smelted in a medium frequency induction furnace. 'Bleeding' from the furnace into the treatment ladle was carried out at 1420 ◦C, with the inoculants being placed at the bottom of the ladle. Table 2 shows the chemical composition of the inoculants.

Table 2. Chemical composition of the inoculants, expressed in weight percent (wt.%).

Inoculants	**Base Chemistry**												
	Si	Ca	Al	Mn	Ti	Ba	C	Bi	S	P	B	La	Fe
FeSi-La	66.0	2.5	0.8	---	---	0.3	---	0.3	---	---	---	0.8	rem.
FeMn	2.0	---	---	69.4	---		5.8		0.014	0.130	---		rem.
SiCa	58.3	16.4	1.1	14.8	0.030		0.6		0.030	0.030	---		rem.
FeB	0.4	---	---	---	---		0.3		---	---	17.9		rem.

The casting was carried out at a temperature of around 60–65 ◦C above the liquidus temperature. Demoulding took place after five days. Before machining, the work-rolls were subjected to tempering at 400 ◦C. Table 3 shows the analysed factors and levels.

Table 3. Description of the Factors and Levels for the DoE.

Factors		**Levels**	
Code	**Metallurgical parameter correspondence**	**Level –1**	**Level +1**
A	FeSi-La (Kg/T)	0	2.7
B	FeB (Kg/T)	3	6
C	Liquidus Temperature (ºC)	1250-1255	1270-1275
D	Si (%)	0.8-0.85	1.1-1.15
E	SiCa (Kg/T)	0.3	0.6
F	Mg (%)	0	0.02

Table 4 shows the array of experiments.

Table 4. Array of experiments.

No.	A	B	C	D	E	F
1	–1	–1	–1	+1	+1	+1
2	+1	–1	–1	–1	–1	+1
3	–1	+1	–1	–1	+1	–1
4	+1	+1	–1	+1	–1	–1
5	–1	–1	+1	+1	–1	–1
6	+1	–1	+1	–1	+1	–1
7	–1	+1	+1	–1	–1	+1
8	+1	+1	+1	+1	+1	+1

Table 5 shows the sequence of generators and confounders in the DoE. The 'generators' column indicates the applied sign algorithm in the construction of columns D, E and F. The 'confounders' column shows those second-order (2 factor) interactions whose effects are confounded in the main effects. For example, the effect of the second-order interactions BD + CE will be confounded with the effect of Factor A [24].

Table 5. Generators and confounders in the array of experiments.

Generators	Confusions
D=AB E=AC F=BC	A+BD+CE B+AD+CF C+AE+BF D+AB+EF E+AC+DF F+BC+DE

The Yates algorithm [25], which can be implemented on a spreadsheet, is usually used to calculate the effects, the main effects, as well as interactions of all kinds. The experimental response is subject to random variation. This variation will follow a normal law, where its standard deviation reflects an experimental error. The effects are linear combinations of the responses. Hence, by the application of the central limit theorem (CLT), they follow a normal law. Each main effect may be considered a random variable, where the obtained value is an estimate of its mean; hence, this value is accompanied by the estimation of its standard deviation. If all the effects were non-significant, they would follow an $N(0,\sigma)$ law and would thus appear aligned in a representation of the effects on a normal probability plot. If any effect is significant, it will follow an $N(\mu,\sigma)$ law, not appearing aligned with the non-significant effects. The standardized effect is the ratio between the difference in the value of the variable and its mean and standard deviation. This represents not only whether the value of the variable is above or below the average, but also how far it deviates from it. To decide whether an effect is significant, we can compare this standardized effect on a normal probability plot. Those effects that deviate from the straight line towards the ends are significant. The significant factors that deviate from the straight line to the left indicate that their −1 level increases the response function with respect to their +1 level. The significant factors at a distance from the straight line to the right indicate that their +1 level increases the response function with respect to their −1 level [26].

For the analysis, the thickness of the work layer was divided into two regions. An outer layer, which started at the periphery of the roll and penetrated into the working layer, reaching a thickness of 15 mm (Region I). Another more interior layer that began 25 mm from the periphery of the roll and whose thickness encompassed another 15 mm, reaching 40 mm in depth from the periphery of the cylinder (Region II). Three 10 mm × 10 mm × 50 mm unnotched Charpy specimens were machined from each of these regions, as well as three bending specimens with a rectangular cross-section, each measuring 10 mm wide, 3mm thick and 60 mm long. The bending tests were performed on an INSTRON 5582 universal testing machine (INSTRON, Barcelona, Spain) equipped with a 100 KN load cell, employing a distance of 50 mm between supports.

The metallographic samples were prepared using one of the pieces of the Charpy specimens once fractured. The Vickers hardness was measured on the other piece, applying a 150 KPa load. The result is obtained as the average value of 10 indentations in each experiment.

The mechanical grinding process was carried out with 60, 120, 240, 400, and 600 grit size SiC paper. Subsequently, the samples were polished in two consecutive stages with 6 µm and 1 µm diamond paste, respectively. Nital 5 was used as the chemical reagent to reveal the microstructure of the material.

The optical microscope employed was a NIKON Epiphot 200 (Nikon, Tokyo, Japan), the images being obtained using the Omnimet Enterprise Image Analysis System. Five micrographs were randomly obtained for each region (Regions I and II) and for each experiment (Experiments 1 to 8). The volume fraction of carbides was calculated using Image ProPlus, version 4.5.0.29 (Media Cybernetics, Rockville, MD, USA), imaging software and its Materials-Pro analysis module. The different types of precipitated carbides were identified under a JEOL JSM-5600 (JEOL, Nieuw-Vennep, The Netherlands) scanning electron microscope (SEM), equipped with the characteristic X-ray scattering microanalysis system (SEM-EDX).

3. Results

Table 6 shows the chemical composition and casting parameters of the peripheral working layers in each of the eight experiments. The elements C, Mn, Si, Cr, Ni, Mo, and Mg were quantified by spark optical emission spectrometry, while the elements B, Nb, and La were quantified by inductively coupled plasma mass spectrometry on an Agilent 7500 ICP-MS device (Agilent Technologies, Madrid, Spain).

Table 6. Chemical composition of the peripheral working layer in the 8 Experiments.

Casting Parameters	units	Experiment Number							
		1	**2**	**3**	**4**	**5**	**6**	**7**	**8**
C	%	3.35	3.46	3.4	3.28	2.94	3.04	3.02	3.04
Mn	%	0.77	0.78	0.79	0.77	0.79	0.83	0.80	0.82
Si	%	1.13	0.88	0.87	1.18	1.16	0.89	0.87	1.15
Cr	%	1.68	1.68	1.71	1.64	1.65	1.71	1.68	1.71
Ni	%	4.44	4.33	4.32	4.38	4.59	4.16	4.62	4.65
Mo	%	0.26	0.25	0.25	0.24	0.25	0.25	0.26	0.26
Nb	%	0.64	0.72	0.68	0.61	0.74	0.75	0.73	0.61
Mg	%	0.005	0.004	-	-	-	-	0.004	0.005
B	%	0.032	0.033	0.071	0.075	0.038	0.041	0.070	0.071
La	%	-	0.0011	-	0.0015	-	0.0016	-	0.0012
Liquidus Temperature	ºC	1252	1254	1253	1250	1273	1272	1272	1270

Figure 1 shows the characteristic microstructure of the working layer. The micrograph in Figure 1a) corresponds to Region II in Experiment 1. The presence of the network of cementite, with M3C stoichiometry, and of martensite needles in a retained austenite background can be identified in this image. The micrograph in Figure 1b corresponds to Region I in Experiment 6. Spheroidal graphite nodules can be observed within the eutectic austenite which subsequently mainly transform into martensite. The micrograph in Figure 1c corresponds to Experiment 3, in the transition zone between the working layer and the core of the roll. In the transition zone of the core part, the presence of spheroidal graphite can be observed within a pearlite matrix, where some ferrite areas can also be seen, in addition to the presence of carbides that could precipitate due to the diffusion of carburizing elements. The darker colouring of the pearlite in the core zone stands out, as compared to the lighter colouring of the martensite in the working layer zone.

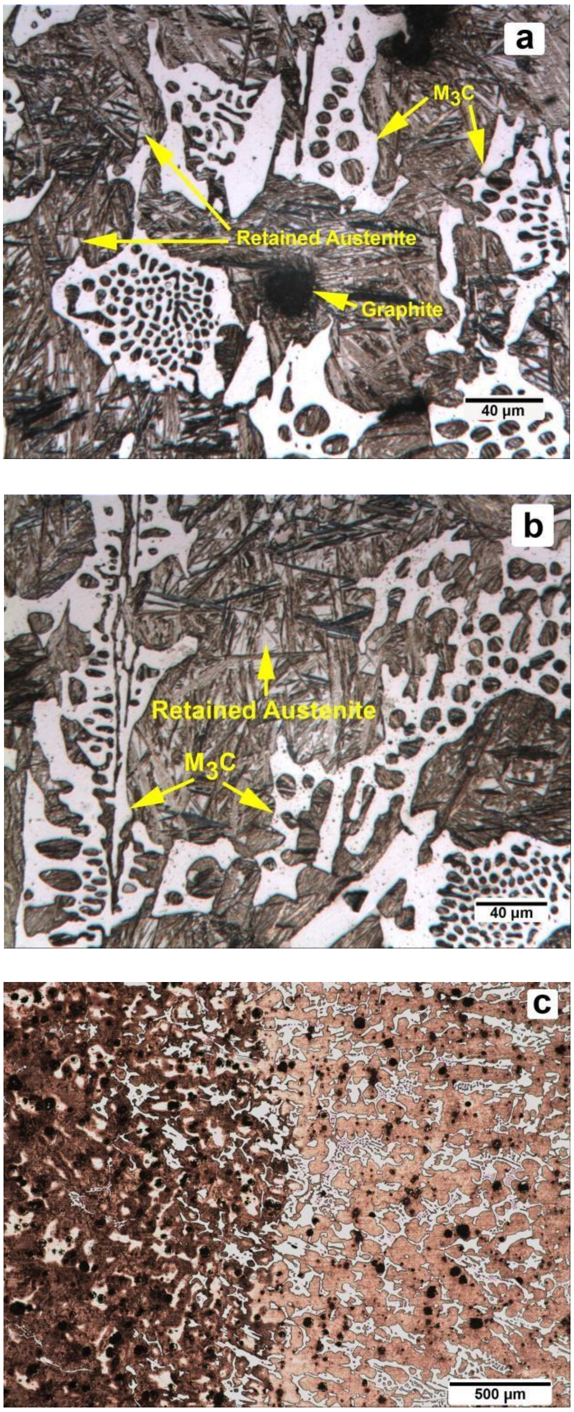

Figure 1. Characteristic microstructure obtained by optical microscopy: (**a**) Experiment 6, Region I of the working layer; (**b**) Experiment 1, Region II of the working layer; and (**c**) Experiment 3, transition zone between the working layer and the core of the roll.

Figure 2 shows the precipitated carbides.

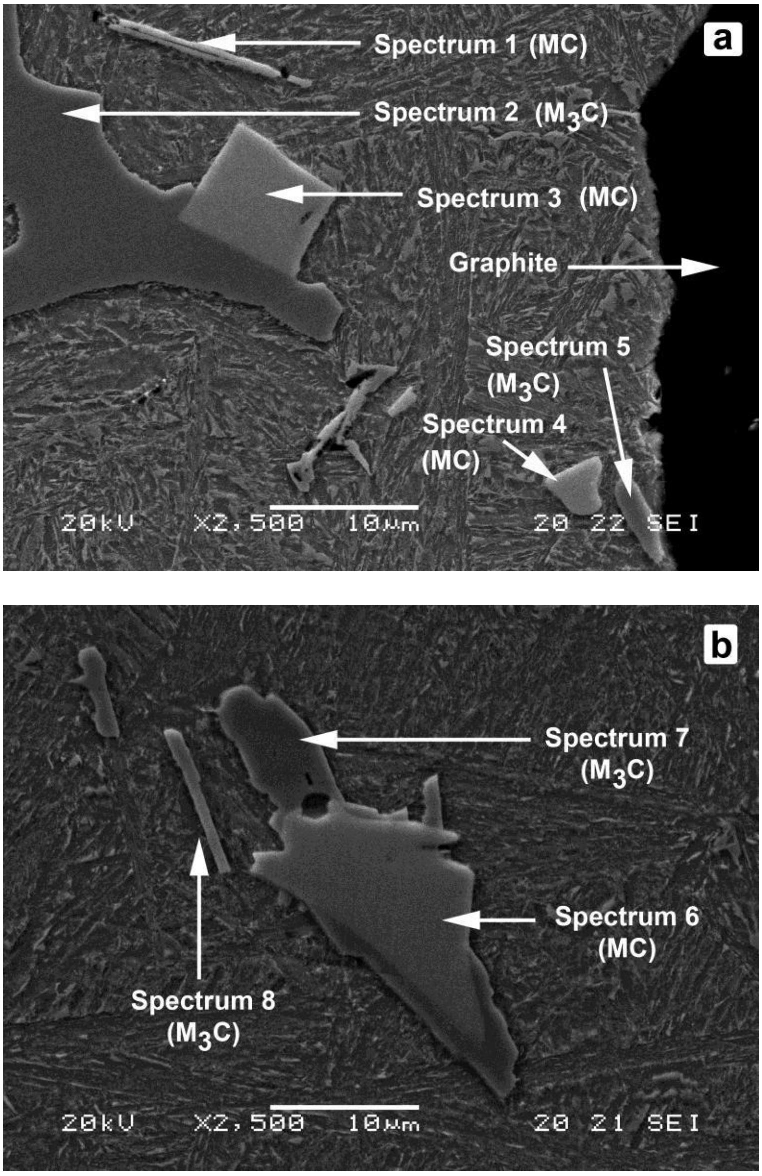

Figure 2: *Cont.*

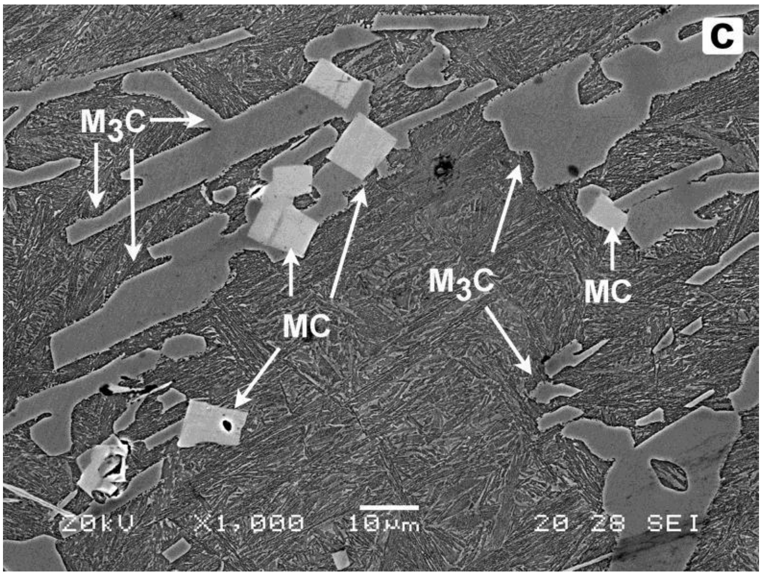

Figure 2. Microstructure obtained under scanning electron microscopy in which the different types of carbides can be distinguished: (**a**) Experiment 8, Region I of the working layer, EDX analysis; (**b**) Experiment 5, Region II of the working layer, EDX analysis; and (**c**) Experiment 8, Region II of the working layer, carbides of MC (NbC) and M_3C (cementite-like carbides) stoichiometry.

The micrograph in Figure 2a corresponds to Region I in Experiment 8. The presence of graphite and two types of disperse carbides can be appreciated in the image. Table 7 shows the results of the microanalysis performed on these two types of carbides (spectra 1 to 5). The lighter-coloured carbides, corresponding to spectra 1, 3 and 4, are carbides of MC stoichiometry, of the NbC type. Elements such as B and Fe can be seen attached to this type of carbide, from which it may be deduced that the FeB acts as a heterogeneous nucleant of this type of carbide. The darker-coloured carbides, spectrum 2 and 5, correspond to carbides of M3C stoichiometry, associated with mixed cementite-like carbides (Fe, Cr)3C.

Table 7. Results of the microanalysis performed by SEM-EDX, corresponding to Figure 2a, b. Atomic (%).

Spectrum	%B	%C	%Fe	%Nb	%Cr
1	36.05	43.47	8.15	12.34	–
2	–	36.11	60.79	–	3.10
3	45.21	27.29	20.61	6.88	–
4	27.61	49.24	1.39	21.76	–
5	–	50.89	49.11	–	–
6	29.96	53.58	0.63	15.83	–
7	–	40.25	57.57	–	2.19
8	-	30.30	67.48	-	2.22

The micrograph in Figure 2b corresponds to Region II in Experiment 5. Table 7 shows the results of the microanalysis performed on the three particles, identified as spectra 6 to 8. Spectra 6 corresponds to NbC carbides, whose precipitation seems to have been promoted by heterogeneous nucleation from FeB particles. Spectra 7 and 8 correspond to a mixed cementite-like carbide.

Figure 2c corresponds to Region II in Experiment 8. Carbides of MC stoichiometry can be identified in this figure, with a brighter colouring and rectangular geometry, as well as carbides of M3C stoichiometry, with a darker colouring, which are found to be the majority. It should be noted that no carbides of M2C stoichiometry, which would be associated with Mo2C, were observed. Hence, it can be deduced that the Mo remains in solid austenite solution, favouring its hardenability.

Tables 8 and 9 show for Regions I and II, respectively, the average values obtained for the studied responses: hardness, volume fraction of Cementite, energy absorbed up to fracture by means of the Charpy test, and flexural strength. These tables also include the standardized effects of the factors and interactions, which are given in the last column (called 'Restricted confounding pattern'). In this column, we indicate the main factors and the second-order interactions with which their effects are confounded. It should be borne in mind that fractional factorial DOEs allow a large number of factors to be studied by means of a very small number of experiments, assuming the loss of information of potential interactions between factors, which are not usually significant in industrial practice. The aim of using a fractional approach is not to make a good fit, but to try to find out which factors have a significant effect on the response variable.

Table 8. Average values and standardized effects for the impact energy absorbed by means of the Charpy test, for the flexural strength and modulus of elasticity obtained by the three-point bending test.

a) Region I

Experiment	Charpy Test		3-Point Bending Test		Restricted Confounding Pattern
	Impact Energy (J/cm^2)		Flexural Strength (MPa)		
	Values	Effect[1]	Values	Effect[1]	
1	3.09	*3.205*	634.2	*586.788*	Mean[2]
2	2.53	0.075	582.8	50.725	A/BC/CE
3	3.11	0.225	493	-34.275	B/AD/Cf
4	2.86	0.615	614	11.575	C/AE/BF
5	2.97	-0.05	548.3	25.375	D/AB/EF
6	3.78	0.48	650.4	15.925	E/AC/DF
7	3.5	0.05	570.2	20.725	F/BC/DE
8	3.8	-0.205	601.4	-60.825	AF/BE/CD

b) Region II

Experiment	Charpy Test		3-Point Bending Test		Restricted Counfounding Pattern
	Impact Energy (J/cm^2)		Flexural Strength (MPa)		
	Values	Effect[1]	Values	Effect[1]	
1	3.21	*3.186*	657.7	*590.438*	Mean[2]
2	2.69	-0.182	621.3	-34.225	A/BC/CE
3	3.07	0.002	479.8	-105.025	B/AD/Cf
4	2.67	0.552	480.4	61.275	C/AE/BF
5	3.46	0.117	627.9	-34.525	D/AB/EF
6	3.38	0.277	664.9	-16.325	E/AC/DF
7	3.37	0.082	664.8	54.375	F/BC/DE
8	3.64	0.057	526.7	-53.025	AF/BE/CD

[1] Standardized effect; [2] Average value of the responses analysed in the 8 experiments.

Table 9. Average values and standardized effects for the volume fraction of cementite and Vickers hardness.

a) Region I

Experiment	Hardness (HV)		V_v Fe_3C (%)		Restricted Confounding Pattern
	Values	Effect[1]	Values	Effect[1]	
1	592	*584.125*	29.31	*23.082*	Mean[2]
2	560	-16.75	28.57	-1.985	A/BC/CE
3	630	32.25	25.09	-0.705	B/AD/Cf
4	543	5.75	20.81	-5.725	C/AE/BF
5	570	9.25	20.23	0.685	D/AB/EF
6	550	42.75	15.63	0.525	E/AC/DF
7	578	21.75	21.67	5.285	F/BC/DE
8	650	36.75	23.35	2.455	AF/BE/CD

b) Region II

Experiment	Hardness (HV)		V_v Fe_3C (%)		Restricted Confounding Pattern
	Values	Values	Values	Effect[1]	
1	540	*575.125*	24.91	*23.956*	Mean[2]
2	607	-3.75	25.90	-0.847	A/BC/CE
3	623	25.75	27.17	-0.392	B/AD/Cf
4	521	4.75	25.4	-3.777	C/AE/BF
5	569	-19.25	23.91	-0.332	D/AB/EF
6	533	13.75	21.89	-0.457	E/AC/DF
7	576	27.25	21.53	-1.272	F/BC/DE
8	632	62.25	20.94	1.047	AF/BE/CD

[1] Standardized effect; [2] Average value of the responses analysed in the 8 experiments.

Figures 3–6 show the representation of the standardized effects on a normal probabilistic plot for the analysed responses in Regions I and II of the working layers of these rolls.

Figure 3a shows that none of the studied factors have a significant effect on the hardness in the outermost part of the working layer (Region I). However, Figure 3b shows that some of the interactions AF, BE, and CD, have a significant effect on the hardness inside this working layer (Region II).

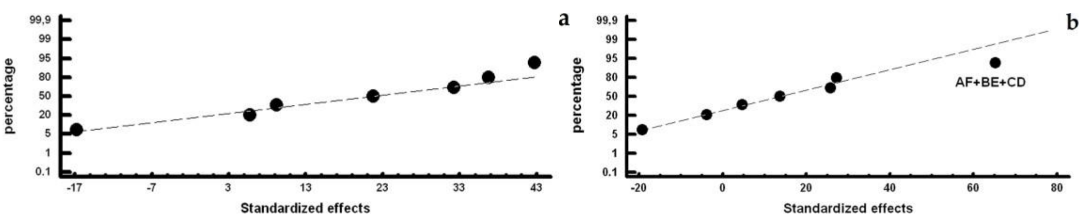

Figure 3. Representation of standardized effects on a normal probability plot versus Vickers hardness: (**a**) Region I and (**b**) Region II.

The effects of these three interactions are analysed separately in Table 10. To increase the hardness inside the working layer, it would appear advisable to place the interaction of Factors A and F at their (+1, +1) levels, the interaction of Factors B and E at their (+1, +1) levels, and the interaction of Factors C and D at their (−1, −1) levels.

Table 10. Analysis of the interactions AF+BE+CD versus hardness in Region II.

A\F	−1	+1	B\E	−1	+1	C\D	−1	+1
−1	596	558	−1	588	537	−1	615	531
+1	527	619	+1	576	628	+1	555	601

That is, it would be advisable to combine inoculation with FeSi-La with the addition of Mg, combine inoculation with 6 kg/T FeB with inoculation with 0.6 kg/T SiCa, and combine a liquidus temperature between 1250 and 1255 ◦C with a low percentage of Si, at around 0.8–0.85%. Of these three interactions, the interaction between factors B and E at their (+1, +1) level, i.e., 6 kg/T FeB in combination with 0.6 kg/T SiCa, seems to have a significantly stronger 'effect'.

Figure 4 shows that the liquidus temperature (factor C) has a significant effect on the volume fraction of cementite. Hence, if we wished to increase its presence, we should place it at its −1 level (1250–1255 ◦C). A low liquidus temperature means an increase in the volume fraction of the eutectic constituent, which is why it is consistent with an increase in the volume fraction of the cementite. Furthermore, Figure 4b) shows that interactions AF + BE + CD has a significant effect on the inside of the working layer. Table 11 analyses the effect of the separate interactions of Factors A with F, B with E, and C with D. From its analysis, it can be concluded that, in order to increase the cementite content, in addition to placing the liquidus temperature between 1250 and 1255 ◦C, the absence of Mg is advisable. Mg has a nucleating effect on spheroidal graphite, and also increases the number of graphite beads [27]. Hence, although it does not have a graphitizing effect, the volume fraction of cementite could be affected by its presence.

Table 11. Analysis of the interactions AF+BE+CD versus Vv Cementite (%) in Region II.

A\F	−1	+1	B\E	−1	+1	C\D	−1	+1
−1	26	23	−1	25	23	−1	27	25
+1	24	23	+1	23	24	+1	22	22

From the analysis, it can be concluded that, in order to increase the Cementite content, in addition to placing the Liquidus Temperature between 1250 and 1255 ◦C, the absence of Mg is advisable.

Figure 5 shows that factors E (inoculation with SiCa) and C (liquidus temperature) have a significant effect on impact toughness. Thus, if we place both factors at their +1 levels, i.e. 0.6 kg/T and 1270–1275 ◦C, respectively, there is an increase in the amount of energy absorbed before impact fracture. This improvement produced by the increase in the amount of SiCa could be due to the effect that this inoculant seems to have on the continuity in the carbide network. An increase in the liquidus temperature leads to the decrease in the volume fraction of cementite. Moreover, Figure 5b) shows that if the ladle is not inoculated with FeSi-La, then there is an improvement in the impact toughness inside the working layer (Region II).

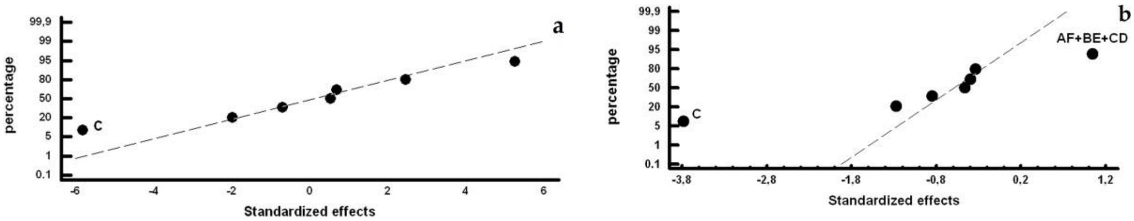

Figure 4. Representation of standardized effects on a normal probability plot versus the volume fraction of cementite, (**a**) Region I and (**b**) Region II.

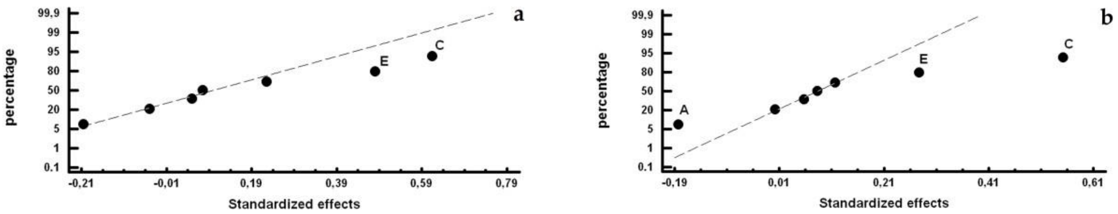

Figure 5. Representation of the standardized effects on a normal probability plot versus the unnotched Charpy test: (**a**) Region I and (**b**) Region II.

Figure 6 shows those factors with a significant effect on flexural strength. Inoculation with FeB is found to have a significant effect in both zones under analysis, Regions I and II. Thus, if we wish to increase this strength, then we should limit the addition of this inoculant to 3 kg/T. In Region I, inoculation with FeSi-La and the interactions AF + BE + CD also seemingly have a significant effect, see Figure 6a. Thus, in order to increase this strength, it would be advisable to inoculate with 2.7 kg/T FeSi-La. Table 12 analyses the interactions AF + BE + CD, showing that, in order to increase the flexural strength in this region, in addition to limiting the addition of FeB to 3 kg/T, it would be advisable to increase the addition of SiCa to 0.6 kg/T.

Table 12. Analysis of the interactions AF + BE + CD versus flexural strength in Region I.

A\F	**−1**	**+1**	**B\E**	**−1**	**+1**	**C\D**	**−1**	**+1**
−1	520.6	602.2	−1	565.5	642.3	−1	537.9	624.1
+1	632.2	592.1	+1	592.1	547.2	+1	610.3	574.8

Figure 6b shows, for Region II, that in addition to inoculation with FeB, the Liquidus Temperature and the addition of Mg also have a significant effect. Hence, in order to increase the flexural strength in this region, it is advisable to place both factors at their +1 level, i.e., 1270–1275 ◦C and 0.02%, respectively.

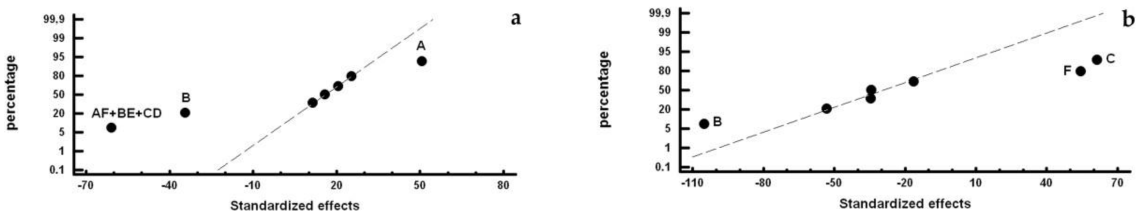

Figure 6. Representation of standardized effects on a normal probability plot versus flexural strength: (**a**) Region I and (**b**) Region II.

4. Conclusions

To improve the resistance to in-service cracking and spalling of the working layer of duplex work-rolls used in hot strip mill finishing stands, manufactured in Ni-hard cast iron alloyed with Mo, Nb and Mg, it is concluded that:

1. Inoculation with SiCa has a positive effect on the toughness of the material and seems to confirm its tendency to break up the carbide network.
2. Inoculation with FeB promotes heterogeneous nucleation of the NbC, but also reduces flexural strength and does not have a significant effect on the hardness of the material.
3. The addition of Mg leads to an improvement in flexural strength.
4. Mo remains in solid austenite solution, favouring the hardenability of the material.

On the other hand, within the levels analysed in this study, neither the %Si nor heterogeneous nucleation with La has a significant effect on the fracture strength of the surface of the aforementioned work layer. To improve this resistance, it is advisable to:

(1) Set the liquidus temperature within the 1270–1275 °C range

(2) Inoculate with 3 kg/T FeB

(3) Inoculate with 0.6 kg/T SiCa

(4) Inoculate with Mg.

Author Contributions: J.A.-L. conceived and designed the experiments; A.C.-V. performed the experiment; J.F.A.-A. analyzed the data and wrote the paper.

Funding: This research received no external funding.

Conflicts of Interest: The authors declare no conflict of interest.

References

1. Bravo, S.V.; Yamamoto, K.; Miyahara, H.; Ogi, K. Control of carbides and graphite in Ni-hard type cast iron for hot strip mills. *Mater. Sci. Forum* **2007**, *561–565*, 1023–1026. [CrossRef]
2. Vadiraj, A.; Balachandran, G.; Kamaraj, M. Effect of misch metal inoculation on microstructure, mechanical and wear properties of hypoeutectic gray cast irons. *Mater. Des.* **2009**, *30*, 4488–4492. [CrossRef]
3. Sergio, V.; Shikawa, S.; Yamamoto, K.; Miyahara, H.; Ogi, K.; Kamimiyada, K. Control of graphite formation in solidification of white cast iron. *Int. J. Cast Met. Res.* **2008**, *21*, 27–30. [CrossRef]
4. Gowda, D.; Kumar, D.C.; Sandeep, G.M.; Parthasarathy, A.; Chandrashekar, S. Tribological characterization of centrifugally cast graphite cast iron under dry and wet conditions. *Mater. Today Proc.* **2018**, *5*, 145–151. [CrossRef]
5. Chen, H.X.; Chang, Z.C.; Lu, J.C.; Lin, H.T. Effect of niobium on wear-resistance of 15% Cr white cast iron. *Wear* **1993**, *166*, 197–201. [CrossRef]
6. Bedolla-Jacuinde, A. Microstructure of vanadium-, niobium- and titanium-alloyed high-chromium white cast irons. *Int. J. Cast Met. Res.* **2001**, *13*, 343–361. [CrossRef]

7. Filipovic, M.; Kamberovic, Z.; Korac, M.; Jordovic, B. Effect of niobium and vanadium additions on the as-cast microstructure and properties of hypoeutectic Fe-Cr-C alloy. *ISIJ Int.* **2013**, *53*, 2160–2166. [CrossRef]
8. Zhang, Z.G.; Yang, C.K.; Zhang, P.; Li, W. Microstructure and wear resistance of high chromium cast iron containing niobium. *China Foundry* **2014**, *11*, 179–184.
9. Mourad, M.M.; El-Hadad, S.; Ibrahim, M.M. Effects of molybdenum addition on the microstructure and mechanical properties of ni-hard white cast iron. Trans. *Indian Inst. Met.* **2015**, *68*, 715–722. [CrossRef]
10. Noda, N.A.; Hu, K.; Sano, Y.; Ono, K.; Hosokawa, Y. Residual stress simulation for hot strip bimetallic roll during quenching. *Steel Res. Int.* **2016**, *87*, 1478–1488. [CrossRef]
11. Belzunce, F.J.; Ziadi, A.; Rodriguez, C. Structural integrity of hot strip mill rolling rolls. *Eng. Fail. Anal.* **2004**, *11*, 789–797. [CrossRef]
12. Drobne, M.; Urska, K.; Tercelj, M.; Fajfar, P.; Ltd, T. Thermal crack propagation during hot rolling and its influence on cast iron work roll degradation. In Proceedings of the Metal 2017: 26th International Conference on Metallurgy and Materials, Brno, Czech Republic, 24–26 May 2017.
13. Jonck, J.; Moema, J.S.; Jooste, J.; van Tonder, P. Investigation of the 'tiger skin' defect on indefinite chill rolls. *J. South. Afr. Inst. Min. Metall.* **2016**, *116*, 907–913. [CrossRef]
14. Ray, A.; Prasad, M.S.; Dhua, S.K.; Sen, S.K.; Jha, S. Microstructural features of prematurely failed hot-strip mill work rolls: Some studies in spalling propensity. *J. Mater. Eng. Perform.* **2000**, *9*, 449–456. [CrossRef]
15. Nilsson, M.; Olsson, M. An investigation of worn work roll materials used in the finishing stands of the hot strip mill for steel rolling. *Proc. Inst. Mech. Eng. Part J J. Eng. Tribol.* **2013**, *227*, 837–844. [CrossRef]
16. Paar, A.; Schneider, R.; Sommitsch, C. Influence of microstructural parameters of indefinite chill alloys on flexural strength and young's modulus. *Mater. Test.* **2018**, *60*, 239–244. [CrossRef]
17. Ibrahim, M.M.; El-Hadad, S.; Mourad, M. Enhancement of wear resistance and impact toughness of as cast hypoeutectic high chromium cast iron using niobium. *Int. J. Cast Met. Res.* **2018**, *31*, 72–79. [CrossRef]
18. Col, M.; Koc, F.G.; Oktem, H.; Kir, D. The role of boron content in high alloy white cast iron (Ni-hard 4) on microstructure, mechanical properties and wear resistance. *Wear* **2016**, *348–349*, 158–165. [CrossRef]
19. Iacoviello, F.; Iacoviello, D.; Di Cocco, V.; De Santis, A.; D'Agostino, L. Classification of ductile cast iron specimens based on image analysis and support vector machine. *Procedia Struct. Integr.* **2017**, *3*, 283–290. [CrossRef]
20. Takeda, H.; Yoneda, H.; Asano, K. Effect of silicon and bismuth on solidification structure of thin wall spheroidal graphite cast iron. *Mater. Trans.* **2010**, *51*, 176–185. [CrossRef]
21. Dun, X.L.; Liu, K.P.; Liu, H.S.; Lai, J.P.; Fu, X.H.; Zhou, J. Effect of multicomponent modifier on microstructure and mechanical properties of high Ni-Cr-Mo cast iron. *Mater. Sci. Technol.* **2011**, *27*, 1840–1845. [CrossRef]

22. Radulovic, M.; Fiset, M.; Peev, K. Effect of rare-earth elements on microstructure and properties of high chromium white iron. *Mater. Sci. Technol.* **1994**, *10*, 1057–1062. [CrossRef]
23. Prat, A.; Tort-Martorell, X.; Grima, P.; Pozueta, L. *Métodos Estadísticos. Control y Mejora de la Calidad*, 2nd ed.; Universidad Politécnica de Cataluña (UPC): Barcelona, Spain, 1997; pp. 165–195, ISBN 9788498802320.
24. Romero, R.; Zúnica, L.R. *Métodos Estadísticos en Ingeniería*; Universidad Politécnica de Valencia: Valencia, Spain, 2005; pp. 275–278, ISBN 9788497057271.
25. Johnson, R. *Probabilidad y Estadística para Ingenieros*, 3rd ed.; Prentice-Hall Hispanoamérica: México DF, México, 1997; pp. 489–494, ISBN 9688809616.
26. Box, G.E.P.; Hunter, W.G.; Hunter, J.S. *Estadística Para Investigadores: diseño, Innovación Y Descubrimiento,* 2nd ed.; Reverté: Barcelona; Spain, 2008; pp. 235–273, ISBN 9788429150445.
27. Song, J.M.; Lui, T.S.; Chen, L.H. Effect of carbon equivalent and spheroidizer addition on the morphology of strip cast white cast iron plate. *Int. J. Cast Met. Res.* **1999**, *12*, 83–91. [CrossRef]

materials

Article

Control over the Percentage, Shape and Size of theGraphite Particles in Martensitic White Castings Alloyed with Cr, Nb and Mg

Alberto Cofiño-Villar, Florentino Alvarez-Antolin *, Juan Asensio-Lozano and Maria Garcia-Garcia

Materials Pro Group, Departamento de Ciencia de los Materiales e Ingeniería Metalúrgica, Universidad de Oviedo, Independencia 13, 33004 Oviedo, Spain; UO229780@uniovi.es (A.C.-V.); jasensio@uniovi.es (J.A.-L.); magarc@uniovi.es (M.G.-G.)

* Correspondence: alvarezflorentino@uniovi.es

Received: 11 December 2018; Accepted: 29 December 2018; Published: 8 January 2019

Abstract: This paper presents the results obtained regarding the control by manufacturers of the percentage, shape, and size of the precipitated graphite in the working layer of duplex work-rolls used in hot strip mill finishing stands. This working layer is manufactured in a martensitic white cast iron alloyed with Cr and Nb to promote the precipitation of M3C and MC carbides, which provide a high wear resistance. The thermal cycling behavior of this layer also has a decisive influence on its service life. In this context, the percentage of graphite and its morphology play a very important role against said thermal cycling. With the aim of studying their effect on the sphericity of graphite, the analyzed industrial manufacturing factors worth highlighting include the liquidus temperature, the %Si, the use of an FeSi inoculant with traces of Lanthanum, inoculation with different amounts of FeB and SiCaMn, and the addition of Mg. At the periphery of the working layer, it was found that the use of the FeSi inoculant with traces of La promoted an increase in the density of counts of graphite, and that inoculation with FeB and the addition of 0.02% Mg diminished the nodularity of the graphite. Furthermore, throughout the entire thickness of the working layer, an increase in the amount of SiCaMn of up to 0.6 kg/T produced an increase in the size of the graphite particles and a marked improvement in their nodularity.

Keywords: work roll; white cast iron; graphite; inoculation; M_3C; MC; nodularity

1. Introduction

The failure mechanisms that arise in the surface of indefinite chill double-poured (ICDP) work rolls used in the finishing stands of hot strip mills involve phenomena of plastic deformation, abrasive wear, and cracking resulting from mechanical or thermal stresses [1]. These work rolls are manufactured by means of vertical centrifugal casting. The outer working layer is a martensitic white cast iron with the presence of graphite particles, while the core is a grey cast iron with a pearlitic matrix and dispersed spheroidal graphite. Its main alloying elements are Ni and Cr. The chemical composition may include Nb and Mo so as to improve the wear resistance of the working layer. The Nb forms carbides of the MC type with a hardness close to 2400 HV [2], while the Cr forms carbides of the M3C type [3], with a hardness close to 1200 HV [3], and the Ni and the Mo increase the hardenability of the material [4].

Thus, its microstructure will mainly be made up of proeutectic austenite, eutectic austenite, MC and M3C carbides, and graphite particles [5]. The austenite will be partially converted to martensite during air cooling after quenching at 1000 ◦C. During the rolling process, the working layer is heated on entering into contact with the sheet steel to be rolled. This heating is counteracted by spraying with water as the materials enters and exits the rolling pass [6]. During the initial stages in the finishing stands, the surface of the work rolls can reach over 500 ◦C, subsequently cooling down to 50 to 80 ◦C during water cooling [7], thereby producing thermal fatigue cycles. During the rolling pass, the work roll, likewise, undergoes compression forces that oppose thermal expansion. Hence, the service life of these rolls depends not only on their wear resistance but also on their fatigue behavior versus cyclic thermal and mechanical stresses [8]. In this context, in addition to the presence of carbides and their network distribution, the percentage of graphite and its morphology also play a very important role against said thermal cycling. Although crack nucleation is predominant in carbides, the subsequent progression of cracks may be favored by laminar graphite morphologies [9,10]. However, thermal conductivity is improved by this morphology compared to compact and spheroidal morphologies [11]. Thus, the laminar morphology of graphite improves the evacuation of heat, but favors the progression of the possible cracks that are generated in the carbide network during the rolling process. In contrast, a spheroidal geometry reduces the evacuation of heat, but constitutes a barrier to the progression of said cracks. Furthermore, graphite performs dry lubrication functions [12], reducing the coefficient of friction between the work roll and the sheet steel to be rolled [13]. One of the quality indicators established for the working layer of these rolls is the volume fraction of graphite. Optimal quality is achieved when this percentage falls within the 2 to 5% range [14]. Hence, one of the objectives of manufacturers and users of this type of work roll should be to control both the volume fraction of graphite and its geometry, in addition to knowing how the different variables of the manufacturing process affect these parameters. This paper presents a research methodology aimed at achieving these objectives in white cast irons alloyed with Ni, Cr, Mo, and Nb. To this end, a fractional Design of Experiments (DOE) is applied to identify those Factors in the manufacturing process that have a significant influence on the percentage of precipitated graphite and its geometry. The analyzed manufacturing Factors were: the use of inoculants based on FeSi alloys that include traces of lanthanum; inoculation with different percentages of Mg, FeB, and SiCaMn; the liquidus temperature, and the percentage of Si. Both the volume fraction and the number of counts of graphite increase with increasing equivalent carbon (EC), while Mg favors the precipitation of graphite with a spheroidal morphology [15,16]. There are many theories that justify the possible spheroidal growth of the graphite. It should be noted that, one of them, which has been proven on iron–carbon–silicon alloys with no sulphur contamination, vacuum caste, and without any presence known of any spheroidizing element (Mg, Ce, RE, etc.). This theory is based on the fact that graphite–liquid surface energy is higher in spheroidal graphite than in flake graphite, so that the crystalline growth of graphite will "curve" to reduce the free surface energy [17], or to decrease the energy–volume ratio [18]. The carbon equivalent implicitly includes factors, such as the %Si and the liquidus temperature, both of which are analyzed in this paper. The composition of FeSi alloys includes elements such as Ca, Al, and Ba, which, due to their high affinity with O, precipitate forming small oxide particles that can act as agents for the nucleation of graphite [19]. The use of inoculants with high percentages of Ca may promote a decrease in the grain size of the primary austenite and discontinuity of the carbide network [20]. La could increase the number of counts of graphite [21] and promote a finer structure of the carbide network [22]. B may combine with the N dissolved in the molten metal forming particles of BN that can act as heterogeneous nucleating agents of graphite [23]. B can also form carbides, thereby improving the wear resistance of the material [24,25]. Nb tends to reduce the eutectic cell, which could result in graphite of smaller size that is more uniformly distributed [19,26]. The formation of Nb carbides in the liquid phase could promote heterogeneous nucleation of graphite [27]. These carbides can also increase the hardness of the resulting material and improve its wear resistance [26]. The study was carried out on an industrial scale, casting eight work rolls with a diameter of 700 mm, a length of between 1800 and 2000 mm, and a thickness of the working layer of 50 mm.

2. Materials and Methods

Table 1 shows the standard chemical composition range for these working layers. The working layer was cast first and then the core was subsequently cast in two stages. In the first stage, an intermediate layer was cast aimed at ensuring optimum binding with the working layer. The remainder of the core was then cast. The working layer was smelted in a medium frequency induction furnace. The inoculants were placed on the bottom of the ladle when "bleeding" the molten iron. This bleeding occurred at a temperature of 1420 ◦C. The casting was carried out at a temperature of around 60 ◦C above the liquidus temperature. Demoulding took place 4 or 5 days after casting. After quenching at 1000 ◦C with air cooling, the roll was subjected to tempering at 400 ◦C.

Table 1. Chemical composition range of the working layer.

C	Si	Mn	Ni	Cr	Nb	Mo
3.2–3.4	0.9–1.0	0.8–1.0	4.4–4.6	1.7–1.8	0.65-0.75	0.25

The experimental procedure employed was based on the Design of Experiments statistical technique [28]. In this case, performing a total of 8 experiments, 6 industrial manufacturing Factors were analyzed, each Factor varying between 2 levels. Table 2 shows the analyzed Factors and levels, while Table 3 displays the Array of Experiments, together with the confounding pattern. These same manufacturing factors were studied in a previous work of the authors, where the resistance of the working layer against mechanical stresses was analyzed, correlating the results with the volume fraction of precipitated carbides [29]. The set of generators associated with this array of experiments is D = AB, E = AC, and F = BC, whose resulting relation definition is I = ABD = ACD = BCF, where I is a column formed only by some (+1) [28]. The resolution of this design is III, i.e., the main effects are confounded with the interactions of two Factors [28]. Table 4 shows the chemical composition of the inoculants employed in this study. Table 5 shows the main casting parameters of the 8 experiments (8 work rolls).

Table 2. Factors and Levels analyzed in the Design of Experiments (DOE).

Factors		Levels	
Code	**Metallurgical parameter correspondence**	**Level –1**	**Level +1**
A	FeSi-La (Kg/T)	0	2.7
B	FeB (Kg/T)	3	6
C	Liquidus Temperature (ºC)	1250-1255	1270-1275
D	Si (%)	0.8-0.85	1.1-1.15
E	SiCaMn (Kg/T)	0.3	0.6
F	Mg (%)	0	0.02

Table 3. Array of Experiments.

No.	A	B	C	D	E	F	Confounding Pattern
1	–1	–1	–1	+1	+1	+1	A+BD+CE
2	+1	–1	–1	–1	–1	+1	B+AD+CF
3	–1	+1	–1	–1	+1	–1	C+AE+BF
4	+1	+1	–1	+1	–1	–1	D+AB+EF
5	–1	–1	+1	+1	–1	–1	E+AC+DF
6	+1	–1	+1	–1	+1	–1	F+BC+DE
7	–1	+1	+1	–1	–1	+1	AF+BE+CD
8	+1	+1	+1	+1	+1	+1	

Table 4. Chemical composition of the inoculants used (% wt.).

Inoculants	Si	Ca	Al	Mn	Ti	Ba	C	Bi	S	P	B	La	Fe
FeSi-La	66.0	2.5	0.8	—	—	0.3	—	0.3	—	—	—	0.8	rem.
FeMn	2.0	—	—	69.4	—		5.8		0.014	0.130	—		rem.
SiCaMn	58.3	16.4	1.1	14.8	0.030		0.6		0.030	0.030	—		rem.
FeB	0.4	—	—	—	—		0.3		—	—	17.9		rem.

Table 5. Casting parameters in each experiment.

Casting Parameters	units	Experiment Number							
		1	2	3	4	5	6	7	8
C	%	3.35	3.46	3.4	3.28	2.94	3.04	3.02	3.04
Si	%	1.13	0.88	0.87	1.18	1.16	0.89	0.87	1.15
Mn	%	0.77	0.78	0.79	0.77	0.79	0.83	0.80	0.82
Ni	%	4.44	4.33	4.32	4.38	4.59	4.16	4.62	4.65
Cr	%	1.68	1.68	1.71	1.64	1.65	1.71	1.68	1.71
Mo	%	0.26	0.25	0.25	0.24	0.25	0.25	0.26	0.26
Mg	%	0.005	0.004	-	-	-	-	0.004	0.005
B	%	0.032	0.033	0.071	0.075	0.038	0.041	0.070	0.071
Nb	%	0.64	0.72	0.68	0.61	0.74	0.75	0.73	0.61
Liquidus Temperature	K	1525	1527	1526	1523	1546	1545	1545	1543

For the analysis of the volume fraction and morphology of the precipitated graphite, samples were obtained from two regions of the working layer. One of them, denominated Zone α, which comprised a thickness of 15 mm from the periphery of said working layer, and another, denominated Zone β, which comprised another 15 mm of thickness from a distance of 25 mm from the periphery up to a distance of 40 mm. The variables used as "responses" to characterize the graphite particles were:

- The volume fraction of graphite, denoted as *Vv*.
- The number of counts per mm^2 of graphite, denoted by N_A.
- The mean Feret diameter, denoted by F_{mean}. Defined as $\frac{[perimeter]^2}{4\pi(area)}$ This parameter defines a perfect nodule when its value is between 1 and 1.4
- The roundness parameter, denoted by R and defined asperfect nodule when its value is between 1 and 1.4.
- The percentage of counts of graphite with a roundness parameter equal to or less than 1.4.

These responses were determined using the Image ProPlus software (version 4.5.0.29) (Media

Cybernetics, Rockville, MD, USA), together with its Materials-Pro analysis module. For this purpose, 10 micrographs were randomly obtained at 100× in each experiment and in each region (Zones α and β). The metallographic samples were in the polished state, without etching with a chemical reagent. The optical microscope employed was a NIKON Epiphot 200 (Nikon, Tokyo, Japan), the images being obtained using the Omnimet Enterprise Image Analysis System. A JEOL JSM-5600 scanning electron microscope (JEOL, Nieuw-Vennep, The Netherlands), equipped with the characteristic energy dispersive X-ray (EDX, JEOL, Nieuw-Vennep, The Netherlands) microanalysis system, was used to obtain representative micrographs of the general microstructure. A CAMEBAX SX-100 electronic probe (CAMECA, Gennevilliers, France), equipped with BSE detectors (CAMECA, Gennevilliers, France), was used to obtain images of backscattered electrons. In these latter two cases, the samples were in the polished state and were etched with the chemical reagent Nital 4.

3. Results

Figure 1 shows the general microstructure of alloys of this type. The presence of M3C and MC carbides and dispersed graphite in an austenitic matrix, which has been transformed into Martensite during its air cooling, can be appreciated.

Figure 1a corresponds to a sample from Experiment 2 in an inner region of the working layer (Zone β), Figure 1b corresponds to a sample from Experiment 3 in an inner region of the working layer (Zone β), and Figure 1c corresponds to a sample from Experiment 6 in an outer region of the working layer (Zone α).

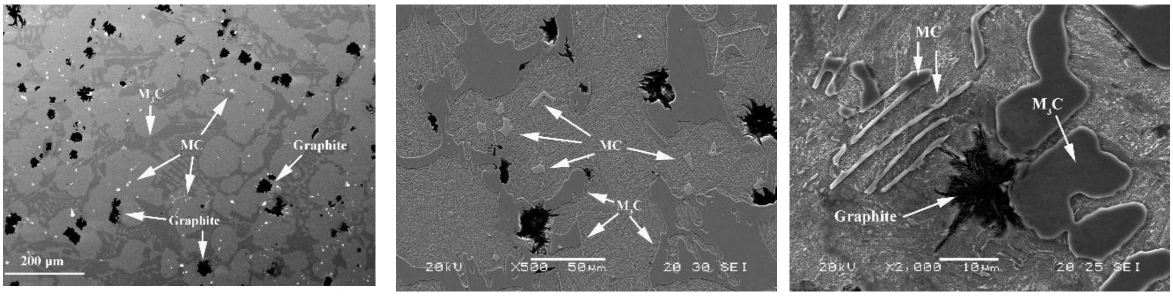

(**a**) (**b**) (**c**)

Figure 1. General microstructure of alloys of this type: (**a**) Micrograph obtained using an electronic microprobe, corresponding to Zone β in Experiment 2; (**b**) Micrograph obtained using a scanning electron microscope, corresponding to Zone β in Experiment 3; (**c**) Micrograph obtained using a scanning electron microscope, corresponding to Zone α in Experiment 6.

The standardized effects were compared on a normal probability plot using the Statgraphics Plus (version 5.1) program (Statgraphics Technologies, The Plain, VA, USA). The standardized effect is the ratio between the difference in the value of the response and its mean and standard deviation. This represents not only whether the value of the variable is above or below the mean but also how far it deviates from it. Those standardized effects that deviate from the straight line towards the ends on the normal probability plot are significant. Those that deviate to the left indicate that the value of the response increases at their −1 level and, analogously, while those that deviate to the right indicate that the value of the response increases at their +1 level [28]. Tables 6–9 show the mean values obtained for the studied responses and the standardized effects corresponding to the Factors and Interactions indicated in the column denominated “Confounding Pattern”. The first row of this column refers to the mean value obtained for each of the analyzed responses considering the eight experiments. Figures 2–6 show the representation of the standardized effects on a normal probabilistic plot for the analyzed responses.

Table 6. Average values and standardized effects for the volume fraction of precipitated graphite (V_V).

Experiment	Zone α		Zone β		Confounding Pattern
	Values	Effect	Values	Effect	
1	1.82	2.149	3.42	2.901	**Mean**
2	2.71	0.268	2.22	-0.003	**A+BC+CE**
3	2.32	-0.128	2.93	-0.108	**B+AD+CF**
4	2.57	-0.413	4.13	-0.548	**C+AE+BF**
5	2.19	-0.148	3.24	0.748	**D+AB+EF**
6	2.13	-0.303	2.94	-0.003	**E+AC+DF**
7	1.73	-0.308	2.02	-0.818	**F+BC+DE**
8	1.72	0.173	2.31	-0.453	**AF+BE+CD**

Table 7. Mean values and standardized effects for the number of count per mm^2 of graphite (N_A).

Experiment	Zone α		Zone β		Confounding Pattern
	Values	Effect	Values	Effect	
1	26.77	90.3	43.07	96.103	**Mean**
2	173.35	52.685	159.36	11.5	**A+BC+CE**
3	26.06	-31.76	156.10	1.885	**B+AD+CF**
4	142.36	-3.67	142.49	-58.305	**C+AE+BF**
5	88.56	-44.345	85.75	-50.0	**D+AB+EF**
6	136.04	-78.755	92.46	-39.84	**E+AC+DF**
7	114.44	-15.91	76.49	-46.195	**F+BC+DE**
8	14.82	-29.205	13.10	14.95	**AF+BE+CD**

Table 8. Mean values and standardized effects for the mean Feret diameter (Fmean).

Experiment	Zone α		Zone β		Confounding Pattern
	Values	Effect	Values	Effect	
1	17	17.361	28.83	19.146	**Mean**
2	11.61	-1.173	11.56	0.863	**A+BC+CE**
3	28.29	7.118	12.63	0.328	**B+AD+CF**
4	12.65	-0.053	16.61	3.478	**C+AE+BF**
5	14.76	2.983	18.49	10.218	**D+AB+EF**
6	11.84	9.343	17.05	7.508	**E+AC+DF**
7	11.74	0.953	14.91	5.903	**F+BC+DE**
8	31	8.108	33.09	-0.408	**AF+BE+CD**

Table 9. Mean values and standardized effects for the Roundness parameter (R).

Experiment	Zone α		Zone β		Confounding Pattern
	Values	Effect	Values	Effect	
1	1.75	1.789	1.75	1.81	**Mean**
2	1.87	-0.048	2	-0.025	**A+BC+CE**
3	1.72	0.113	1.72	-0.09	**B+AD+CF**
4	1.90	-0.043	1.98	-0.105	**C+AE+BF**
5	1.72	-0.043	2.01	0.025	**D+AB+EF**
6	1.59	-0.198	1.66	-0.28	**E+AC+DF**
7	2.06	0.113	1.81	-0.065	**F+BC+DE**
8	1.70	-0.073	1.55	0.02	**AF+BE+CD**

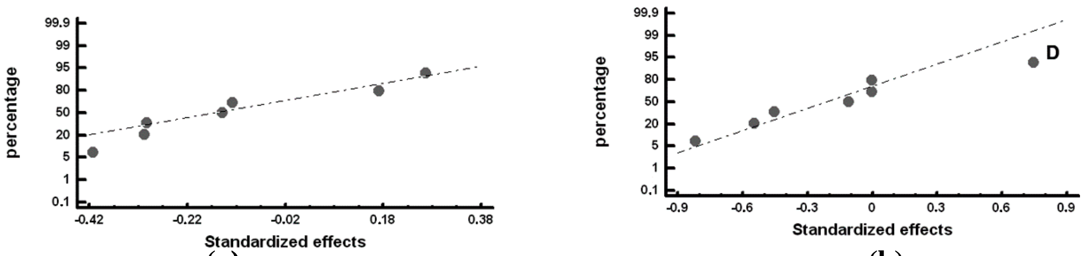

(**a**) (**b**)

Figure 2. Standardized effects on the volume fraction of graphite on a normal probability plot: (**a**)Factors with a significant effect on the outermost region of the working layer (Zone α); (**b**) Factorswith a significant effect on the inner region of the working layer (Zone β).

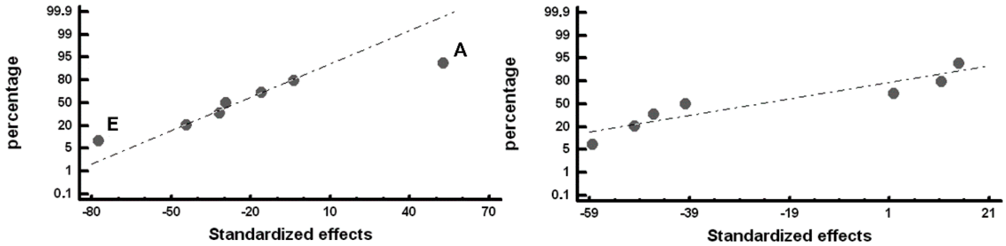

(**a**) (**b**)

Figure 3. Standardized effects on the number of counts per mm^2 of graphite, N_A, on a normal probability plot: (**a**) Factors with a significant effect on the outermost region of the working layer (Zone α); (**b**). Factors with a significant effect on the inner region of the working layer (Zone β).

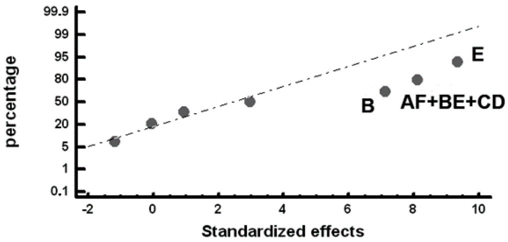

(**a**)

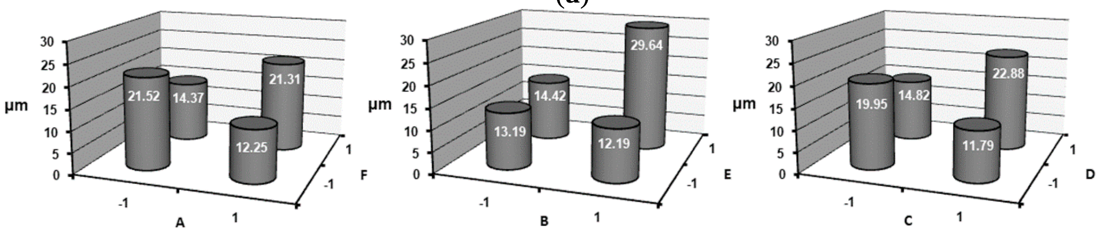

(**b**)

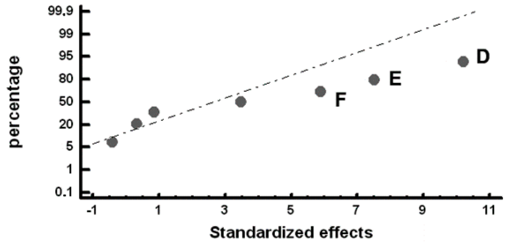

(**c**)

Figure 4. Standardized effects on the mean Feret diameter, F_{mean}, on a normal probability plot: (**a**) Factors with a significant effect on the outermost region of the working layer (Zone α); (**b**) Detailed analysis of Interaction AF + BE + CD, which has a significant effect; (**c**) Factors with a significant effecton the inner region of the working layer (Zone β).

Figure 2 shows the standardized effects on the volume fraction of graphite on a normal probability plot. Figure 2a shows that, in the outermost region of the working layer (Zone α), none of the analyzed Factors has a significant effect on the volume fraction of graphite. However, Figure 2b shows that Factor D (%Si) has a significant effect on the volume fraction of graphite in the inner region of the working layer (Zone β): situating this Factor at its +1 level (1.1–1.15 %Si) leads to an increase in the volume fraction of precipitated graphite.

Figure 3 shows the Factors with a significant effect on the number of counts of graphite per mm2, N_A. Figure 3a shows that Factor A (inoculation with FeSi-La) and Factor E (inoculation with SiCaMn) have a significant effect on N_A in the outermost region of the working layer: inoculation with FeSi-La and a low level of SiCaMn favor an increase in this variable. However, Figure 3b shows that none of the analyzed Factors has a significant effect on N_A in the inner region.

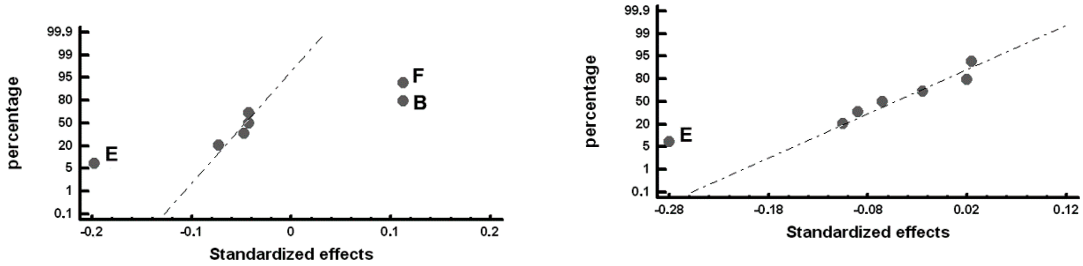

(**a**) (**b**)

Figure 5. Standardized effects on the Roundness parameter, *R*, on a normal probability plot: (**a**) Factors with a significant effect on the outermost region of the working layer (Zone *α*); (**b**) Factors with a significant effect on the inner region of the working layer (Zone *β*).

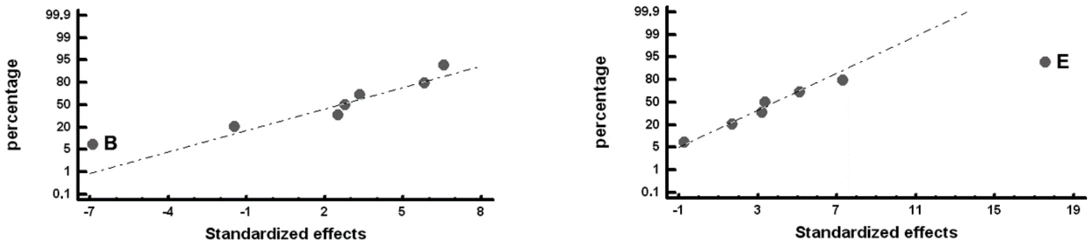

(**a**) (**b**)

Figure 6. Standardized effects on the percentage of graphite with a nodular morphology, on a normal probability plot: (**a**) Factors with a significant effect on the outermost region of the working layer (Zone *α*); (**b**) Factors with a significant effect on the inner region of the working layer (Zone *β*).

Figure 4 shows the Factors with a significant effect on the size of the counts of graphite, represented by the mean Feret diameter (Fmean). In Figure 4a, it can be observed that Factor E (inoculation with SiCaMn) and Factor B (addition of FeB) significantly influence this variable in Zone α of the working layer: both Factors at their +1 level increase Fmean. It, hence, follows that if Factor E at its −1 level increases the number of counts of graphite, it is because when it is placed at this level, it also reduces the size of said graphite. Interaction AF + BE + CD is also found to have a significant effect. Figure 4b provides a detailed analysis of this interaction, in which it is verified that it is interaction BE that has a significant effect, increasing the variable Fmean when both Factors are at their +1 level. In Figure 4c, it can be observed that Factor F (%Mg), Factor E (SiCaMn), and Factor D (%Si) have a significant effect on Fmean in the inner region of the working layer (Zone β): placing these Factors at their +1 level produces an increase in the value of this variable.

Figure 5 shows the Factors with a significant effect on the roundness parameter of the particles of graphite. Figure 5a shows the significant effect of Factor E (SiCaMn), Factor B (FeB), and Factor F (%Mg) in Zone α of the working layer: if these Factors are respectively situated at their −1, +1, +1 levels, this parameter increases and the nodularity of the graphite decreases. The deleterious effect of the %Mg on the nodularity of the graphite is worth noting.

This result could be justified by the fact that the residual Mg associated with the Mg added at Level +1 (0.02%) is insufficient to achieve a nodular geometry, promoting a “star-shaped” geometry that results in high roundness parameters [30]. Several graphite particles with this geometry can be observed in Figure 1a. Figure 5b shows the significant effect of Factor E (SiCaMn) in Zone β of the working layer. As occurred in Zone α of the working layer, if this Factor is situated at its −1 level, the roundness parameter increases. The addition of Mg does not have a significant effect in this region.

Furthermore, Figure 6 shows the Factors with a significant effect on the % graphite with a nodular geometry, i.e., with a roundness parameter below 1.4. In Zone α of the working layer, Factor B (FeB) is significant: To increase the % nodular graphite, this Factor must be placed at its −1 Level; see Figure 6a. Similarly, in Zone β of the working layer, the effect of Factor E (SiCaMn) is found to be significant: placing this Factor at its +1 level will increase the percent of particles of graphite with a spheroidal morphology; see Figure 6b.

4. Conclusions

This paper presents a research method for manufacturers and users of duplex work rolls used in hot strip mill finishing stands whose working layers is manufactured in Ni-hard cast iron alloyed with Nb and Mg that enables them to control the volume fraction and morphology of precipitated graphite. As to the manufacturing Factors and their Levels analyzed in this paper, it is concluded that:

1. Inoculation with SiCaMn has a significant effect on the shape and size of the precipitated graphite. An increase of 0.3 to 0.6 kg/T will lead to:
    a. an increase in the size of the precipitated graphite, and
    b. an improvement in the nodularity of the graphite.
2. Inoculation with FeB has a significant effect on the shape and size of the precipitated graphite inthe outermost region of the working layer. An increase of 3 to 6 kg/T will lead to:
    a. an increase in the size of the precipitated graphite,
    b. a deterioration in the nodularity of the graphite, and
    c. a reduction in the percentage of graphite with a nodular morphology.
3. In the outermost region of the working layer in contact with the sheet steel to be rolled:
    a. treatment with Mg, up to values of around 0.02%, has a deleterious effect on the nodularityof the graphite.
    b. inoculation with FeSiLa produces an increase in the density of graphite nodules.

Author Contributions: Methodology, J.A.-L. and F.A.-A.; software, A.C.-V.; validation, F.A.-A., J.A.-L., M.G.-G. and A.C.-V.; formal analysis, F.A.-A. and A.C.-V.; investigation, A.C.-V.; writing—original draft preparation, F.A.-A.; writing—review and editing, F.A.-A.; visualization, F.A.-A.; supervision, J.A.-L.

Funding: This research received no external funding.

Conflicts of Interest: The authors declare no conflict of interest.

References

1. Nilsson, M.; Olsson, M. An investigation of worn work roll materials used in the finishing stands of the hotstrip mill for steel rolling. *Proc. Inst. Mech. Eng. Part J J. Eng. Tribol.* **2013**, *227*, 837–844. [CrossRef]
2. Bedolla-Jacuinde, A. Microstructure of vanadium-, niobium- and titanium-alloyed high-chromium white cast irons. *Int. J. Cast Met. Res.* **2001**, *13*, 343–361. [CrossRef]
3. Pero-Sanz, J.A. *Fundiciones Férreas*; Dossat: Madrid, Spain, 1994; pp. 124–126.
4. Pero-Sanz, J.A. *Ciencia e Ingeniería de Materiales*, 4th ed.; Dossat: Madrid, Spain, 2000; p. 673.
5. Bravo, S.V.; Yamamoto, K.; Miyahara, H.; Ogi, K. Control of carbides and graphite in Ni-hard type cast iron for hot strip mills. In Proceedings of the Pricm 6: Sixth Pacific Rim International Conference on Advanced Materials and Processing, Cheju Isl, South Korea, 5–9 November 2007; Volume 561–565, p. 1023.
6. Guerrero, M.P.; Pérez, A.; Colás, R. Heat Transfer to the work rolls during hot rolling of steel. In Proceedings of the Rolls 2000 International Convention Centre Birmingham, Brno, Czech Republic, 23–25 May 2012; pp. 108–112.
7. Belzunce, F.J.; Ziadi, A.; Rodriguez, C. Structural integrity of hot strip mill rolling rolls. *Eng. Fail. Anal.* **2004**, *11*, 789–797. [CrossRef]
8. Noda, N.A.; Hu, K.J.; Sano, Y.; Ono, K.; Hosokawa, Y. Residual Stress Simulation for Hot Strip Bimetallic Roll during Quenching. *Steel Res. Int.* **2016**, *87*, 1478–1488. [CrossRef]
9. Tercelj, M.; Fajfar, P.; Godec, M.; Kugler, G. Characteristics of the thermal fatigue resistance for 3.1C, 0-8Si, 0.9Mn, 1.7Cr, 4.5Ni and 0-3Mo ICDP cast iron roll at 600 degrees C. *Mater. Tehnol.* **2017**, *51*, 515–521. [CrossRef]
10. Bombac, D.; Kugler, G.; Markoli, B.; Tercelj, M. Hot work roller surface layer degradation progress during thermal fatigue in the temperature range 500–700 degrees C. *Int. J. Fatigue* **2017**, *104*, 355–365. [CrossRef]
11. Holmgren, D.; Dioszegi, A.; Svensson, I.L. Effects of nodularity on thermal conductivity of cast iron. *Int. J. Cast Met. Res.* **2007**, *20*, 30–40. [CrossRef]
12. Sergio, V.; Ishikawa, S.; Yamamoto, K.; Miyahara, H.; Ogi, K.; Kamimiyada, K. Control of graphite formation in solidification of white cast iron. *Int. J. Cast Met. Res.* **2008**, *21*, 27–30. [CrossRef]
13. Gowda, D.; Kumar, D.C.; Sandeep, G.M.; Parthasarathy, A.; Chandrashekar, S. Tribological Characterization of Centrifugally Cast Graphite Cast Iron under Dry and Wet conditions. *Mater. Today Proc.* **2018**, *5*, 145–151. [CrossRef]
14. Valek, T.; Hampl, J. Prediction of Metallurgic Quality of ICDP Material before Tapping. *Phys. Procedia* **2011**, *22*, 191–196. [CrossRef]

15. Song, J.M.; Lui, T.S.; Chen, L.H. Effect of carbon equivalent and spheroidizer addition on the morphology of strip cast white cast iron plate. *Int. J. Cast Met. Res.* **1999**, *12*, 83–91. [CrossRef]
16. Konig, M.; Wessen, M. Influence of alloying elements on microstructure and mechanical properties of CGI. *Int. J. Cast Met. Res.* **2010**, *23*, 97–110. [CrossRef]
17. Geilenberg, H. A critical Review of the Crystalization of Graphite from Metallic Solutions after the "Surface Tension Theory". In *Recent Reaearch on Cast Iron*; Merchant, H.D., Ed.; Gordon and Breach: Materials Park, OH, USA, 1968; p. 195.
18. Sadocha, J.P.; Gruzleski, J.E. The Mechanism of Graphite Spheroid Formation in Pure Fe-C-Si Alloys. In *The Metallurgy of Cast Iron*; Lux, B., Ed.; Georgi Publishing: Materials Park, OH, USA, 1975; p. 443.
19. Strande, K.; Tiedje, N.; Chen, M. A Contribution to the Understanding of the Combined Effect of Nitrogen and Boron in Grey Cast Iron. *Int. J. Metalcast.* **2017**, *11*, 61–70. [CrossRef]
20. Dun, X.L.; Liu, K.P.; Liu, H.S.; Lai, J.P.; Fu, X.H.; Zhou, J. Effect of multicomponent modifier on microstructure and mechanical properties of high Ni-Cr-Mo cast iron. *Mater. Sci. Technol.* **2011**, *27*, 1840–1845. [CrossRef]
21. Onsoien, M.I.; Skaland, T.; Grong, O. Mechanisms of graphite formation in ductile cast iron containing cerium and lanthanum. *Int. J. Cast Met. Res.* **1999**, *11*, 319–324. [CrossRef]
22. Hamidzadeh, M.A.; Meratian, M.; Saatchi, A. Effect of cerium and lanthanum on the microstructure and mechanical properties of AISI D2 tool steel. *Mater. Sci. Eng. Struct. Mater. Prop. Microstruct. Process.* **2013**, *571*, 193–198. [CrossRef]
23. Eppich, R. Cast Iron Alloy Containing Boron. U.S. Patent WO 2006/133355 A3, 28 December 2006.
24. Col, M.; Koc, F.G.; Oktem, H.; Kir, D. The role of boron content in high alloy white cast iron (Ni-Hard 4) on microstructure, mechanical properties and wear resistance. *Wear* **2016**, *348*, 158–165. [CrossRef]
25. Tasgin, Y.; Kaplan, M.; Yaz, M. Investigation of effects of boron additives and heat treatment on carbides and phase transition of highly alloyed duplex cast iron. *Mater. Des.* **2009**, *30*, 3174–3179. [CrossRef]
26. Zhou, W.B.; Zhu, H.B.; Zheng, D.K.; Zheng, H.X.; Hua, Q.; Zhai, Q.J. Niobium alloying effect in high carbon equivalent grey cast iron. *China Foundry* **2011**, *8*, 36–40.
27. Chen, X.R.; Xu, J.; Hu, H.; Mohrbacher, H.; Kang, M.; Zhang, W.; Guo, A.M.; Zhai, Q.J. Effects of niobium addition on microstructure and tensile behavior of as-cast ductile iron. *Mater. Sci. Eng. Struct. Mater. Prop. Microstruct. Process.* **2017**, *688*, 416–428. [CrossRef]
28. Prat-Bartés, A.; Tort-Martorell, X.; Grima-Cintas, P.; Pozueta-Fernández, L.; Solé-Vidal, I. *Métodos Estadísticos*, 2nd ed.; Cataluña, U.P.d., Ed.; UPC: Barcelona, Spain, 2004; p. 376. ISBN 84-8301-786-5.
29. Cofiño-Villar, A.; Alvarez-Antolin, J.F.; Asensio-Lozano, J. Enhanced Fracture Strength in the Working Layer of Rolls Manufactured in Ni-Hard Cast Iron Alloyed with Mo, Nb and Mg. *Metals* **2018**, *8*, 725. [CrossRef]
30. Elliott, R. *Cast Iron Technology*; Buttherworths-Heinemann: Oxford, UK, 1988; p. 10. ISBN 9781483192307.

materials

Article

Enhancement of the Quality of the Shell-Core Bond Interface in Duplex Work Rolls Manufactured by Centrifugal Casting Used in Hot Strip Mills

Alberto Cofiño-Villar, Florentino Alvarez-Antolin * and Juan Asensio-Lozano

Materials Pro Group, Departamento de Ciencia de los Materiales e IngenieríaMetalúrgica, Universidad de Oviedo; Independencia 13, 33004 Oviedo, Spain; UO229780@uniovi.es (A.C.-V.); jasensio@uniovi.es (J.A.-L.)

***** Correspondence: alvarezflorentino@uniovi.es; Tel.: +34-985-181-949

Received: 29 March 2019; Accepted: 18 April 2019; Published: 20 April 2019

Abstract: To ensure the formation of a sound shell-core bond interface free of defects between the shell and the core in work rolls used in the finishing stands of hot strip mills, a complete fusion of this interface must be achieved, avoiding excessive mixing of the two components and the formation of hard, fragile microstructures. The shell is made of white cast iron, alloyed with Ni and Cr, and the core is manufactured of grey cast iron spheroidal graphite in a pearlitic matrix. It is thus advisable to inoculate the shell with 0.6 kg/T SiCaMn, as this promotes discontinuity in the carbide network and leads to an increase in the impact toughness of the bond interface. Furthermore, inoculation of the shell with FeSi-La should be avoided, as this inoculant leads to an increase in graphite counts, promoting it with a lamellar morphology at the edge of the bond and hence reducing the impact toughness in this interface. Addition of Mg to the shell has been found to produce an increase in hardness in the regions adjacent to the bond interface.

Keywords: shell-core bond; work rolls; centrifugal casting; hot strip mill; Cr_3C; NbC

1. Introduction

Indefinite chill double-poured (ICDP) work rolls are used in the finishing stands of hot strip mills (HSMs). These rolls usually comprise an outer shell made of cast iron, alloyed with Ni and Cr, and a grey cast iron core containing spheroidal graphite in a mostly pearlitic matrix. The term "indefinite" refers to the fact that part of the carbon in the shell appears in the form of carbides, while another, small part appears in the form of graphite [1]. The graphite performs dry lubrication functions [2] and reduces the coefficient of friction during the rolling process [3]. In the early phases of the hot strip mill, during the rolling passes, the shell or working layer is subjected to severe thermal fatigue cycles, reaching over 500 ◦C when it comes into contact with the steel strip and cooling down to 50 ◦C via the application of jets of water at the beginning and end of the rolling pass [4,5]. The presence of graphite facilitates the evacuation of heat due to its high thermal conductivity [6–8], flake graphite being more favorable for this purpose than graphite with a spheroidal morphology [9,10], although the latter improves mechanical strength [11]. During each rolling pass, the roll is thus subjected to compression forces that oppose thermal expansion. The majority of carbides will be formed with Cr with a stoichiometry of M3C, whose hardness can reach 1200 HV [12].

The presence of mixed carbides in a martensitic matrix ensures high wear resistance [13].To enhance wear resistance, Nb and Mo can be added, which form carbides with a stoichiometry of MC, obtaining hardness values that can reach 2400 HV [14].The Ni and almost all the Mo will be in solid solution to increase the hardenability of the austenite [15], which is mostly transformed into martensite after a heat treatment at 1000 ◦C and air cooling. These rolls are manufactured by centrifugal casting [16–21]. First, the shell of the roll (outer working layer) is cast, and once this outer shell has solidified, the core is cast in two stages. In the first stage, the part of the core intended to achieve an optimal bond with the shell is cast.This intermediate layer is necessary to create a good bond between the working layer and the core. Subsequently, the remainder of the core and roll necks are casted by gravity and solidify statically. The bonding between the working layer and the core is important since poor bonding can cause bond-related spalls [22]. Demolding takes place 4 or 5 days after casting. After heat treatment at 1000 ◦C with air cooling, the roll is subjected to tempering at 400 ◦C. To ensure the formation of a sound bond interface free of defects, complete bonding of the shell-core interface must be achieved, avoiding excessive mixing of the two components [23]. This bonding region will inevitably be contaminated with alloy elements, such as Cr, resulting in a microstructure of grey cast iron that combines spheroidal graphite and ledeburite [24]. During the casting process and the slow cooling during solidification until demolding, diffusive phenomena take place between the shell and the core, especially among the alloy elements of the shell towards the core. Hard, fragile microstructures may be formed in the shell-core bonding region that might weaken this bond when subjected to the pressures exerted during the rolling pass. The presence of non-metallic inclusions or microcavities can also adversely affect this bond. All this can lead to fracture and spalling between the shell and the core [25]. Employing a design of experiments (DOE), the aim of this paper is to identify those manufacturing factors involved in the manufacture of the shell that might have a significant effect on the quality of the shell-core interface. The impact toughness test is a reliable test method for assessing the quality of this bi-metal bond [26–28]. The analyzed factors were: The use of FeSi alloy inoculants with traces of lanthanum; inoculation with different percentages of SiCaMn, FeB, and Mg; the percentage of Si; and the liquidus temperature. Previous studies by the authors have analyzed the influence of these factors on the mechanical and microstructural properties of the working layers [29,30]. The present paper analyzes their effect on the shell-core bond interface in work rolls.

1. Materials and Methods

Table 1 shows the most usual chemical composition range for both the shell and the core of the work roll.

Table 1. Chemical composition range of the shell and the core (wt.%).

Part of the Roll	C	Si	Mn	Ni	Cr	Nb	Mo	Mg
Shell	3.2–3.4	0.9–1.0	0.8–1.0	4.4–4.6	1.7–1.8	0.65–0.75	0.25	-
Core	3–3.02	2.2–2.3	0.2–0.4	0.1–0.2	0–0.1	-	0–0.02	0.06–0.08

The experimental procedure employed is based on the design of experiments (DOE) statistical technique [31]. The purpose of applying this technique is to modify certain normal working conditions deliberately so as to produce changes in some of the responses under study. In this case, deliberate changes in six industrial manufacturing factors were analyzed, carrying out eight experiments in all, at an industrial scale. Table 2 shows the analyzed factors and levels, while Table 3 displays the resulting array of experiments. The set of generators associated with this array of experiments is D = AB, E = AC and F = BC. This means that the interactions ABD, ACE, and BCF are confounded with the mean.

The resolution of this design of experiments is III, which means that the main effects are confounded with the interactions of two factors [31]. The effect of a factor is the variation in the response function as a consequence of the variation of said factor. These effects are defined as the main effects. The effect of one factor may often depend on the value that another takes. When this occurs, these factors are said to interact. The importance of the main effects tends to be greater than that of the interactions of two factors, while the importance of the latter is in turn greater than that of the interactions of three factors, and so on. The "Confounding Pattern" column in Table 3 indicates those second-order interactions whose effects are confounded with the main effects. For example, the effect of the second-order interactions BD and CE will be confounded with the effect of factor A [31]. In this design of experiments (DOE), we analyze six factors, with two levels for each factor. Thus, if the DOE were not fractional, it would be necessary to estimate 26 effects (64 effects) in all. However, as the DOE is fractional, we only estimate eight effects (26−3): Hence, seven other effects are confounded in each effect (64/8 = 8). The confounding pattern should include all the effects confounded with one another. However, given that the number of confounding patterns is very high (8). Table 3 shows a restricted confounding pattern in which only the main effects and the two-factor interactions are represented.

Table 2. Factors and levels analyzed in the design of experiments (DOE).

Factors			Levels	
Code	**Description**	**Units**	**−1 Level**	**+1 Level**
A	FeSi-La	wt.%	0	0.27
B	FeB	wt.%	0.3	0.6
C	Liquidus Temperature	K	1523–1528	1543–1548
D	Si	wt.%	0.8–0.85	1.1–1.15
E	SiCaMn	wt.%	0.03	0.06
F	Mg	wt.%	0	0.04

Table 3. Array of experiments.

No.	A	B	C	D	E	F	Confounding Pattern
1	–1	–1	–1	+1	+1	+1	
2	+1	–1	–1	–1	–1	+1	A/BD/CE
3	–1	+1	–1	–1	+1	–1	B/AD/CF
4	+1	+1	–1	+1	–1	–1	C/AE/BF
5	–1	–1	+1	+1	–1	–1	D/AB/EF
6	+1	–1	+1	–1	+1	–1	E/AC/DF
7	–1	+1	+1	–1	–1	+1	F/BC/DE
8	+1	+1	+1	+1	+1	+1	AF/BE/CD

The experimental response is subject to random variation. This variation will follow a normal law, where its standard deviation reflects experimental error. The effects are linear combinations of the responses. Hence, applying the central limit theorem (CLT), they follow a normal law. Each main effect may be considered a random variable where the obtained value is an estimate of its mean. If all the effects were non-significant, they would follow an N(0,σ) law and would thus appear aligned in a representation of the effects on a normal probability plot. If any effect is significant, it will follow an N(μ,σ) law, not appearing aligned with the non-significant effects [31]. The standardized effect is the ratio between the difference in the value of the response of each experiment and the mean value of all the experiments and its standard deviation. This represents not only whether the value of the variable is above or below the mean, but also how far it deviates from it. Those standardized effects that deviate from the straight line towards the ends on the normal probability plot are significant. Those that deviate to the left indicate that the value of the response increases at their −1 level, while, analogously, those that deviate to the right indicate that the value of the response increases at their +1 level.

Table 4 shows the chemical composition of the inoculants used to manufacture the shell. The spheronization treatment was carried out in a covered ladle. The procedure consisted of introducing a 13 mm wire into the liquid alloy through an opening in the cover. The wire alloy was FeSiMg.

The research was conducted at an industrial scale, for which purpose eight rolls with a diameter between 680 and 700 mm, a length between 1800 and 2000 mm, and a thickness of the working layer between 50 and 55 mm were cast. Table 5 provides the casting parameters of each layer in the eight experiments.

Table 4. Chemical composition of the inoculants used to manufacture the shell (wt.%). Remainder Fe.

Inoculants	Si	Ca	Al	Mn	Ti	Ba	C	Bi	S	P	B	La	Mg
FeSi-La	66.0	2.5	0.8	-	-	0.3	-	0.3	-	-	-	0.8	
FeSiMg	28.7	-	-	-	-	-	-	-	-	-	-	-	15.0
SiCaMn	58.3	16.4	1.1	14.8	0.03		0.6		0.03	0.03	-		
FeB	0.4	-	-	-	-		0.3		-	-	17.9		

Table 5. Casting parameters in each experiment. (wt.%)

Casting Parameters	units	Experiment Number							
		1	2	3	4	5	6	7	8
C	%	3.35	3.46	3.4	3.28	2.94	3.04	3.02	3.04
Si	%	1.13	0.88	0.87	1.18	1.16	0.89	0.87	1.15
Mn	%	0.77	0.78	0.79	0.77	0.79	0.83	0.80	0.82
Ni	%	4.44	4.33	4.32	4.38	4.59	4.16	4.62	4.65
Cr	%	1.68	1.68	1.71	1.64	1.65	1.71	1.68	1.71
Mo	%	0.26	0.25	0.25	0.24	0.25	0.25	0.26	0.26
Mg	%	0.005	0.004	-	-	-	-	0.004	0.005
B	%	0.032	0.033	0.071	0.075	0.038	0.041	0.070	0.071
Nb	%	0.64	0.72	0.68	0.61	0.74	0.75	0.73	0.61
Liquidus Temperature	K	1525	1527	1526	1523	1546	1545	1545	1543

Three unnotched Charpy specimens measuring 10 mm × 10 mm × 50 mm were extracted from the bonding region between the shell and the core of the eight work rolls, the shell-core interface being parallel to the longest dimension. Accordingly, the direction of impact with the Charpy pendulum (HOYTOM, Leioa, Spain) was perpendicular to this bond interface. Three Charpy tests were performed for each experiment. Furthermore, a Vickers hardness profile was determined in each of the Charpy specimens, thereby enabling the transition between the shell and the core to be described. A load of 0.5 kg was applied for this purpose. In all, 23 Vickers indentations with a length of 8.8 mm were made in each Charpy specimen, with a separation of 400 µm between each indentation. The hardness profile of each experiment corresponds to the mean values of three measurements.

The factors with significant influence on the following responses were determined by means of the DOE:

1. Impact toughness using a Charpy pendulum.
2. Hardness of the part of the shell adjacent to the bond edge. To obtain this value, the hardness data obtained at a thickness of 2 mm from this edge were considered.
3. Hardness of the part of the core adjacent to the bond edge. Likewise, the hardness data obtainedat a thickness of 2 mm from this edge were considered to obtain this value.

The optical microscope employed was a NIKON Epiphot 200 (Nikon, Tokyo, Japan), and the different types of precipitated carbides were identified under a JEOL JSM-5600 (JEOL, Nieuw-

Vennep, The Netherlands) scanning electron microscope (SEM), equipped with the characteristic X-ray scattering microanalysis system (SEM-EDX).

3. Results

Figure 1 shows representative images of the microstructure in the shell-core bonding region. The appreciable penetration of M3C carbides towards the core is worth noting. The matrix phase in the part of the bond corresponding to the shell is martensite, while the constituent matrix of the bond in the part of the core is pearlite. In this latter part, ferrite regions (direct ferritization) can be observed around the spheroidal graphite. Figure 1e,f shows the presence of MC (NbC) carbides at the edge of the bond, even appearing in the core, in the region adjacent to the bond.

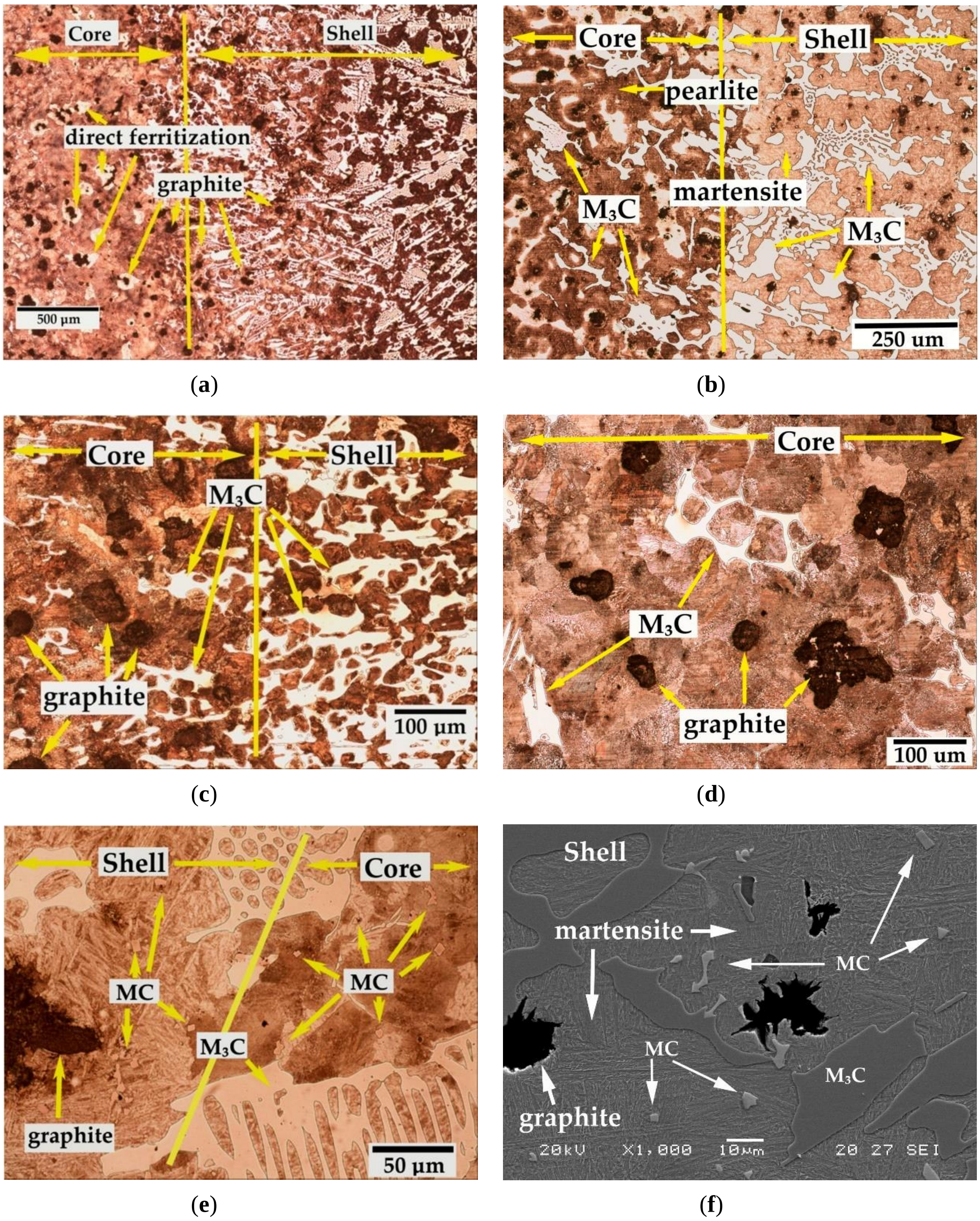

Figure 1. Microstructure of the shell-core bonding region. (**a**) Bonding region corresponding to experiment 2. Ferrite regions can be observed around the spheroidal graphite. Micrograph obtained by optical

microscopy. ×50 magnifications, (**b**) Bonding region corresponding to experiment 3. Martensite is the matrix phase in the part of the bond corresponding to the shell and pearlite is the constituent matrix of the bond in the part of the core. Micrograph obtained by optical microscopy. ×100 magnifications, (**c**) Bonding region corresponding to experiment 2. The penetration of M3C carbides towards the core is observed. Micrograph obtained by optical microscopy. ×200 magnifications, (**d**) Bonding region corresponding to experiment 8. M3C carbides are observed in the part of the core adjacent to the bond. Micrograph obtained by optical microscopy. ×200 magnifications, (**e**) Bonding region corresponding to experiment 1. MC (NbC) carbides are observed in the core. Micrograph obtained by optical microscopy. ×500 magnifications, (**f**) Bonding region corresponding to experiment 7. Presence of mixed carbides in a martensitic matrix. Micrograph obtained by scanning electron microscopy. ×1000 magnifications.

Table 6 shows the mean values obtained for the studied responses and the standardized effects corresponding to the factors and interactions indicated in the column denominated "Confounding Pattern". The row corresponding to the mean shows the average value obtained for each of the responses in the eight experiments.

Table 6. Mean values and standardized effects. HV0.5 (Vickers hardness with a load of 0.5 kg).

Experiment	Charpy test		Hardness of the shell		Hardness of the core		Confounding Pattern
	J/cm^2	Effect	HV0.5	Effect	HV0.5	Values	
1	3.45	3.18	590	619.37	290	296.75	Mean
2	2.69	-0.36	707	-1.75	281	-7.50	A+BC+CE
3	3.66	0.13	595	17.25	313	22.00	B+AD+CF
4	2.57	0.18	547	19.25	294	4.50	C+AE+BF
5	3.26	0.11	619	-14.25	297	8.00	D+AB+EF
6	3.07	0.56	527	-36.25	275	6.50	E+AC+DF
7	3.09	0.09	677	94.75	302	4.00	F+BC+DE
8	3.69	0.28	693	68.25	322	13.00	AF+BE+CD

Figures 2–5 show the representation of these standardized effects on a normal probabilistic plot, highlighting those that have a significant effect on these responses.

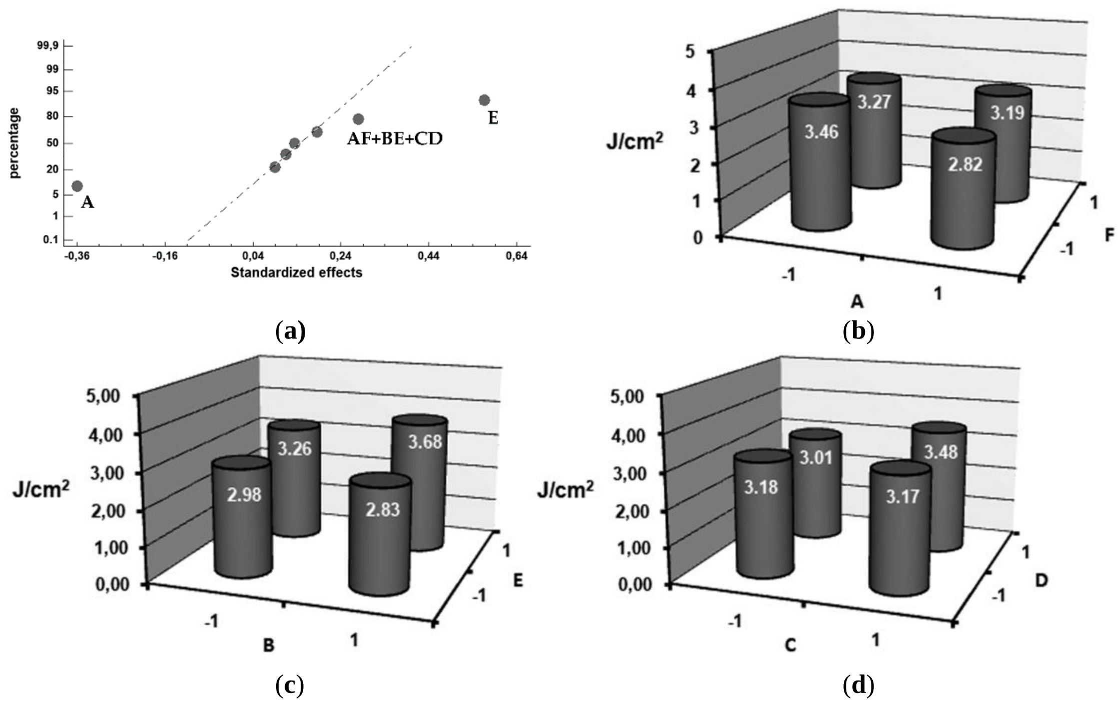

Figure 2. Factors that have a significant effect on impact toughness in the bond interface. (**a**) Standardized effects on a normal probability plot, (**b**) Analysis of interaction AF, (**c**) Analysis of interaction BE, (**d**) Analysis of interaction CD.

Figure 2a shows that the factors with a significant effect on impact toughness are E (inoculation with SiCaMn) and A (inoculation with FeSi-La). Setting both factors at their respective +1 (0.6 kg/T SiCaMn) and −1 (without FeSi-La) levels leads to an increase in said toughness. In a previous study by the authors, it was found that inoculation with SiCaMn promoted discontinuity of the carbide network [32], which increased the toughness of the shell [29]. In this case, it is verified that this effect also reaches the region of the shell in contact with the core.

In previous studies by the authors, it was similarly found that if the ladle is not inoculated with FeSi-La, then there is an improvement in the impact toughness inside the working layer [29,30,32]. In the present study, we have verified that this effect is maintained in the region of the shell-core bond. Previous studies [33,34] found that the aforementioned inoculant increases the number of graphite nodules and favors the precipitation of graphite with a lamellar morphology. If this inoculant should accumulate in the inner region of the working layer in contact with the core, it could damage the toughness of the shell-core bond. Given that FeSi-La has a density lower than the molten metal, it is suspected that FeSi-La tends to accumulate in the inner region of the shell during the centrifugation process. Figure 3a–c shows an example of this phenomenon. These micrographs show the region of the shell-core bond in a number of experiments in which FeSi-La was used as inoculant. The presence of flake graphite can be observed in these bonding regions.

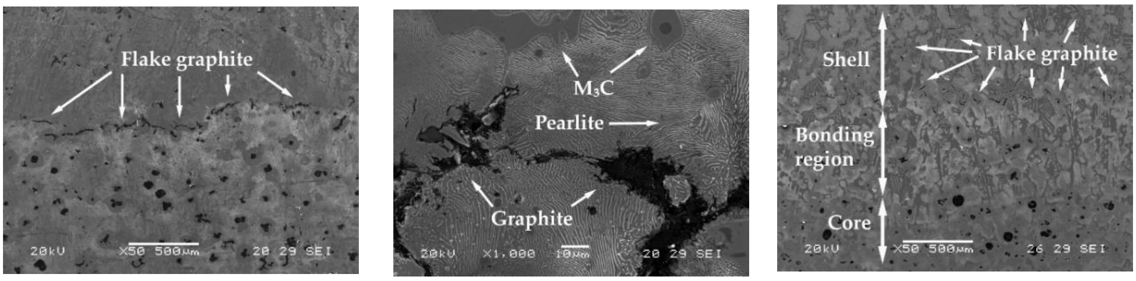

(**a**) (**b**) (**c**)

Figure 3. Flake graphite located in the region of the shell adjacent to the bond interface. This mainly appears in those experiments in which the shell was inoculated with FeSi-La, (**a**) Bonding region corresponding to experiment 2. Micrograph obtained by scanning electron microscopy. ×50 magnifications, (**b**) Bonding region corresponding to experiment 2. In addition to the presence of flake graphite, the presence of eutectic M_3C carbides and austenite fully transformed into pearlite can also be observed. Micrograph obtained by scanning electron microscopy. ×1000 magnifications, (**c**) Bonding region corresponding to experiment 4. Micrograph obtained by scanning electron microscopy. ×500 magnifications.

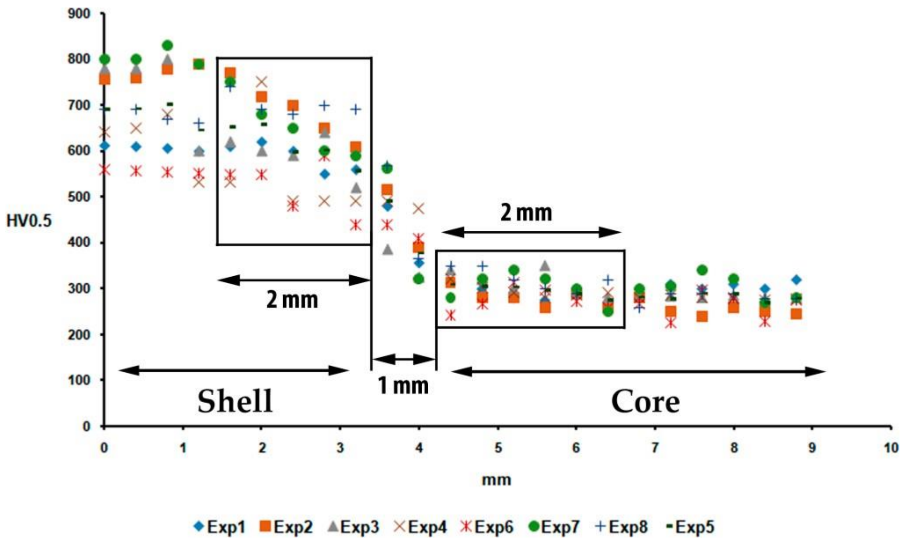

Figure 4. Hardness profiles in the shell-core bonding region. The statistically analyzed data were collected from a width of 2 mm in the regions of the shell and the core adjacent to the bond interface between both. Exp (Experiment).

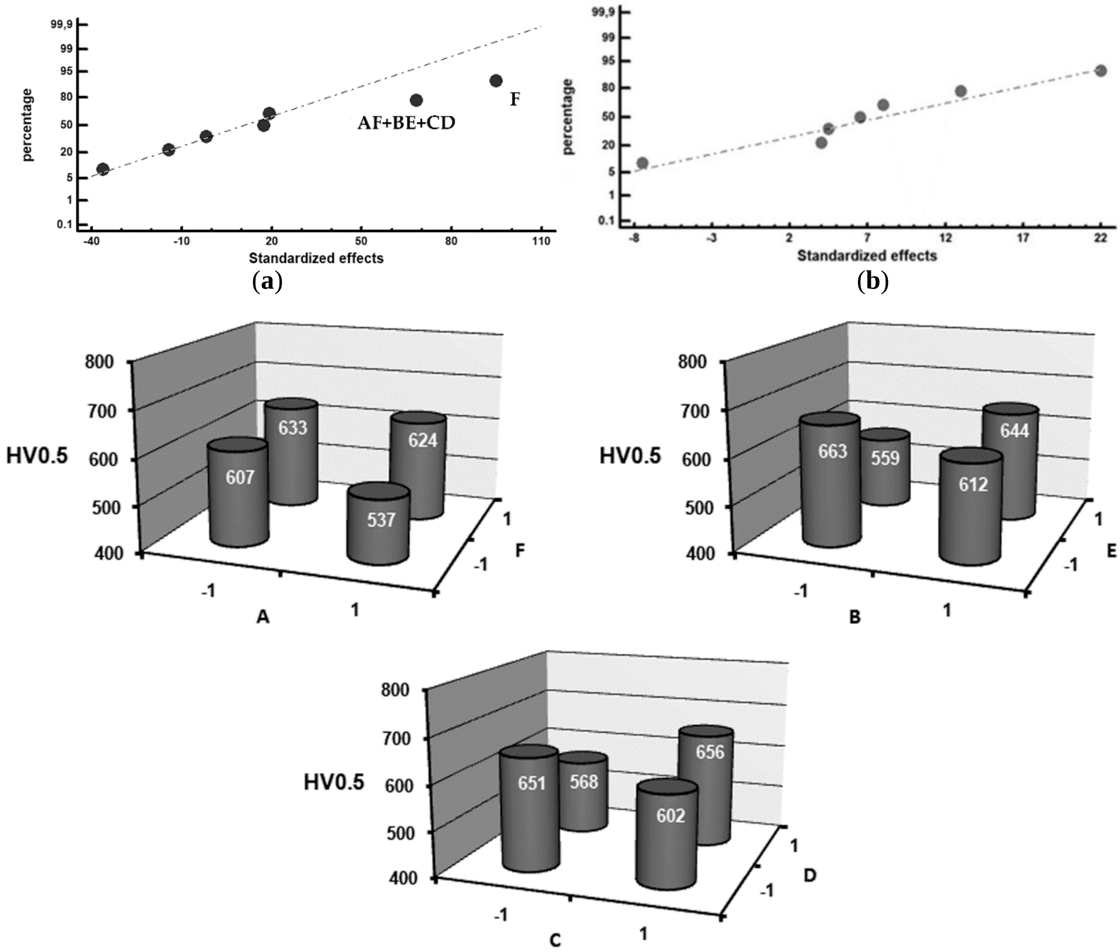

(**a**) (**b**)

(**c**) (**d**)

(**e**)

Figure 5. Factors that have a significant effect on hardness in the bond interface, (**a**) Standardized effects, on a normal probability plot, on the hardness in the shell region adjacent to the bond interface; (**b**)Standardized effects, on a normal probability plot, on the hardness in the core region adjacent to the bond interface; (**c**) Analysis of interaction AF; (**d**) Analysis of interaction BE; (**e**) Analysis of interaction CD.

It can also be seen that some of the interactions, namely AF, BE and CD, have a significant effect on toughness. Figure 2b through to Figure 2d shows the results of the analysis of these interactions. It appears that interaction BE, i.e., simultaneously setting both factors at their +1 level (inoculation with 6 kg/T FeB and 0.6 kg/T SiCaMn), produces an increase in toughness.

Figure 4 shows the hardness profiles obtained in the bonds in the eight experiments. It can be observed that there is a clear difference in hardness in the bond interface on the shell side between the different experiments. However, only minor differences are perceived on the side of the bond interface corresponding to the core. The statistically analyzed data correspond to a width of 2 mm in both regions. Figure 5 shows the representation of standardized effects, on a normal probability plot, of the average hardness values in the bonding region. Figure 5a corresponds to the bonding region of the shell, while Figure 5b corresponds to the bonding region of the core. Mg is seen to have a significant influence on the hardness of the bonding region adjacent to the shell. Setting this factor at its +1 level (its addition up to 0.04 wt.%) produces an increase in hardness. This could be due to its lightness, its concentration increasing in the innermost region of the shell during its solidification by centrifugation. Mg produces high subcooling during eutectic solidification. Consequently, it shows a high tendency to form white eutectic versus its grey counterpart, especially if the Si content is below 2% [12]. None of the analyzed factors are found to have a significant effect on hardness in the core region adjacent to the bond interface. It can also be seen that some of the interactions, namely AF, BE and CD, have a significant effect on toughness. Figure 5c through to Figure 5e shows the results of the analysis of these interactions. In interaction AF, the significant effect of factor F can seemingly be seen. If this factor is set at its +1 level, increases in hardness in this interaction occur. For interaction BE, there appears to be an increase in hardness when these factors are simultaneously set at their −1 (recall the graphitizing effect of SiCaMn) and +1 (bear in mind the bleaching effect of FeB in this case) levels. Regarding interaction CD, this appears to produce an increase in hardness if the liquidus temperature (factor C) and %Si (factor D) are both at their −1 levels (this would be equivalent to a greater volume fraction of eutectic constituent and a lower fraction in graphite volume), or both at their +1 levels (a smaller volume fraction of the eutectic constituent and greater hardening due to the Si solid solution).

4. Conclusions

To enhance the quality of the shell-core interface in work rolls used in the finishing stands of hot strip mills, manufactured by indefinite chill double-poured centrifugal casting, it is advisable to:

1. Inoculate the shell (working layer) with 0.6 kg/T SiCaMn, as this promotes discontinuity in the carbide network and leads to an increase in the impact toughness of the bond interface.

2. Avoid inoculation with FeSi-La, as this inoculant promotes an increase in the number of graphite nodules per unit area and a lamellar morphology of this graphite, reducing the impact toughnessin this bond interface.

3. Furthermore, the addition of Mg at values around 0.04 wt.% has been found to produce an increase in hardness in the shell region adjacent to the bond interface. This is due to two simultaneous phenomena:

    a. The tendency of Mg to accumulate in the innermost region of the shell during centrifugalcasting as a result of its low density.

    b. Its tendency to favor the precipitation of white eutectic versus grey eutectic when the Si content is low.

Author Contributions: Methodology, J.A.-L. and F.A.-A.; software, A.C.-V.; validation, F.A.-A., J.A.-L., and A.C.-V.; formal analysis, F.A.-A. and A.C.-V.; investigation, A.C.-V.; writing—original draft preparation, F.A.-A.;writing—review and editing, F.A.-A.; visualization, F.A.-A.; supervision, J.A.-L.

Funding: This research received no external funding.

Conflicts of Interest: The authors declare no conflict of interest.

References

1. Strilkova, L.; Valek, T.; Tanger, L.T.D. Microstructural investigation of icdp iron designed for working layers of composite centrifugally cast rolls in hot rolling mills. In Proceedings of the 21st International on Conference Metallurgy and Materials, Brno, Czech Republic, 23–25 May 2012; pp. 788–794.
2. Sergio, V.; Ishikawa, S.; Yamamoto, K.; Miyahara, H.; Ogi, K.; Kamimiyada, K. Control of graphite formationin solidification of white cast iron. *Int. J. Cast Met. Res.* **2008**, *21*, 27–30. [CrossRef]
3. Gowda, D.; Kumar, D.C.; Sandeep, G.M.; Parthasarathy, A.; Chandrashekar, S. Tribological characterizationof centrifugally cast graphite cast iron under dry and wet conditions. *Mater. Today Proc.* **2018**, *5*, 145–151. [CrossRef]
4. Belzunce, F.J.; Ziadi, A.; Rodriguez, C. Structural integrity of hot strip mill rolling rolls. *Eng. Fail. Anal.* **2004**, *11*, 789–797. [CrossRef]

5. Guerrero, M.P.; Pérez, A.; Colás, R. *Heat Transfer to Work Rolls during Hot Rolling Steel*; International Convention Centre Birmingham: Birmingham, UK, 1996; pp. 108–112.
6. Wan, J.; Qing, J.J.; Xu, M.Z. Designing a novel graphitic white iron for metal-to-metal wear systems. *Metall. Mater. Trans. A-Phys. Metall. Mater. Sci.* **2019**, *50A*, 1162–1174. [CrossRef]
7. Holmgren, D.; Svensson, I.L. Thermal conductivity—structure relationships in grey cast iron. *Int. J. Cast Met. Res.* **2005**, *18*, 321–330. [CrossRef]
8. Elmabrouk, O.; Erfan, O.M.; Kalkanli, A. The effect of magnisium to sulfur ratio on the graphite morphology of graphite cast iron produced at differrent section thicknesses. *Manuf. Sci. Technol.* **2012**, *383–390*, 5880–5885.
9. Wang, G.Q.; Chen, X.; Li, Y.X.; Liu, Z.L. Effects of inoculation on the pearlitic gray cast iron with high thermal conductivity and tensile strength. *Materials* **2018**, *11*, 1876. [CrossRef]
10. Ding, X.F.; Huang, H.; Matthias, W.; Huang, S.Y.; Lu, Y.H.; Feng, Q. Development of high performance cast iron with combination of improved mechanical and thermal properties through mo addition. *Metall. Mater.Trans. A-Phys. Metall. Mater. Sci.* **2018**, *49A*, 3173–3177. [CrossRef]
11. Lekakh, S.N.; Qing, J.; Richards, V.L.; Amer Foundry, S. Investigation of cast iron processing to produce controlled dual graphite structure in castings. *Trans. Am. Foundry Soc.* **2012**, *120*, 297–306.
12. Pero-Sanz, J.A. Fundiciones Férreas. Dossat: Madrid, Spain, 1994; p. 154.
13. Xin, Z.; Perks, M.C. Centrifugal Casting Hss Roll for Narrow Strip Rod Mills. In Proceedings of the 42nd Mechanical Working and Steel Processing Conference, Toronto, ON, Canada, 22–25 October 2000; Iron and Steel Society: Toronto, ON, Canada, 2000; pp. 183–191.
14. Bedolla-Jacuinde, A. Microstructure of vanadium-, niobium-and titanium-alloyed high-chromium white cast irons. *Int. J. Cast Met. Res.* **2001**, *13*, 343–361. [CrossRef]
15. Mourad, M.M.; El-Hadad, S.; Ibrahim, M.M. Effects of molybdenum addition on the microstructure and mechanical properties of ni-hard white cast iron. *Trans. Indian Inst. Met.* **2015**, *68*, 715–722. [CrossRef]
16. Antolin, J.F.A.; Perez, C.H.A.; Lozano, J.A. Identification of metallurgical manufacturing factors with a significant effect on the flexural strength of mottled ni-hard cast irons through a design of experiments approach. *Int. J. Met.* **2017**, *11*, 467–474.
17. Gowda, H.S.D.; Mukunda, P.G.; Herbert, M.A. Correlation of tribological properties with microstructure and mechanical properties of graphite cast irons centrifugally cast for engine liner. *Trans. Indian Inst. Met.* **2014**,*67*, 731–740. [CrossRef]
18. Qihong, C.; Zhan-Wen, W.; Yi, J.; Yehua, J.; Fei, L.; Hanguang, F. A study of centrifugal cast high boron high speed steel. *Mater. Werkst.* **2014**, *45*, 582–590. [CrossRef]
19. Yamamoto, M.; Narita, I.; Miyahara, H. Fractal analysis of solidification microstructure of high carbon high alloy cast roll manufactured by centrifugal casting. *Tetsu Hagane J. Iron Steel Inst. Jpn.* **2013**, *99*, 72–79. [CrossRef]
20. Bai, Y.L.; Luan, Y.K.; Song, N.N.; Kang, X.H.; Li, D.Z.; Li, Y.Y. Chemical compositions, microstructure and mechanical properties of roll core used ductile iron in centrifugal casting composite rolls. *J. Mater. Sci. Technol.* **2012**, *28*, 853–858. [CrossRef]
21. Fu, H.G.; Xiao, Q.; Xing, H.D. A study of segregation mechanism in centrifugal cast high speed steel rolls. *Mater. Sci. Eng. A Struct. Mater. Prop. Microstruct. Process.* **2008**, *479*, 253–260. [CrossRef]

22. Mitrovic, D.; Mrvar, P.; Petric, M. Characterization of cast-iron gradient castings. *Mater. Tehnol.* **2015**, *49*, 871–875. [CrossRef]

23. Fernandez-Pariente, I.; Ziadi, A.; Belzunce, F.J. Study of the high strenght steel-nodular iron interphase developed in bimetallic rolls produced by centrifugal casting. *Bol. Soc. Esp. Ceram. Y Vidr.* **2004**, *43*, 263–266.

24. Schon, C.G.; Sinatora, A. Hot rolling mill roll microstructure interpretation: A computational thermodynamics study. *J. Phase Equilibria* **2001**, *22*, 470–474. [CrossRef]

25. Sinha, P.; Indimath, S.S.; Mukhopadhyay, G.; Bhattacharyya, S. Failure of a work roll of a thin strip rollingmill: A case study. *Struct. Integr.* **2014**, *86*, 940–948. [CrossRef]

26. Ozdemir, Z. Effect of heat treatment on the impact toughness of 'high-chromium cast iron—Low alloy steel' bimetal components. *Met. Sci. Heat Treat.* **2017**, *58*, 738–741. [CrossRef]

27. Yazdani, M.; Toroghinejad, M.R.; Hashemi, S.M. Effects of heat treatment on interface microstructure and mechanical properties of explosively welded ck60/st37 plates. *J. Mater. Eng. Perform.* **2016**, *25*, 5330–5342. [CrossRef]

28. Imran, M.K.; Masood, S.H.; Brandt, M.; Bhattacharya, S.; Mazumder, J. Direct metal deposition (dmd) of h13 tool steel on copper alloy substrate: Evaluation of mechanical properties. *Mater. Sci. Eng. A Struct. Mater. Prop. Microstruct. Process.* **2011**, *528*, 3342–3349. [CrossRef]

29. Cofino-Villar, A.; Alvarez-Antolin, J.F.; Asensio-Lozano, J. Enhanced fracture strength in the working layer of rolls manufactured in ni-hard cast iron alloyed with mo, nb and mg. *Metals* **2018**, *8*, 725. [CrossRef]

30. Cofino-Villar, A.; Alvarez-Antolin, F.; Asensio-Lozano, J.; Garcia-Garcia, M. Control over the percentage, shape and size of the graphite particles in martensitic white castings alloyed with cr, nb and mg. *Materials* **2019**, *12*, 185. [CrossRef]

31. Prat-Bartés, A.; Tort-Martorell, X.; Grima-Cintas, P.; Pozueta-Fernández, L.; Solé-Vidal, I. *Métodos Estadísticos*, 2nd ed.; Barcelona: Barcelona, Spain, 2004; p. 376.

32. Dun, X.L.; Liu, K.P.; Liu, H.S.; Lai, J.P.; Fu, X.H.; Zhou, J. Effect of multicomponent modifier on microstructure and mechanical properties of high ni-cr-mo cast iron. *Mater. Sci. Technol.* **2011**, *27*, 1840–1845. [CrossRef]

33. Asensio-Lozano, J.; Alvarez-Antolin, J.F.; Voort, G.F.V. Identification and quantification of active manufacturing factors for graphite formation in centrifugally cast nihard cast irons. *J. Mater. Process. Tech.* **2008**, *206*, 202–215. [CrossRef]

34. Asensio-Lozano, J.; Alvarez-Antolin, J.F. Saturated fractional design of experiments: Toughness and graphite phase optimizing in nihard cast irons. *J. Mater. Eng. and Perform.* **2008**, *17*, 216–223. [CrossRef]

metals

Article

Improvement in the Resistance to Wear of Work-Rolls Used in Finishing Stands of the Hot Strip Mills

Alberto Cofiño-Villar, Florentino Alvarez-Antolin * and Carlos Hugo Alvarez-Perez

Department of Material Science and Metallurgical Engineering, University of Oviedo, 33004 Oviedo, Spain; UO229780@uniovi.es (A.C.-V.); alvarezhugo@uniovi.es (C.H.A.-P.)

* Correspondence: alvarezflorentino@uniovi.es

Received: 22 October 2021; Accepted: 19 November 2021; Published: 21 November 2021

Abstract: Work-rolls manufactured through the Indefinite Chill Double Poured (ICDP) method present an exterior work layer manufactured in a martensitic white cast iron alloyed with 4.5 %Ni, 1.7 %Cr, and 0.7 %Nb (wt.%). In its microstructure, there are abundant carbides of the type M3C and MC, which give high resistance to wear, and graphite particles which improve the service behaviour of the rolls against thermal cycling. The core of the rolls is manufactured in grey cast iron of pearlitic matrix and spheroidal graphite. These work-rolls are used in the finishing stands in Hot Strip Mills for rolling slabs proceeding from continuous casting at 1200 ◦C. Through the application of a Design of Experiments (DoE), an attempt has been made to identify those manufacturing factors which have a significant effect on resistance to wear of these rolls and to find an optimal combination of levels of these factors which allow for improvement in resistance to wear. To increase resistance to wear, it is recommended to situate, simultaneously, the liquidus temperature and the percentage of Si in the respective ranges of 1250–1255 ◦C and 1.1–1.15 (wt.%). Higher liquidus temperatures favour the presence of the pro-eutectic constituent rather than the eutectic constituent. The outer zone of the work layer, in contact with the metal sheet, which is being rolled, does not show the graphitising effect of Si (0.8–1.15 wt.%). On the contrary, it confirms the hardening effect of the Si in solid solution of the ferrite. The addition of 0.02% of Mg (wt.%) and the inoculation of 6 kg/T of FeB tend to eliminate the graphitising effect of the Si, thus favouring that the undissolved carbon in the austenite is found to form carbides in contrast to the majority formation of graphite.

Keywords: hot strip mills; white cast iron; hot wear; graphite; Fe_3C and NbC carbides

1. Introduction

The work-rolls manufactured with the Indefinite Chill Double Poured (ICDP) method are used in the last two finishing stands of the hot strip mills (HSMs). The term "indefinite" refers to the fact that part of the carbon in the shell appears in the form of carbides, while another small part appears in the form of graphite [1]. The dispersed interdendritic graphite is the result of the solidification of the residual eutectic liquid that provides an optimum combination of wear life and enhanced thermal shock resistance. In the hot strip mills, the flat slabs, proceeding from continuous casting, are rolled [2]. The rolled slabs are heated to temperatures of 1200 ◦C or higher, in order to go through a large reduction in the hot strip mill at a range of temperatures between 1100–1200 ◦C. Subsequently, in the finishing stand, the metal sheet reaches a final reduction for the winding of the metal sheet. The finishing temperature usually oscillates between 820 ◦C and 920 ◦C.

The finishing stand is made up of seven rolling stands. The work-rolls of these stands should have a high level of resistance to wear, resistance to rusting, resistance to fracture, and an excellent surface finish [2,3].The work layer is exposed to periodic cycles of heating and cooling during contact with the metal and subsequent cooling with water. The maximum temperatures reached on the surface of the work-roll could exceed 500 ◦C. This heating is countered with jets of water, both before and after passing through rolling. The minimum temperatures could reach 100 ◦C [4].

During rolling, the work-roll is exposed to compression forces which resist thermal dilation, and which cause cycles of mechanical forces complementary to thermal cycles. Therefore, the service life of the material will depend on its resistance to wear as well as its resistance to thermal and mechanical cycles [3,5,6]. These rolls are manufactured by vertical centrifugal casting. In the first step, the work layer is cast and, once this outer shell has solidified, the core is cast. The core is cast in two steps. In the first step, the part of the core intended to achieve an optimal bond with the shell is cast. Subsequently, the remainder of the core and roll necks are casted by gravity and solidify statically; Figure 1 shows this process. The exterior work layer is a martensitic white cast iron with graphite particles, and the core is a grey cast iron with a pearlitic matrix and spheroidal graphite. The main alloying elements in the work layer are Ni (4.4–4.6 wt.%) and Cr (1.7–18 wt.%). To improve resistance to wear, Nb (0.7 wt.%) and Mo (0.25 wt.%) are also included in its chemical composition [7–9]. The Nb forms carbides with an MC stoichiometry and with a hardness close to 2400 HV, while, in the Cr in compositions of lower than 15%, carbides of the type M3C and with a hardness of close to 1200 HV are formed [10,11]. The Ni and the Mo increase hardenability [12]. The microstructure is made up of pro-eutectic austenite and a double eutectic constituent; on the one hand, that which is derived from a ledeburitic eutectic is formed by austenite and carbides, and, on the other hand, that which is formed by austenite and graphite [13]. The presence of graphite increases resistance to thermal shock. At the same time, the graphite performs functions of dry lubrication, thus reducing the coefficient of friction between the roll and the sheet of steel [4,14–18].

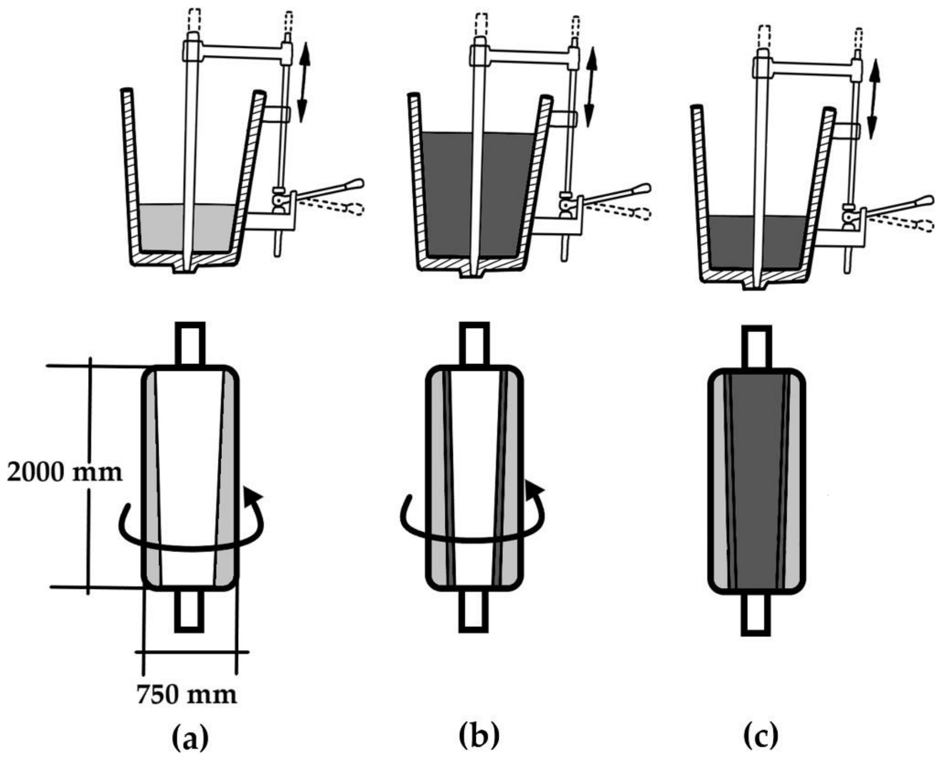

Figure 1. Manufacture by centrifugal casting: (**a**) casting of outer working layer; (**b**) casting of the core intended to achieve an optimal bond with the outer working layer; (**c**) casting of the remainder of the core and roll necks by gravity and static solidification.

The aim of this study is to identify those manufacturing factors which have a significant effect on resistance to wear on the work layer. Apart from the microstructural characteristics of the work layer, the rate of wear will depend mainly on temperature, the speed of sliding, and the load applied [19]. Among the studied factors are the use of alloys of FeSi with traces of Lanthanum as an inoculant and the inoculation of the hot metal with different contents of Mg, FeB, and SiCaMn.

Also, the effects of the variation in the Liquidus Temperature were studied, as well as the percentage of Si. The liquidus temperature indicates the volume fraction of the eutectic constituent. If the liquidus temperature is low, it means that the eutectic constituent is the majority, compared to the proeutectic austenite. The ledeburitic matrix exhibits high wear resistance, poor toughness, and low thermal shock resistance due to the ceramic nature of the cementite carbides. These car- bides exhibit true continuity in the microstructure; thus, they become the true mechanical matrix [20]. Inoculation with La produces an increase in the number of beads, by unit area, of graphite, and the thinning of the carbide network [21–23]. B has a whitening effect, thus increasing the volume fraction of carbides and improving the resistance to wear of the material [24,25]. The Nb tends to reduce the size of the eutectic cell, which could produce graphite of a smaller size and that is more uniformly distributed. The NbC incrementally improves abrasive wear resistance, and, on the other hand, could favour the heterogeneous nucleation of the graphite [25–27]. At the same time, inoculation with FeB favours heterogeneous nucleation of the NbC. The Mg performs as a nucleating agent of the graphite, thus favouring its spheroidal morphology [28–30]. However, the Mg produces subcooling during eutectic solidification, which favours the formation of ledeburitic eutectics [10]. In previous studies, it was concluded that inoculation with SiCaMn, apart from increasing the volume fraction of graphite and its nodularity, produced fractioning in the continuity of the carbide network, which favours an improvement in the toughness performance of the work layer [23,28]. On the other hand, it was shown that, with effective quantities of Mg (around 0.02%), a deterioration in the nodularity of the graphite was produced [23]. This same effect was observed with the inoculation of FeB [23]. In previous works, the properties of the working layer were characterized. Hardness of the working layer is between 550 and 650 HV. The flexural strength, obtained through a three-point bending test, is between 500 and 660 MPa. The toughness is rather low. The impact energy, obtained by means of an unnotched Charpy test, is just 3–4 J/cm2 [28].

2. Materials and Methods

Table 1 shows the range of habitual compositions both for the outer layer as well as for the core.

Table 1. Range of chemical composition of the outer layer and of the core (wt. %).

Work-roll	C	Si	Mn	Ni	Cr	Nb	Mo	Mg
Work layer	3.2–3.4	0.9–1.0	0.8–1.0	4.4–4.6	1.7–1.8	0.65-0.75	0.25	--
Core (ASTM Grade 100-70-03)	3-3.02	2.2-2.3	0.2-0.4	0.1-0.2	0-0.1	--	0-0.02	0.06-0.08

The manufacturing process can be summed up as the following: initially the work layer is cast and, after that, the core, in two steps. In the first step, the part of the core which will be joined to the work layer is cast. In the second step, the rest of the core is cast. The work layer is smelted in a medium frequency induction oven. The bleeding from the oven to the ladle is carried out at around 1420 ◦C. When tapping occurs, the inoculants are to be found at the bottom of the ladle. Casting is carried out at around 90 ◦C above the liquidus temperature. Five days after casting, the roll is unmoulded. After quenching at 1000 ◦C with air cooling, the roll was subjected to tempering at 400 ◦C.

The methodology used in this research was that of Design of Experiments (DoE). Through this methodology, the aim is to deliberately modify certain work conditions to generate variations in one or a number of characteristics of the product (responses). These variations in responses should allow for reaching a deeper understanding of this product. In industrial processes, it is habitual that only a small number of factors are responsible for the majority of variations in responses. Therefore, the main effects are defined as those which are a consequence of each separate factor. That is to say, the main effect of a certain factor is defined as a change in the response function upon varying that factor between its level -1 and its level +1.

The interactions between 2 factors are defined as the variation between the average of a factor with another factor at its level -1, and the average effect of the same factor with another factor at its level +1. The interactions between various factors would be defined in a similar way [31]. Complete Design of Experiments factorials require a large number of experiments, which grows exponentially depending on the number of factors studied. For example, when k factors are analysed, the number of experiments is 2k, where 2 is the number of levels applied to each factor (-1 and +1). However, fractional factorial designs allow for the study of a large number of factors, thus reducing the number of experiments [32]. This implies that the interactions of two, three, or more effects become confounded between main effects and other interactions of two factors. This loss of information is not usually of importance in industrial practice.

The experimental response is subject to random variation. This variation will follow a normal law, where its typical deviation reflects experimental error. The effects are linear combinations of the responses, so that by applying the Central Limit Theorem, they will follow a normal law. Starting from a normal law, the distribution function associated with it can be represented graphically. This will appear as a straight line if it is represented on the scale of a 'normal probability paper'. If all the effects were not significant, these would follow a law ley $N(0,\sigma)$, so that they would appear in a linear fashion. If any of the effects were significant, then they would follow a law $N(\mu,\sigma)$, so that they would not appear in line with other effects. Those significant effects which are separated from the straight line to the left and above this line indicate that its level -1 increases the response function. Those significant factors which are separated from the line to the right and below this line indicate that its level +1 increases the response function [32,33].

Table 2 shows the studied factors and the levels which limit this study. The factors A, B, and E are inoculants. Table 3 shows the chemical composition of the inoculants used in this study. Table 4 shows the matrix of experiments. The column 'generators' indicates the algorithm of signs applied in the construction of columns D, E, and F. The column 'restricted confounding pattern' shows those second order interactions whose effects are confounded with the main effects. For example, in this case, the effects of the interactions BD and CE will be confounded with the effect of factor A. The columns for the signs D, E, and F have been constructed as the product of columns AB, AC, and BC respectively.

Table 2. Factors and levels analysed in the Design of Experiments.

Factors		**Levels**	
Code	**Metallurgical parameter correspondence**	**Level –1**	**Level +1**
A	FeSi-La (Kg/T)	0	2.7
B	FeB (Kg/T)	3	6
C	Liquidus Temperature (ºC)	1250-1255	1270-1275
D	Si (wt. %)	0.8-0.85	1.1-1.15
E	SiCaMn (Kg/T)	0.3	0.6
F	Mg (wt. %)	0	0.02

Table 3. Chemical composition of inoculants given in weight %.

Inoculants	Base Chemistry												
	Si	Ca	Al	Mn	Ti	Ba	C	Bi	S	P	B	La	Fe
FeSi-La	66.0	2.5	0.8	---	---	0.3	---	0.3	---	---	---	0.8	rem[1].
SiCaMn	58.3	16.4	1.1	14.8	0.030		0.6		0.030	0.030	---		rem[1].
FeB	0.4	---	---	---	---		0.3		---	---	17.9		rem[1].

[1]Remainder.

Table 4. Matrix of experiments.

No.	A	B	C	D	E	F	Confounding Patterns
1	–1	–1	–1	+1	+1	+1	A+BD+CE B+AD+CF C+AE+BF D+AB+EF E+AC+DF F+BC+DE AF+BE+CD
2	+1	–1	–1	–1	–1	+1	
3	–1	+1	–1	–1	+1	–1	
4	+1	+1	–1	+1	–1	–1	
5	–1	–1	+1	+1	–1	–1	
6	+1	–1	+1	–1	+1	–1	
7	–1	+1	+1	–1	–1	+1	
8	+1	+1	+1	+1	+1	+1	

The mathematical model applied to estimate the volume fraction of carbides and the resistance to wear is formed by the main effects and the interactions of two factors. Therefore, both the volume fraction of carbides as well as the resistance to wear would be approximated in the following function (1):

$$\begin{aligned} Y = {} & B_0 + B_1x_1 + B_2x_2 + B_3x_3 + B_4x_4 + B_5x_5 + B_6x_6 + B_7x_7 \\ & + B_8x_8 \\ & + B_{12}x_1x_2 + B_{13}x_1x_3 + B_{14}x_1x_4 + B_{15}x_1x_5 + B_{16}x_1x_6 \\ & + B_{17}x_1x_7 + B_{18}x_1x_8 \\ & + B_{23}x_2x_3 + B_{24}x_2x_4 + B_{25}x_2x_5 + B_{26}x_2x_6 + B_{27}x_2x_7 \\ & + B_{28}x_2x_8 \\ & B_{34}x_3x_4 + B_{35}x_3x_5 + B_{36}x_3x_6 + B_{37}x_3x_7 + B_{38}x_3x_8 \\ & B_{45}x_4x_5 + B_{46}x_4x_6 + B_{47}x_4x_7 + B_{48}x_4x_8 + B_{56}x_5x_6 \\ & + B_{57}x_5x_7 + B_{58}x_5x_8 \\ & B_{67}x_6x_7 + B_{68}x_6x_8 + B_{78}x_7x_8 \end{aligned} \tag{1}$$

From this model, the optimum combination of levels allows for the maximisation of resistance to wear. The statistical software used for this was Statgraphics Centurion XVI, version 16.1.03.

The thickness of the work layer was studied in two zones (Figure 2a): an external zone, starting at the exterior edge of the roll reaches a depth of 15 mm (named Zone I); a more interior zone that begins at 25 mm from the outer edge of the roll and whose thickness reaches another 15 mm (named Zone III). In both zones, the volume fraction of carbides was determined using the software Image ProPlus (version 4.5.0.29) and its module of analysis Materials-Pro. In order to do this, 5 micrographs of each zone were obtained randomly. The different types of precipitated carbides were identified under a JEOL JSM-5600 (JEOL, Nieuw-Vennep, The Netherlands) scanning electron microscope (SEM), equipped with the characteristic X-ray scattering microanalysis system (SEM-EDX).

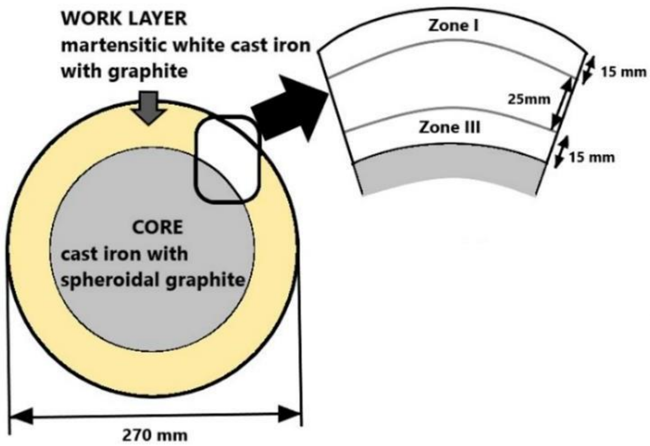

Figure 2. Analysis zones in the work layer.

Resistance to wear was measured with a Pin on Disc test (ASTM G99), using a linear speed of 0.36 m/s and a load of 20 N. The distance covered was 8000 m. Each of the pins corresponded to each of the experiments. The cross section of the pin was circular with a 3 mm diameter. The disc was of steel DIN 42CrMo4 (AISI 4140) in an oil quenched state without tempering. At the time of testing, its hardness was 650 HV. Wear resistance was measured as weight loss (mg). The tests were carried out at 250 and 350 ◦C.

The chemical analysis of each experiment was determined by Inductively Coupled Plasma Mass Spectrometry (ICP-MS), (HP 7500c, Agilent, Santa Clara, CA, USA).

3. Results and Discussion

Table 5 shows the chemical composition and the liquidus temperature of each of the work layers which form part of the matrix of experiments. The pouring temperature was always the liquidus temperature + 90 ◦C.

Table 5. Casting parameters of each experiment.

Casting Parameters	units	Experiment Number							
		1	2	3	4	5	6	7	8
C	%	3.35	3.46	3.4	3.28	2.94	3.04	3.02	3.04
Si	%	1.13	0.88	0.87	1.18	1.16	0.89	0.87	1.15
Mn	%	0.77	0.78	0.79	0.77	0.79	0.83	0.80	0.82
Ni	%	4.44	4.33	4.32	4.38	4.59	4.16	4.62	4.65
Cr	%	1.68	1.68	1.71	1.64	1.65	1.71	1.68	1.71
Mo	%	0.26	0.25	0.25	0.24	0.25	0.25	0.26	0.26
Mg	%	0.024	0.018	--	--	--	--	0.022	0.028
B	%	0.032	0.033	0.071	0.075	0.038	0.041	0.070	0.071
Nb	%	0.64	0.72	0.68	0.61	0.74	0.75	0.73	0.61
Liquidus Temperature	ºC	1252	1254	1253	1250	1273	1272	1272	1270

Figure 3 shows the general microstructure of some of the experiments. These micrographs are referred to as the work layer. The microstructure is formed by proeutectic austenite and two eutectic constituents, one of these formed by austenite and graphite. Figure 3a shows the continuity of the ledeburitic carbides in the microstructure. The austenite is largely found to be transformed into martensite [27]. In Figure 3b–d, it may be observed that the graphite has a compact morphology without reaching a nodular geometry. Among the carbides, two types appear to be observed. One of these is of greater size and with a darker tone (type M3C, associated with Cr), and the other is of much smaller size with a lighter tone (type MC carbides, associated with Nb).

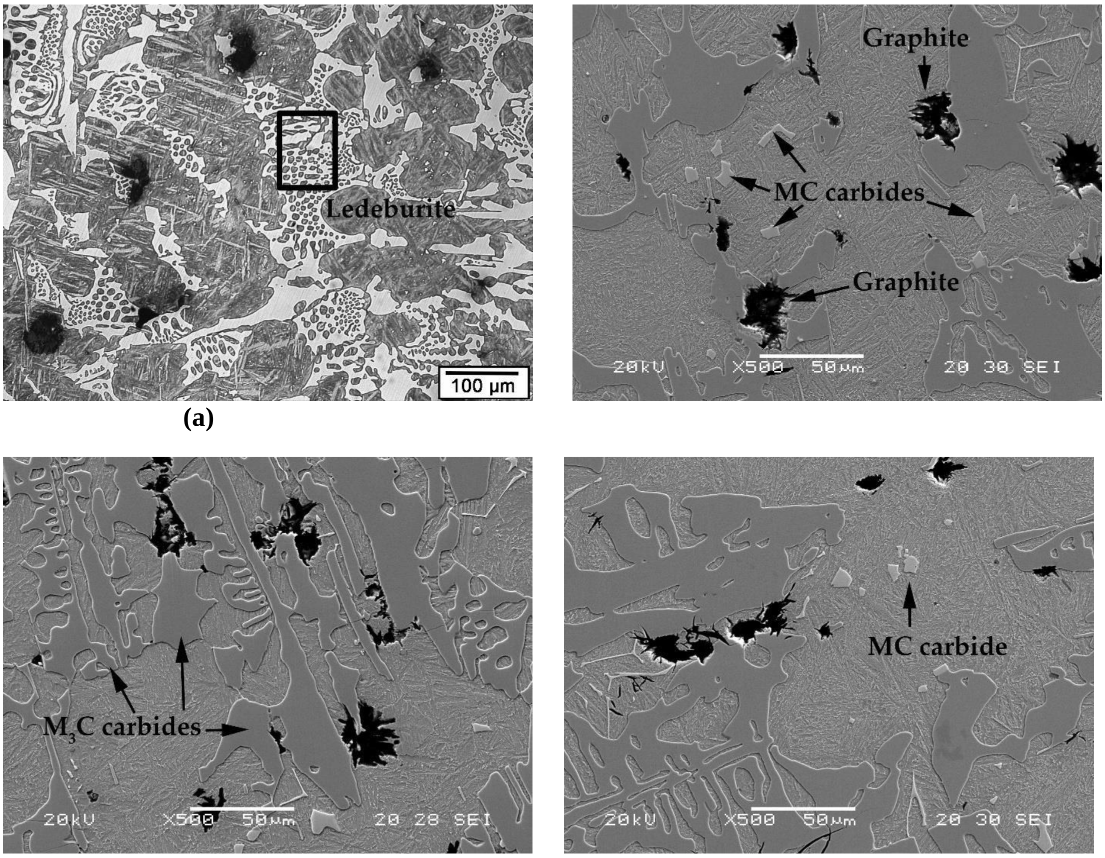

Figure 3. General microstructure of the work layer. (**a**) Experiment 1 in zone III; (**b**) experiment 3 in zone I; (**c**) experiment 4in zone III; (**d**) experiment 7 in zone I.

In Figure 4, the different precipitated phases can be observed. Table 6 shows the results of the semi-quantitative micro-analysis carried out on these types of carbides (spectrums 1 to 5). The lighter toned carbides (spectrums 1, 2, and 4) are carbides of stoichiometry MC, associated with the Nb. Fe and B appear fixed in this type of carbide, and, therefore, it may be deduced that FeB acts as a heterogeneous nucleant in this type of carbide [27]. The darker toned carbides (spectrums 3 and 5) are mixed carbides with stoichiometry M3C, of the type (Fe,Cr)3C.

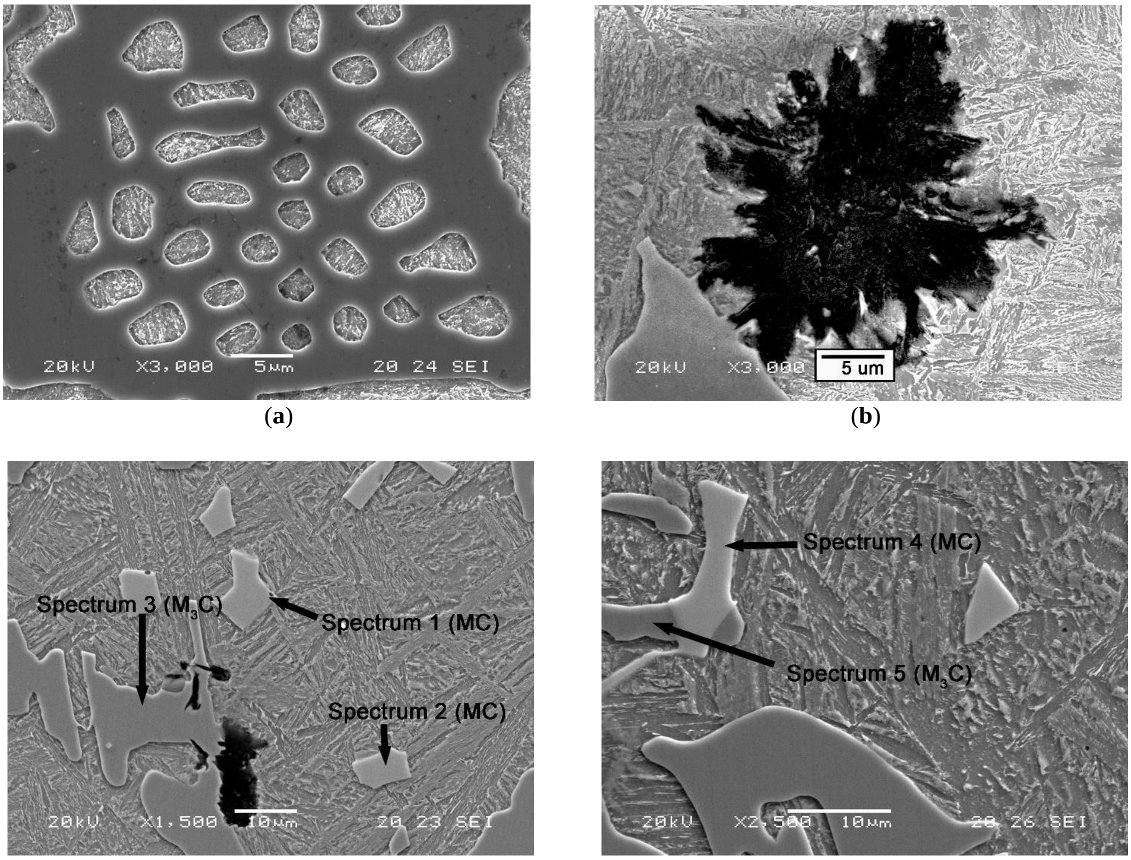

(**a**) (**b**)

(**c**) (**d**)

Figure 4. Main phases and constituents. (**a**) Experiment 2 in zone I, ledeburite; (**b**) experiment 3 in zone III, graphite; experiment 3 in zone I, carbides; (**d**) experiment 6 in zone I, carbides.

Table 6. Results of the micro-analysis carried out with SEM-EDX. Spectrums highlighted in Figure 2 (weight %). Due to the low fluorescence yield of boron, its analysis by EDX shows a high error. Therefore, the boron analysis should be considered "semi-quantitative".

Spectrum	% B	% Fe	% Nb	% Cr
1	9.8	1.8	66.8	–
2	16.3	1.6	46.0	–
3	–	85.1	–	4.9
4	13.1	1.5	59.4	–
5	–	84.3	–	3.0

Table 7 shows the results obtained compared to the volume fraction of carbides. The average percentage of the eight experiments was very similar in both zones. In zone I it was 23.08% and in zone III it was 23.95%. Figure 5 shows a graphic representation of the effects through a normal probability paper.

Table 7. Average values and standardised effects on the volume fraction of carbides.

No.	Zone I	Effects	Zone III	Effects	Effects
1	29.31	23.08	24,9	23.95	Average
2	28.57	-1.99	25,9	-0.84	A+BC+CE
3	25.09	-0.71	27,2	-0.39	B+AD+CF
4	20.81	-5.73	25,4	-3.77	C+AE+BF
5	20.23	0.69	23,9	-0.33	D+AB+EF
6	15.63	0.53	21,9	-0.45	E+AC+DF
7	21.67	5.29	21,5	-1.27	F+BC+DE
8	23.35	2.46	20,9	1.04	AF+BE+CD

In zone I, the factors C (liquidus temperature) and F (% Mg) have a significant effect. Therefore, in order to increase the volume fraction of carbides, both factors should be situated at their respective levels -1 (1250–1255 ◦C) and +1 (0.02% Mg). The Mg generates greater sub-cooling in the eutectic reaction 'austenite + graphite'; thus, without a very elevated content in Si, this favours the formation of eutectic austenite + carbides.

In zone III, where the cooling speed is slightly lower, the factors with a significant effect are C (liquidus temperature) and F (% Mg), and the confounded interactions are AF + BE + CD. To increase the volume fraction of carbides, the factors C and F should be situated in their respective levels -1 (1250–1255 ◦C) and -1 (0% Mg). Given the 'contradiction' in the effect of factor F with respect to zones I and III, the effect should be analysed in greater detail. In Table 8, the effect of factor F on zone III is analysed, including the effect of the confounded interactions with the main effect. In this table, the effects of the interactions AF + BE + CD are also analysed. From this analysis it may be deduced that the effect of factor F (% Mg) is negligible with respect to the effect of the interaction BC. In this case, to increase the volume fraction of carbides, it would be necessary to situate these factors at their respective levels B = + 1 and C = - 1; that is to say, inoculation with 6 Kg/T of FeB and fixing the liquidus temperature between 1550 and 1555 ◦C. Thus, if an increase in the percentage of carbides is required, both factors should be situated at their respective levels -1; that is to say, liquidus temperature of 1255–1255 ◦C and a % Si of 0.8–0.85.

Therefore, in order to increase the volume fraction of carbides in both zones of the work layer, the liquidus temperature should be situated at 1250-1255 ◦C (level -1). This range of temperatures favours the increase in the eutectic constituent in comparison with a liquidus temperature in the range of 1570–1575 ◦C (level +1). In zone I, where the speed of cooling is slightly higher, the graphitising effect of Si is not confirmed. However, in zone III, where the speed of cooling is slightly slower, the effect is more significant. Because of this, in order to increase the volume fraction of carbides in this zone, the percentage of Si should be situated at its level −1 (0.8–0.85 %Si). It may be highlighted that the Mg requires greater sub-cooling during solidification of the eutectic constituent, which favours the formation of ledeburitic eutectic. Its effects are significant in zone I, where cooling is more rapid.

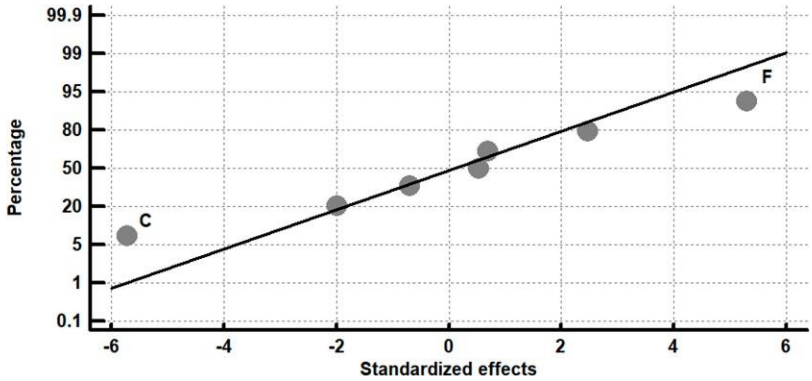

(**a**)

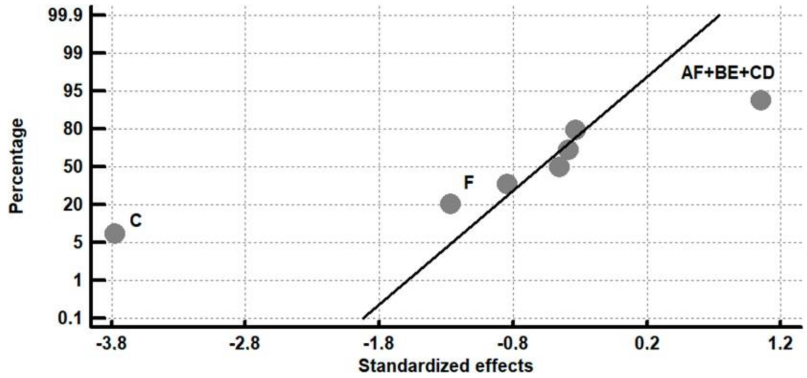

(**b**)

Figure 5. Representation of the effects in a normal probability paper on Vol.% carbides. (**a**) Zone I; (**b**) zone III.

Table 8. Vol.% carbides in zone III. Analysis of the effects corresponding to the interactions AF + BE + CD and F + BC + DE.

(a). Effects of AF+BE+CD.

A(↓)×F(→)	**-1**	**+1**	**B(↓)×E(→)**	**-1**	**+1**	**C(↓)×D(→)**	**-1**	**+1**
-1	25.5	23.2	**-1**	23.9	23.4	**-1**	26.5	25.2
+1	23.6	23.4	**+1**	23.5	24.1	**+1**	21.7	22.4

(b). Effects of F+BC+DE.

F	**-1**	**+1**	**B(↓)×C(→)**	**-1**	**+1**	**D(↓)×E(→)**	**-1**	**+1**
-1	24.6		**-1**	25.4	22.9	**-1**	23.7	24.5
+1		23.3	**+1**	26.3	21.2	**+1**	24.7	22.9

Table 9 shows the results obtained in the wear tests in zone I. The average value of wear in the eight experiments at 250 ◦C was 22.6 mg, while the average value of the eight experiments at 350 ◦C was 25.9 mg. Figure 6 shows a graphic representation of the effects. Figure 6a,c represent the effects on a normal probability paper, and Figure 6b,d represent the effects in a Pareto diagram.

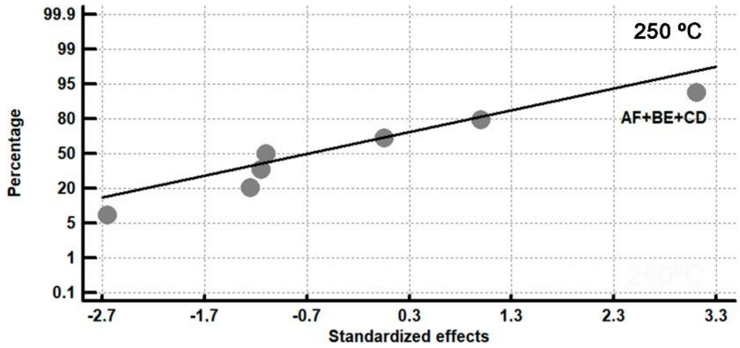

(**a**)

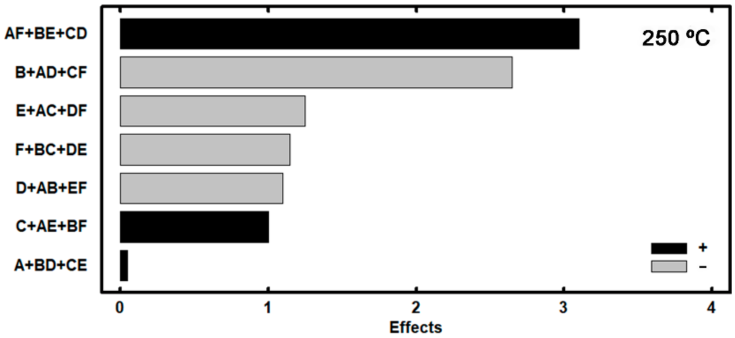

(**b**)

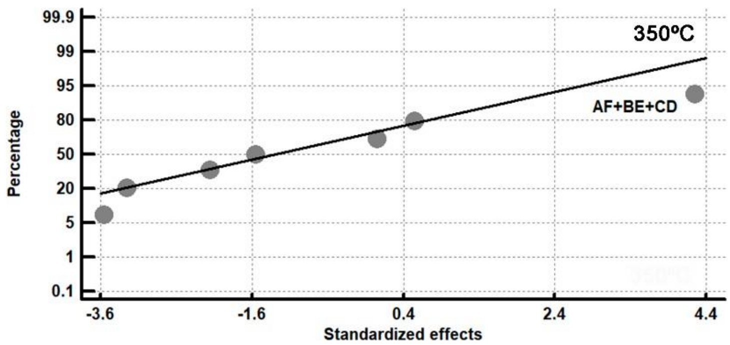

(**c**)

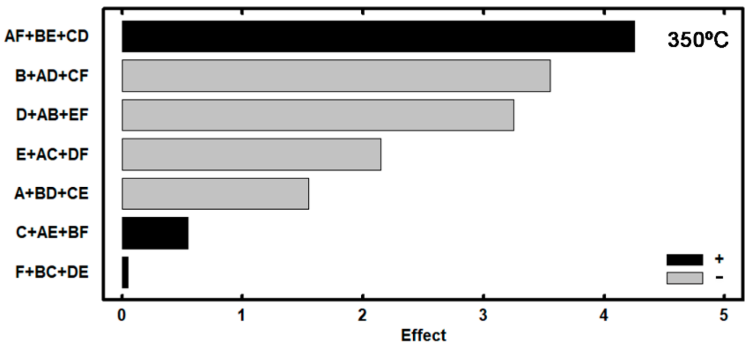

(**d**)

Figure 6. Graphic representation of wear in zone I (**a**) 250 °C. Representation of the effects on a normal probability paper; (**b**) 250 °C. Representation of the effects in a Pareto diagram; (**c**) 350 °C. Representation of the effects on a normal probability paper; (**d**) 350 °C. Representation of the effects in a Pareto diagram.

Table 9. Average values and standardised effects with respect to zone I. Values in mg.

No.	250ºC	Effects	350ºC	Effects	Effects
1	20.1	22.6	23.4	25.9	Average
2	25.6	0.0	31.5	-1.5	A+BC+CE
3	22.8	-2.6	27.3	-3.5	B+AD+CF
4	19.9	1.0	20.4	0.5	C+AE+BF
5	26.6	-1.1	30.3	-3.2	D+AB+EF
6	23.4	-1.2	25.6	-2.1	E+AC+DF
7	20.8	-1.1	25.8	0.0	F+BC+DE
8	21.6	3.1	23.1	4.2	AF+BE+CD

In both cases, a single significant effect is confirmed which corresponds to the 'con- founded' interactions AF, BE, and CD. Table 10 shows a detailed analysis of these inter- actions, highlighting the combination of factors that generates less wear. This seems to suggest a contradiction in the effects in the interactions AF at 250 ◦Cand at 350 ◦C. If one of these is found at its level +1, the other should be situated at its level − 1.

Table 10. Analysis of the interactions AF, BE, and CD.

a). Wear in zone I at 250 ºC

A(↓)×F(→)	-1	+1	B(↓)×E(→)	-1	+1	C(↓)×D(→)	-1	+1
-1	24.7	<u>20.4</u>	**-1**	24.5	21.7	**-1**	24.2	<u>20.0</u>
+1	21.6	23.6	**+1**	<u>20.3</u>	22.2	**+1**	22.1	24.1

(b). Wear in zone I at 350 ºC

A(↓)×F(→)	-1	+1	B(↓)×E(→)	-1	+1	C(↓)×D(→)	-1	+1
-1	28.8	24.6	**-1**	30.9	24.5	**-1**	29.4	<u>21.9</u>
+1	<u>23.0</u>	27.3	**+1**	<u>23.1</u>	25.2	**+1**	25.7	26.7

As a consequence of applying a mathematical model of the interactions of two factors, and in analysing all the possible combinations of level, the optimum combination which allows the minimising of wear may be determined. Table 11 shows this combination.

Table 11. Optimum combination of levels to minimise wear in zone I.

	Factors	250ºC	350ºC	value
A	FeSi-La (Kg/T)	+1	+1	0
B	FeB (Kg/T)	+1	+1	6
C	Liquidus temperature	-1	-1	1250-1255
D	Si (%)	+1	+1	1.1-1.15
E	SiCa (Kg/T)	-1	-1	0.3
F	Mg (%)	-1	-1	0
	Estimated level of wear (mg)	18.3	18.6	

It must be taken into account that the optimum combination of levels coincides at both temperatures. This optimum combination forces factors C (liquidus temperature) and D (%Si) to be situated at their levels -1 (1250–1255 ◦C) and +1 (1.1–1.15 %Si), respectively. A low liquidus temperature would reflect a higher content of the eutectic constituent, while a high percentage of Si could elevate the graphitising potential of the alloy. However, it must be pointed out that this 'graphitising' effect is not confirmed in zone I due to the fact that this is the zone which shows a greater cooling speed. On the other hand, the Si has a tendency to favour the formation of pearlite in martensitic white cast iron.

However, the high content of Ni and Cr avoid the formation of this constituent, thus favouring the transformation of martensite into austenite. At the same time, the high content of Si raised the

Ms temperature, thus reducing the quantity of retained austenite. This favours an increase in the quantity of martensite.

The hardening effect of the Si in solid solution with ferrite must also be highlighted. This means an additional 'stimulus' in the increase of resistance to wear. The system recommends situating Factor A at its +1 level and Factor F at its -1 level. With respect to this, it must be pointed out that, in the exterior zone of the work layer, zone I, the number of beads of graphite per unit of area increases when Factor A is situated at level +1 and that the size of these beads is smaller when Factors A and F are situated at their respective levels +1 and -1 [22]. Therefore, it may be deduced that it could be favourable to resistance to wear that the precipitation of graphite were produced with a high density of graphite beads and in a small size. At the same time, the 'whitening' effect of FeB (level +1) and the reduction in the 'graphitising' effect of the SiCaMn at its level -1 seem to be favourable.

Table 12 shows the results obtained from the wear tests in Zone III. The average value for wear in the eight experiments at 250 ◦C was 25.7 g, while the average value for the eight experiments at 35 ◦C was 29.8 mg. These values are greater than those reached in zone I. Figure 7 shows a graphic representation of the effects. Figure 7a,c show the effects on a normal probability paper and Figure 7b,d show the effects in a Pareto diagram.

Table 12. Average values and standardised effects with respect to zone III. Values in mg.

No.	250ºC	Effects	350ºC	Effects	Effects
1	19.2	25.7	21.5	29.8	Average
2	27.7	-1.6	30.4	2.1	A+BC+CE
3	27.5	-2.3	32.4	-0.7	B+AD+CF
4	26.5	1	28.6	3.1	C+AE+BF
5	33.8	-2.3	34.2	-2.4	D+AB+EF
6	26.8	-5.3	34.4	-0.4	E+AC+DF
7	25.6	-5.8	26.7	-5.2	F+BC+DE
8	18.8	2.4	30	3.9	AF+BE+CD

In both cases, the lack of factors with a significant effect is confirmed. However, it may be observed that the factor with the greatest effect in both cases is Factor F, which included the confounded effects of interactions BC and DE. In Table 13, these effects are analysed. In both cases, the interaction which has a larger effect on resistance to wear at both temperatures is interaction DE. It may be deduced that, in order to increase resistance to wear, both factors should be situated at their levels +1; that is to say, %Si = 1.1–1.15 and the inoculation with 6 Kg/T of SiCaMn.

Table 13. Analysis of the effect of factor F and interactions BE + CD.

(a). Effects of F+BC+DE. Wear in zone III at 250 ºC (mg).

F	-1	+1	B(↓)×C(→)	-1	+1	D(↓)×E(→)	-1	+1
-1	28.6		**-1**	23.4	30.3	**-1**	26.6	27.1
+1		22.8	**+1**	27.0	22.2	**+1**	30.1	19.0

(b). Effects of F+BC+DE. Wear in zone III at 350 ºC (mg).

F	-1	+1	B(↓)×C(→)	-1	+1	D(↓)×E(→)	-1	+1
-1	32.4		**-1**	25.9	30.5	**-1**	28.5	33.4
+1		27.1	**+1**	34.3	28.3	**+1**	31.4	25.7

In the tests carried out at 250 ◦C, factor E and the interactions AC + DF also appear to have a large effect. In Table 14, these effects are analysed separately. It can be seen that the interaction DF has a more significant effect. It is concluded that, in order to increase resistance to wear, both factors should be situated at their levels +1; that is to say, %Si = 1.1–1.15 and % Mg = 0.02.

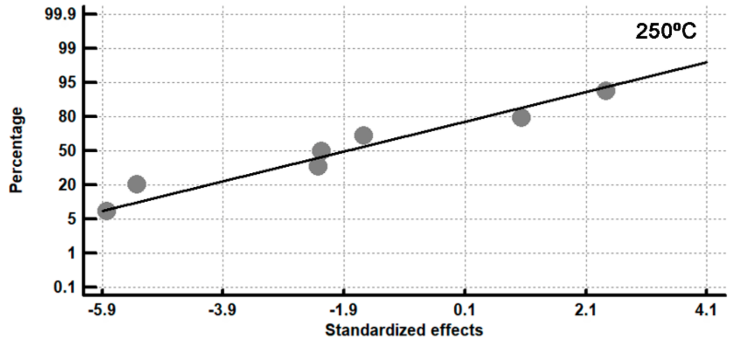

(**a**)

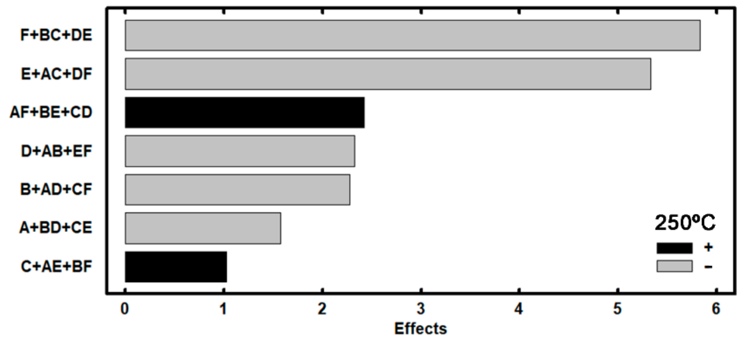

(**b**)

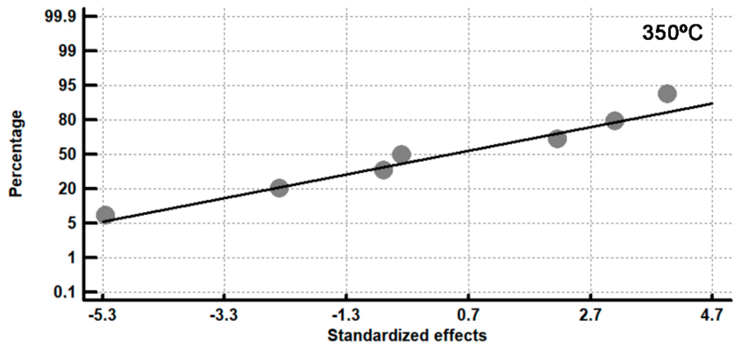

(**c**)

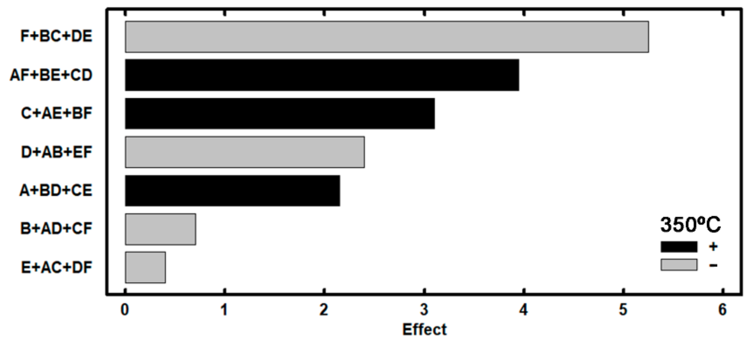

(**d**)

Figure 7. Graphic representation of wear in zone III. (a) 250 °C, representation of effects on a normal probability paper. (b) 250 °C, representation of effects in a Pareto diagram; (c) 350 °C, representation of effects on a normal probability paper; (d) 350 °C, representation of effects in a Pareto diagram.

Table 14. Analysis of the effect of factor E and the interactions AC + DF. Wear in zone III at 250 ˚C (mg).

E	**-1**	**+1**	**A(↓)×C(→)**	**-1**	**+1**	**D(↓)×F(→)**	**-1**	**+1**
-1	28.4		**-1**	23.3	29.7	**-1**	27.1	26.6
+1		23.1	**+1**	27.1	22.8	**+1**	30.1	19.0

On the other hand, in the tests carried out at 350 ◦C, interactions AF + BE + CD also appear to have a large effect. In Table 15, the effect of these interactions is analysed separately. It is concluded that the largest effect is a consequence of the interaction AF in such a way that, in order to reduce the message level, this interaction should be fixed at the following levels: A = -1 and F = +1. Also, the interaction CD at its levels C = -1 and D = +1 shows a large effect.

Table 15. Analysis of the effect of interactions AF + BE + CD. Wear in zone III at 350 ˚C (mg).

AF	**-1**	**+1**	**B(↓)×E(→)**	**-1**	**+1**	**C(↓)×D(→)**	**-1**	**+1**
-1	33.3	24.1	**-1**	32.3	27.9	**-1**	31.4	25.0
+1	31.5	30.2	**+1**	27.6	31.2	**+1**	30.5	32.1

As a consequence of applying a mathematical model to the interactions of three factors, and analysing all the possible combinations of levels, the optimum combination can be determined, and this would allow for minimising wear in this zone III. Table 16 shows this combination. It can be confirmed that this combination of levels is in agreement with the results shown in Tables 13–15.

Table 16. Optimal combination of levels for minimising wear in zone III.

	Factors	**250ºC**	**350ºC**	**value**
A	FeSi-La (Kg/T)	-1	-1	0
B	FeB (Kg/T)	+1	+1	6
C	Liquidus temperature	-1	-1	1250-1255
D	Si (%)	+1	+1	1.1-1.15
E	SiCa (Kg/T)	+1	+1	0.6
F	Mg (%)	+1	+1	0.02
	Estimated level of wear (mg)	17.0	20.8	

In this interior zone of the work layer, it is observed that resistance to wear improves when the liquidus temperature is maintained at its level -1. That is to say, similar to what happened in zone I, the presence of the eutectic constituent rather than the proeutectic austenite should be favourable. Situating factor D (%Si) at its level +1 and taking advantage of the hardening effect of Si on the proeutectic constituent are also favourable. It must be taken into account that a high %Si increases the Ms temperature, thus reducing the quantity of retained austenite and the Si in a solid ferrite solution substantially hardens this phase. On the other hand, it must be highlighted that the 'whitening effect' of the Mg favours the precipitation of metastable eutectic (austenite + carbides) rather than stable (austenite + graphite).

4. Conclusions

Work rolls manufactured through the process Indefinite Chill Double Poured (ICDP) present an exterior work layer manufactured in a martensitic white cast iron alloyed with Cr, Ni, and Nb. These rolls are used in the finishing stands of Hot Strip Mills. Through the application of a Design of Experiments (DoE), the aim was to increase resistance to wear. In order to do this:

1. In the exterior zone of the work layer it is recommended that the liquidus temperature and the percentage of Si be situated in their respective ranges of 1250–1255 ◦C and1.1–1.15%. More elevated temperatures favour the presence of the proeutectic

constituent as opposed to the eutectic constituent. In this zone, where the speed of cooling during solidification is greater, the graphitising effect of Si is not confirmed. However, the results confirm the hardening effect of Si in a solid ferrite solution after tempering of the martensite. At the same time, the 'whitening' effect of inoculation with 6 kg/T of FeB, and that the size of precipitated graphite particles is small, with a high number of 'beads' per unit of area, may both be considered favourable;

2. Resistance to wear in more interior areas of the work layer is increased, as in the previous case, with liquidus temperatures between 1250–1255 ◦C and the content of Si between 1.1–1.15%. However, in this zone, the graphitising effect is confirmed, and, therefore, the addition of Mg as a micro-alloy as well as the inoculation with 6 kg/T de FeB, is favourable. All of this evidences that the undissolved carbon in the austenite is found to be forming carbides rather than the majority formation of graphite.

Author Contributions: Conceptualization, F.A.-A.; methodology, F.A.-A.; software, F.A.-A.; validation, A.C.-V., F.A.-A.; formal analysis, F.A.-A.; investigation, A.C.-V. and C.H.A.-P.; resources, F.A.-A. and C.H.A.-P.; data curation, F.A.-A.; writing—original draft preparation, F.A.-A.; writing—review and editing, F.A.-A. and A.C.-V.; visualization, F.A.-A.; supervision, F.A.-A.; project administration, F.A.-A.; funding acquisition, F.A.-A. All authors have read and agreed to the published version of the manuscript.

Funding: This research received no external funding.

Conflicts of Interest: The authors declare no conflict of interest.

Citation: Cofiño-Villar, A.; Alvarez-Antolin, F.; Alvarez-Perez, C.H. Improvement in the Resistance to Wear of Work-Rolls Used in Finishing Stands of the Hot Strip Mills. Metals 2021, 11, 1873. https://doi.org/10.3390/met11111873

Academic Editor: Cristiano Fragassa

Publisher's Note: MDPI stays neutral with regard to jurisdictional claims in published maps and institutional affiliations.

References

1 Strilkova, L.; Valek, T.; Tanger, L.T.D. Microstructural investigation of icdp iron designed for working layers of composite centrifugally cast rolls in hot rolling mills. In Proceedings of the 21st International on Conference Metallurgy and Materials, Brno, Czech Republic, 23–25 May 2012; pp. 788–794.

2 Palit, P.; Patel, S.N.; Mathur, J.; Shenoy, S. Analysis of a Progressive Failure of a Work Roll in Hot Strip Mill. *Journal of Failure Analysis and Prevention* **2019**, *19*, 1297-1303, doi:10.1007/s11668-019-00688-w.

3 Ramirez-Ramirez, J.H.; Colas, R.; Garza-Montes-de-Oca, N.F. High Temperature Oxidation of a Work Roll Grade High-Chromium White Cast Iron. *Journal of Iron and Steel Research International* **2013**, *20*, 122-129, doi:10.1016/s1006-706x(13)60187-9.

4 Bombac, D.; Kugler, G.; Markoli, B.; Tercelj, M. Hot work roller surface layer degradation progress during thermal fatigue in the temperature range 500-700 degrees C. *International Journal of Fatigue* **2017**, *104*, 355-365, doi:10.1016/j.ijfatigue.2017.08.008.

5 Nilsson, M.; Olsson, M. An investigation of worn work roll materials used in the finishing stands of the hot strip mill for steel rolling. *Proceedings of the Institution of Mechanical Engineers Part J-Journal of Engineering Tribology* **2013**, *227*, 837-844, doi:10.1177/1350650113478333.

6 Ray, A.; Prasad, M.S.; Dhua, S.K.; Sen, S.K.; Jha, S. Microstructural features of prematurely failed hot-strip mill work rolls: Some studies in spalling propensity. *Journal of Materials Engineering and Performance* **2000**, *9*, 449-456, doi:10.1361/105994900770345854.

7 Filipovic, M.; Kamberovic, Z.; Korac, M.; Jordovic, B. Effect of Niobium and Vanadium Additions on the As-Cast Microstructure and Properties of Hypoeutectic Fe-Cr-C Alloy. *Isij International* **2013**, *53*, 2160-2166, doi:10.2355/isijinternational.53.2160.

8 Zhang, Z.G.; Yang, C.K.; Zhang, P.; Li, W. Microstructure and wear resistance of high chromium cast iron containing niobium. *China Foundry* **2014**, *11*, 179-184.

9 Bedolla-Jacuinde, A. Microstructure of vanadium-, niobium- and titanium-alloyed high-chromium white cast irons. *International Journal of Cast Metals Research* **2001**, *13*, 343-361, doi:10.1080/13640461.2001.11819416.

10 Pero-Sanz, J.A. *Fundiciones Férreas*; Dossat: 1994; p. 154.

11 Antolin, J.F.A.; Garrote, L.F.; Lozano, J.A. Application of Rietveld Refinement to the correlation of the microstructure evolution of white cast irons with 18 and 25 %-wt. Cr after oil quench and successive temper treatments, with abrasive wear and bending testing. *Revista De Metalurgia* **2018**, *54*, 11, doi:10.3989/revmetalm.113.

12 Mourad, M.M.; El-Hadad, S.; Ibrahim, M.M. Effects of Molybdenum Addition on the Microstructure and Mechanical Properties of Ni-Hard White Cast Iron. *Transactions of the Indian Institute of Metals* **2015**, *68*, 715-722, doi:10.1007/s12666-014-0504-6.

13 Bravo, S.V.; Yamamoto, K.; Miyahara, H.; Ogi, K. Control of carbides and graphite in Ni-hard type cast iron for hot strip mills. *Pricm 6: Sixth Pacific Rim International Conference on Advanced Materials and Processing, Pts 1-3* **2007**, *561-565*, 1023.

14 Sergio, V.; Ishikawa, S.; Yamamoto, K.; Miyahara, H.; Ogi, K.; Kamimiyada, K. Control of graphite formation in solidification of white cast iron. *International Journal of Cast Metals Research* **2008**, *21*, 27-30, doi:10.1179/136404608x361611.

15 Gowda, D.; Kumar, D.C.; Sandeep, G.M.; Parthasarathy, A.; Chandrashekar, S. Tribological Characterization of Centrifugally Cast Graphite Cast Iron under Dry and Wet conditions. *Materials Today-Proceedings* **2018**, *5*, 145-151.

16 Holmgren, D.; Dioszegi, A.; Svensson, I.L. Effects of nodularity on thermal conductivity of cast iron. *International Journal of Cast Metals Research* **2007**, *20*, 30-40, doi:10.1179/136404607x202690.

17 Tercelj, M.; Fajfar, P.; Godec, M.; Kugler, G. Characteristics of the thermal fatigue resistance for 3.1C, 0-8Si, 0.9Mn, 1.7Cr, 4.5Ni and 0-3Mo ICDP cast iron roll at 600 degrees C. *Materiali in Tehnologije* **2017**, *51*, 515-521, doi:10.17222/mit.2016.259.

18 Drobne, M.; Urska, K.; Tercelj, M.; Fajfar, P.; Ltd, T. Thermal crack propagation during hot rolling and its influence on cast iron work roll degradation. *Metal 2017: 26th International Conference on Metallurgy and Materials* **2017**, 408-413.

19 Stott, F.H.; Jordan, M.P. The effects of load and substrate hardness on the development and maintenance of wear-protective layers during sliding at elevated temperatures. *Wear* **2001**, *250*, 391-400, doi:10.1016/s0043-1648(01)00601-9.

20 Asensio, J.; Álvarez, J.F.; Vander, G.F. 2008. Microstructural control of FeB-inoculated mottled low-alloy white iron by a design of experiments approach. *International Journal of Materials Research* **2008**, *11*, 1237-1247. DOI: 10.3139/146.101758

21 Onsoien, M.I.; Skaland, T.; Grong, O. Mechanisms of graphite formation in ductile cast iron containing cerium and lanthanum. *International Journal of Cast Metals Research* **1999**, *11*, 319-324, doi:10.1080/13640461.1999.11819293.

22 Hamidzadeh, M.A.; Meratian, M.; Saatchi, A. Effect of cerium and lanthanum on the microstructure and mechanical properties of AISI D2 tool steel. *Materials Science and Engineering a-Structural Materials Properties Microstructure and Processing* **2013**, *571*, 193-198, doi:10.1016/j.msea.2013.01.074.

23 Cofino-Villar, A.; Alvarez-Antolin, F.; Asensio-Lozano, J.; Garcia-Garcia, M. Control over the Percentage, Shape and Size of the Graphite Particles in Martensitic White Castings Alloyed with Cr, Nb and Mg. *Materials* **2019**, *12*, 10, doi:10.3390/ma12010185.

24 Col, M.; Koc, F.G.; Oktem, H.; Kir, D. The role of boron content in high alloy white cast iron (Ni-Hard 4) on microstructure, mechanical properties and wear resistance. *Wear* **2016**, *348*, 158-165, doi:10.1016/j.wear.2015.12.007.

25 Tasgin, Y.; Kaplan, M.; Yaz, M. Investigation of effects of boron additives and heat treatment on carbides and phase transition of highly alloyed duplex cast iron. *Materials & Design* **2009**, *30*, 3174-3179, doi:10.1016/j.matdes.2008.11.015.

26 Zhou, W.B.; Zhu, H.B.; Zheng, D.K.; Zheng, H.X.; Hua, Q.; Zhai, Q.J. Niobium alloying effect in high carbon equivalent grey cast iron. *China Foundry* **2011**, *8*, 36-40.

27 Chen, X.R.; Xu, J.; Hu, H.; Mohrbacher, H.; Kang, M.; Zhang, W.; Guo, A.M.; Zhai, Q.J. Effects of niobium addition on microstructure and tensile behavior of as-cast ductile iron. *Materials Science and Engineering a-Structural Materials Properties Microstructure and Processing* **2017**, *688*, 416-428, doi:10.1016/j.msea.2017.01.032.

28 Cofino-Villar, A.; Alvarez-Antolin, J.F.; Asensio-Lozano, J. Enhanced Fracture Strength in the Working Layer of Rolls Manufactured in Ni-Hard Cast Iron Alloyed with Mo, Nb and Mg. *Metals* **2018**, *8*, 13, doi:10.3390/met8090725.

29 Takeda, H.; Yoneda, H.; Asano, K. Effect of Silicon and Bismuth on Solidification Structure of Thin Wall Spheroidal Graphite Cast Iron. *Materials Transactions* **2010**, *51*, 176-185, doi:10.2320/matertrans.M2009255.

30 Konig, M.; Wessen, M. Influence of alloying elements on microstructure and mechanical properties of CGI. *International Journal of Cast Metals Research* **2010**, *23*, 97-110, doi:10.1179/136404609x12505973098972.

31 Johnson, R. *Probabilidad y Estadística para Ingenieros*, 3rd ed. ed.; México., P.-H.H., Ed.; 1997; pp. 489-494.

32 Prat-Bartés, A.; Tort-Martorell, X.; Grima-Cintas, P.; Pozueta-Fernández, L.; Solé-Vidal, I. *Métodos Estadísticos*, 2nd ed.; UPC: Barcelona, 2004; p. 376.

33 Silva, R.G.; Estay, C.S.; Pavez, G.M.; Vinuela, J.Z.; Torres, M.J. Influence of Geometric and Manufacturing Parameters on the Compressive Behavior of 3D Printed Polymer Lattice Structures. *Materials* **2021**, *14*, 16, doi:10.3390/ma14061462.

4. CONCLUSIONES

En esta tesis se han estudiado los efectos que los niveles definidos en el diseño de experimentos tienen sobre las propiedades de la capa de trabajo de cilindros de laminación dúplex, empleados para las cajas acabadoras de trenes de bandas en caliente. Los resultados obtenidos como repuestas al diseño de experimentos permiten concluir que:

1. Inocular con 2.7 Kg/T de FeSi-La produce:
   a. Aumento de la resistencia a la flexión en la capa de trabajo.
   b. Aumento del número de partículas de grafito por unidad de área.
2. Por el contrario, no inocular con 2.7 Kg/T de FeSi-La genera:
   a. Aumento de la resistencia al impacto en la capa de trabajo.
   b. Aumento de la resistencia al impacto en la zona de unión entre capa de trabajo y núcleo.
3. Inocular con 6 Kg/T de FeB produce:
   a. Un aumento del tamaño de las partículas de grafito, representado por la media de Feret.
   b. Un aumento en el parámetro R (redondez) de las partículas de grafito, lo que implica una reducción en la nodularidad de las partículas, ya que se considera que una partícula es redonda cuando el parámetro R ≤ 1.4.
4. Inocular con 3 Kg/T de FeB produce:
   a. Un aumento de la resistencia a la flexión de la capa de trabajo.
   b. Un aumento en el porcentaje de partículas redondas.
1. Si se realiza la colada del material entre 1250ºC y 1255ºC se obtiene que:
   a. Se aumenta la fracción en volumen de cementita en la capa de trabajo.
   b. Se produce un aumento de la resistencia al desgaste en la capa de trabajo.
2. Si se realiza la colada del material entre 1270ºC y 1275ºC se obtiene que:
   a. Se aumenta la resistencia al impacto de la capa de trabajo.
   b. Se aumenta la resistencia a la flexión de la capa de trabajo.
3. La presencia de un porcentaje de Si entre 1.1 y 1.15 % en peso genera:
   a. Un aumento en la fracción en volumen de cementita en la capa de trabajo.
   b. Un aumento de la media de Feret.
   c. Un aumento en la fracción en volumen de grafito en la capa de trabajo.

    d. Un aumento en la resistencia al desgaste de la capa de trabajo.
4. La inoculación con 0.6 Kg/T de SiCaMn produce:
    a. Un aumento de la resistencia a la flexión en la capa de trabajo.
    b. Un aumento en la resistencia al impacto en la capa de trabajo.
    c. Un aumento en la resistencia al impacto en la zona de unión.
    d. Un aumento en el porcentaje de partículas de grafito redondas.
    e. Un aumento en el tamaño de las partículas de grafito.
5. La inoculación con 0.3 Kg/T de SiCaMn produce:
    a. Un aumento en el parámetro redondez.
    b. Un aumento en el número de partículas de grafito.
6. La presencia de un porcentaje de Mg del 0.02% en peso se obtiene que:
    a. Se aumenta la resistencia a la flexión en la capa de trabajo
    b. Se aumenta la dureza de la zona de unión
    c. Se aumenta el tamaño de partícula de grafito.
    d. Se aumenta el parámetro redondez.

Por otro lado, se confirma que el molibdeno presente en esta aleación se mantiene en solución sólida en la austenita, mejorándose así la templabilidad de esta.

Atendiendo a los factores expuestos anteriormente se puede mejorar la resistencia a la fractura superficial de la superficie de trabajo si:

1. Se fija la temperatura líquidus en su valor +1 (1270-1275ºC).
2. Se inocula con 3 kg/T de FeB.
3. Se inocula con 0.6 kg/T de SiCaMn.
4. Se inocula con Mg.

Para obtener un aumento de la calidad de la unión entre la capa de trabajo y en núcleo se recomienda:

1. Inocular con 0.6 kg/T de SiCaMn, por su efecto de mejora de la resistencia al impacto.
2. Evitar la inoculación con FeSi-La, debido a que aumenta el número de partículas de grafito por unidad de área, promoviendo al mismo tiempo una morfología laminar de este, reduciendo significativamente la resistencia al impacto de la zona de unión.

Para obtener una mejora de la resistencia al desgaste se recomienda:

3. En la zona más externa de la capa de trabajo se tiene que:
    a. Mantener la temperatura líquidus en el rango 1250ºC-1255ºC
    b. Fijar el contenido de Si en el rango 1.1%-1.15%

c. Inocular con 6 kg/T de FeB

Elevadas temperaturas líquidus favorecen la presencia del constituyente pro eutéctico, además las velocidades de enfriamiento durante la fabricación son lo suficientemente altas como para que la presencia de silicio no tenga un efecto grafitizante. Sin embargo, sí que se confirma el efecto endurecedor por solución sólida en la ferrita tras revenido. Además, el efecto blanqueante de la inoculación con FeB y la presencia de partículas de grafito, de pequeño tamaño y en gran número, es favorable.

4. Por otro lado, en la zona más interior de la capa de trabajo se mejora la resistencia al desgaste si:

    a. Se sitúa la temperatura líquidus en el rango 1250ºC-1255ºC

    b. Se sitúa el contenido de Si entre 1.1% y 1.15%

    c. Se inocula con Mg

    d. Se inocula con 6kg/T de FeB

En este caso el efecto grafitizante del Si sí que tiene lugar, por lo que la presencia de Mg como microaleante, así como la inoculación con FeB es favorable. Además, se confirma que el carbono no disuelto en la austenita se encuentra formando carburos en vez de formar grafito.

Bibliografía

1. Kalpakjian, S.; Schmid, S.R.; Manufactura, ingeniería y tecnología; 5ª edición; Pearson Educación; México; 2008; p. 347-350.
2. Enríquez Berciano, J.L.; Tremps Guerra, E.; de Elío de Bengy, S.; Fernández Segovia, D.; Monografias sobre Tecnología del acero parte IV Laminación; Madrid; España; 2010.
3. Schröder, K. H.; A basic understanding of the mechanics of rolling mill rolls; 2004; p. 4-8.
4. El Wahabi, M.; Caracterización termomecánica de aceros inoxidables auteníticos AISI-304, E.T.S d'Enginyeria Industrial de Barcelona; 2002.
5. Pero-Sanz Elorz, J.A.; Ciencia e Ingeniería de Materiales 4ª edición; Dossat; Madird, España; 2000; p. 536-546.
6. Belzunce, F.J.; Ziadi, A.; Rodriguez, C. Structural integrity of hot strip mill rolling rolls. Eng. Fail. Anal. 2004, Vol. 11, p. 789–797.
7. Guerrero, M.P.; Pérez, A.; Colás, R. Heat Transfer to the work rolls during hot rolling of steel. In Proceedings of the Rolls 2000 International Convention Centre Birmingham, Brno, Czech Republic, 2012, Vol. 23–25, p. 108–112.
8. Nilsson, M.; Olsson, M. An investigation of worn work roll materials used in the finishing stands of the hot strip mill for steel rolling. Proc. Inst. Mech. Eng. Part J J. Eng. Tribol. 2013, Vol. 227, p. 837–844.
9. Noda, N.A.; Hu, K.; Sano, Y.; Ono, K.; Hosokawa, Y. Residual stress simulation for hot strip bimetallic roll during quenching., Steel Res. Int., 2016, Vol. 87, p. 1478–1488.
10. Equipo técnico del Centro de Formación de Arcelor Mittal Asturias, El Proceso Siderúrgico 2ª edición, La Toba, Avilés, España; Arcelor Mittal, 2007.
11. Atamert, S.; Stekly, J.J.K.; Roll life Beyond 2000; In Proceedings of the Rolls 2000 International Convention Centre Birmingham, Brno, Czech Republic, 2012, Vol. 23–25, p. 57-64.
12. Delaunois, F., Stanciu, V.I. & Sinnaeve, M. Resistance to High-Temperature Oxidation and Wear of Various Ferrous Alloys Used in Rolling Mills., Metall Mater Trans A 49. 2018, p. 822–835.
13. Tercejl, M.; Fajfar, P.; Godec, M.; Kugler, G.; Charecteristics of the Thermal Fatigue Resistance for 3.1C, 0.8Si, 0.9Mn, 1.7Cr, 4.5Ni AND 0.3Mo ICDP Cast Iron Roll at 600 °C, Materiali In Tehnologije, 2017, Vol. 51, Issue 3, p. 515-521.
14. Jonck, J.; Moema, J.S.; Jooste, J.; van Tonder, P. Investigation of the 'tiger skin' defect on indefinite chill rolls. J. South. Afr. Inst. Min. Metall. 2016, Vol. 116, p. 907–913.
15. Ray, A.; Prasad, M.S.; Dhua, S.K.; Sen, S.K.; Jha, S. Microstructural features of prematurely failed hot-strip mill work rolls: Some studies in spalling propensity. J. Mater. Eng. Perform. 2000, Vol. 9, p. 449–456.

16. Palit P.; Patel, S. N.; Mathur, J.; Shenoy, S.; Analysis of a Progressive Failure of a Work Roll in Hot Strip Mill; Journal of Failure Analysis and Prevention. 2019, Vol. 19, p. 1297-1303.

17. Schröder, K.H.; State of the art of rolls for the production of flat rolled products; World Steel and Metalworking, 1984/85; Vol 6; p. 120-124.

18. Schröder, K.H.; Heavy spalls originating in the cores of high chromium rolls; Metalurgical Plant and Technology; 1986.

19. Kulmburg, A.; Zusammenhang zwischen Gefüge und Eigenschaften bei Werkezeugstählen; Radex-Rundschau Heft ½; 1980; p. 115-126.

20. Werkstoffkunde Stahl Band:2; 4ª Edición, Springer, Berlin, Heidelberg, Alemania, 1985.

21. Stott, F.H.; Jordan, M.P. The effects of load and substrate hardness on the development and maintenance of wear-protective layers during sliding at elevated temperatures. Wear 2001, Vol. 250, p. 391–400.

22. Strilkova, L.; Valek, T.; Tanger, L.T.D. Microstructural investigation of icdp iron designed for working layers of composite centrifugally cast rolls in hot rolling mills. In Proceedings of the 21st International on Conference Metallurgy and Materials, Brno, Czech Republic, 2012, Vol. 23–25, p. 788–794.

23. Vadiraj, A.; Balachandran, G.; Kamaraj, M. Effect of misch metal inoculation on microstructure, mechanical and wear properties of hypoeutectic gray cast irons. Mater. Des. 2009, Vol. 30, p. 4488–4492.

24. Sergio, V.; Shikawa, S.; Yamamoto, K.; Miyahara, H.; Ogi, K.; Kamimiyada, K. Control of graphite formation in solidification of white cast iron. Int. J. Cast Met. Res. 2008, Vol. 21, p. 27–30.

25. Gowda, D.; Kumar, D.C.; Sandeep, G.M.; Parthasarathy, A.; Chandrashekar, S. Tribological characterization of centrifugally cast graphite cast iron under dry and wet conditions. Mater. Today Proc. 2018, Vol. 5, p. 145–151.

26. Brandner, M.; Windhager, M.; Ziehenberger, K.H.; Improvementes in plate mill work rolls; in Saruc 2008 conference; Witbank, Republic of South Africa; 2008.

27. Fernandez-Pariente, I.; Ziadi, A.; Belzunce, F.J. Study of the high strenght steel-nodular iron interphase developed in bimetallic rolls produced by centrifugal casting. Bol. Soc. Esp. Ceram. Y Vidr. 2004, Vol. 43, p. 263–266.

28. Schon, C.G.; Sinatora,A. Hot rolling mill roll microstructure interpretation: Acomputational thermodynamics study. J. Phase Equilibria 2001, Vol. 22, p. 470–474.

29. Sinha, P.; Indimath, S.S.; Mukhopadhyay, G.; Bhattacharyya, S. Failure of a work roll of a thin strip rolling mill: A case study. Struct. Integr. 2014, Vol. 86, p. 940–948.

30. Antolin, J.F.A.; Perez, C.H.A.; Lozano, J.A. Identification of metallurgical manufacturing factors with a significant effect on the flexural strength of mottled ni-hard cast irons through a design of experiments approach. Int. J. Met. 2017, Vol. 11, p. 467–474.

31. Gowda, H.S.D.; Mukunda, P.G.; Herbert, M.A. Correlation of tribological properties with microstructure and mechanical properties of graphite cast irons centrifugally cast for engine liner. Trans. Indian Inst. Met. 2014, Vol. 67, p. 731–740.

32. Qihong, C.; Zhan-Wen, W.; Yi, J.; Yehua, J.; Fei, L.; Hanguang, F. A study of centrifugal cast high boron high speed steel. Mater. Werkst. 2014, Vol. 45, p. 582–590.

33. Yamamoto, M.; Narita, I.; Miyahara, H. Fractal analysis of solidification microstructure of high carbon high alloy cast roll manufactured by centrifugal casting. Tetsu Hagane J. Iron Steel Inst. Jpn. 2013, Vol. 99, p. 72–79.

34. Bai, Y.L.; Luan, Y.K.; Song, N.N.; Kang, X.H.; Li, D.Z.; Li, Y.Y. Chemical compositions, microstructure and mechanical properties of roll core used ductile iron in centrifugal casting composite rolls. J. Mater. Sci. Technol. 2012, Vol, 28, p. 853–858.

35. Fu, H.G.; Xiao, Q.; Xing, H.D. A study of segregation mechanism in centrifugal cast high speed steel rolls. Mater. Sci. Eng. A Struct. Mater. Prop. Microstruct. Process. 2008, Vol. 479, p. 253–260.

36. Collins, D.B.; HSS Rolls through 2000; In Proceedings of the Rolls 2000 International Convention Centre Birmingham; Czech Republic, 2012, Vol. 23–25, p. 90-100.

37. Hashimoto, M.; Shibao, S.; Recent technical trends of hot strip mill rolls at Nippon Steel Corporation; In Proceedings of the Rolls 2000 International Convention Centre Birmingham; Brno, Czech Republic, 2012, Vol. 23–25, p. 76-89.

38. Price, R.; Gisborne, H.T.; Hanlon, D.N.; Rainforth, W.M.; Sellars, C.M.; Aplication of new casting technologies for duplex rolls In Proceedings of the Rolls 2000 International Convention Centre Birmingham; Brno, Czech Republic, 2012, Vol. 23–25, p. 250-261.

39. Lowe, E.M.; FeWTiC-Iron, Tungsten and Titanium carbide duplex rolls; In Proceedings of the Rolls 2000 International Convention Centre Birmingham; Brno, Czech Republic, 2012, Vol. 23–25, p. 116-125.

40. Pero-Sanz Elorz, J.A.; Fundiciones Férreas; Dossat; Madrid; España; 1994; p. 123-129.

41. Mourad, M.M.; El-Hadad, S.; Ibrahim, M.M. Effects of molybdenum addition on the microstructure and mechanical properties of ni-hard white cast iron. Trans. Indian Inst. Met. 2015, Vol. 68, p. 715–722.

42. Chen, H.X.; Chang, Z.C.; Lu, J.C.; Lin, H.T. Effect of niobium on wear-resistance of 15% Cr white cast iron. Wear 1993, Vol. 166, p. 197–201.

43. Zhang, Z.G.; Yang, C.K.; Zhang, P.; Li, W. Microstructure and wear resistance of high chromium cast iron containing niobium. China Foundry 2014, Vol. 11, p. 179–184.

44. Kamimiyada, K; Ishikawa, S; Miyahara, H; Konno, Y; Effect of MC Type Carbides on Wear Resistance of High Wear Resistant Cast Iron Rolls Developed for Work Rolls of Hot Strip Mills. ISIJ International, 2021, Vol 61, Issue 10, p. 2597-2604.

45. Bedolla-Jacuinde, A. Microstructure of vanadium-, niobium- and titanium-alloyed high-chromium white cast irons. Int. J. Cast Met. Res. 2001, Vol. 13, p. 343–361.

46. Filipovic, M.; Kamberovic, Z.; Korac, M.; Jordovic, B. Effect of niobium and vanadium additions on the as-cast microstructure and properties of hypoeutectic Fe-Cr-C alloy. ISIJ Int. 2013, Vol. 53, p. 2160–2166.

47. Col, M.; Koc, F.G.; Oktem, H.; Kir, D. The role of boron content in high alloy white cast iron (Ni-hard 4) on microstructure, mechanical properties and wear resistance. Wear 2016, Vol. 348–349, p. 158–165.

48. Dun, X.L.; Liu, K.P.; Liu, H.S.; Lai, J.P.; Fu, X.H.; Zhou, J. Effect of multicomponent modifier on microstructure and mechanical properties of high Ni-Cr-Mo cast iron. Mater. Sci. Technol. 2011, Vol. 27, p. 1840–1845.

49. Bravo, S.V.; Yamamoto, K.; Miyahara, H.; Ogi, K. Control of carbides and graphite in Ni-hard type cast iron for hot strip mills. Mater. Sci. Forum 2007, Vol. 561–565, p. 1023–1026.

50. Drobne, M.; Urska, K.; Tercelj, M.; Fajfar, P.; Ltd, T. Thermal crack propagation during hot rolling and its influence on cast iron work roll degradation. In Proceedings of the Metal 2017: 26th International Conference on Metallurgy and Materials, Brno, Czech Republic, 2017, Vol. 24–26.

51. Tercelj, M.; Fajfar, P.; Godec, M.; Kugler, G. Characteristics of the thermal fatigue resistance for 3.1C, 0-8Si, 0.9Mn, 1.7Cr, 4.5Ni and 0-3Mo ICDP cast iron roll at 600 degrees C.Mater. Tehnol. 2017, Vol. 51, p. 515–521.

52. Bombac, D.; Kugler, G.; Markoli, B.; Tercelj, M. Hot work roller surface layer degradation progress during thermal fatigue in the temperature range 500–700 degrees C. Int. J. Fatigue 2017, Vol. 104, p. 355–365

53. Holmgren, D.; Dioszegi, A.; Svensson, I.L. Effects of nodularity on thermal conductivity of cast iron. Int. J. Cast Met. Res. 2007, Vol. 20, p. 30–40.

54. Wan, J.; Qing, J.J.; Xu, M.Z. Designing a novel graphitic white iron for metal-to-metal wear systems. Metall. Mater. Trans. A-Phys. Metall. Mater. Sci. 2019, Vol. 50A, p. 1162–1174.

55. Elmabrouk, O.; Erfan, O.M.; Kalkanli, A. The efect of magnesium to sulfur ratio on the graphite morphology of graphite cast iron produced at different section thicknesses. Manuf. Sci. Technol. 2012, Vol. 383–390, p. 5880–5885

56. Wang, G.Q.; Chen, X.; Li, Y.X.; Liu, Z.L. Effects of inoculation on the pearlitic gray cast iron with high thermal conductivity and tensile strength. Materials 2018, Vol. 11, p. 1876.

57. Lekakh, S.N.; Qing, J.; Richards, V.L.; Amer Foundry, S. Investigation of cast iron processing to produce controlled dual graphite structure in castings. Trans. Am. Foundry Soc. 2012, Vol. 120, p. 297–306.

58. Iacoviello, F.; Iacoviello, D.; Di Cocco, V.; De Santis, A.; D’Agostino, L. Classification of ductile cast iron specimens based on image analysis and support vector machine. Procedia Struct. Integr. 2017, Vol. 3, p. 283–290.

59. Valek, T.; Hampl, J. Prediction of Metallurgic Quality of ICDP Material before Tapping. Phys. Procedia 2011, 22, p. 191–196.

60. Song, J.M.; Lui, T.S.; Chen, L.H. Effect of carbon equivalent and spheroidizer addition on the morphology of strip cast white cast iron plate. Int. J. Cast Met. Res. 1999, 12, 8 p. 3–91.

61. Konig, M.;Wessen, M. Influence of alloying elements on microstructure and mechanical properties of CGI. Int. J. Cast Met. Res. 2010, 23, p. 97–110.

62. Strande, K.; Tiedje, N.; Chen, M. A Contribution to the Understanding of the Combined Effect of Nitrogen and Boron in Grey Cast Iron. Int. J. Metalcast. 2017, 11, p. 61–70.

63. Takeda, H.; Yoneda, H.; Asano, K. Effect of silicon and bismuth on solidification structure of thin wall spheroidal graphite cast iron. Mater. Trans. 2010, Vol. 51, p. 176–185.

64. Johnson, R. Probabilidad y Estadística para Ingenieros, 3rd ed.; Prentice-Hall Hispanoamérica: México DF, México, 1997; p. 489–494.

65. Box, G.E.P.; Hunter, W.G.; Hunter, J.S. Estadística Para Investigadores: diseño, Innovación Y Descubrimiento, 2nd ed.; Reverté: Barcelona; Spain, 2008; p. 235–273.

66. Prat, A.; Tort-Martorell, X.; Grima, P.; Pozueta, L. Métodos Estadísticos. Control y Mejora de la Calidad, 2nd ed.; Universidad Politécnica de Cataluña (UPC): Barcelona, Spain, 1997; p. 165–195.